Forschungszentrum Karlsruhe
in der Helmholtz-Gemeinschaft

NACHRICHTEN

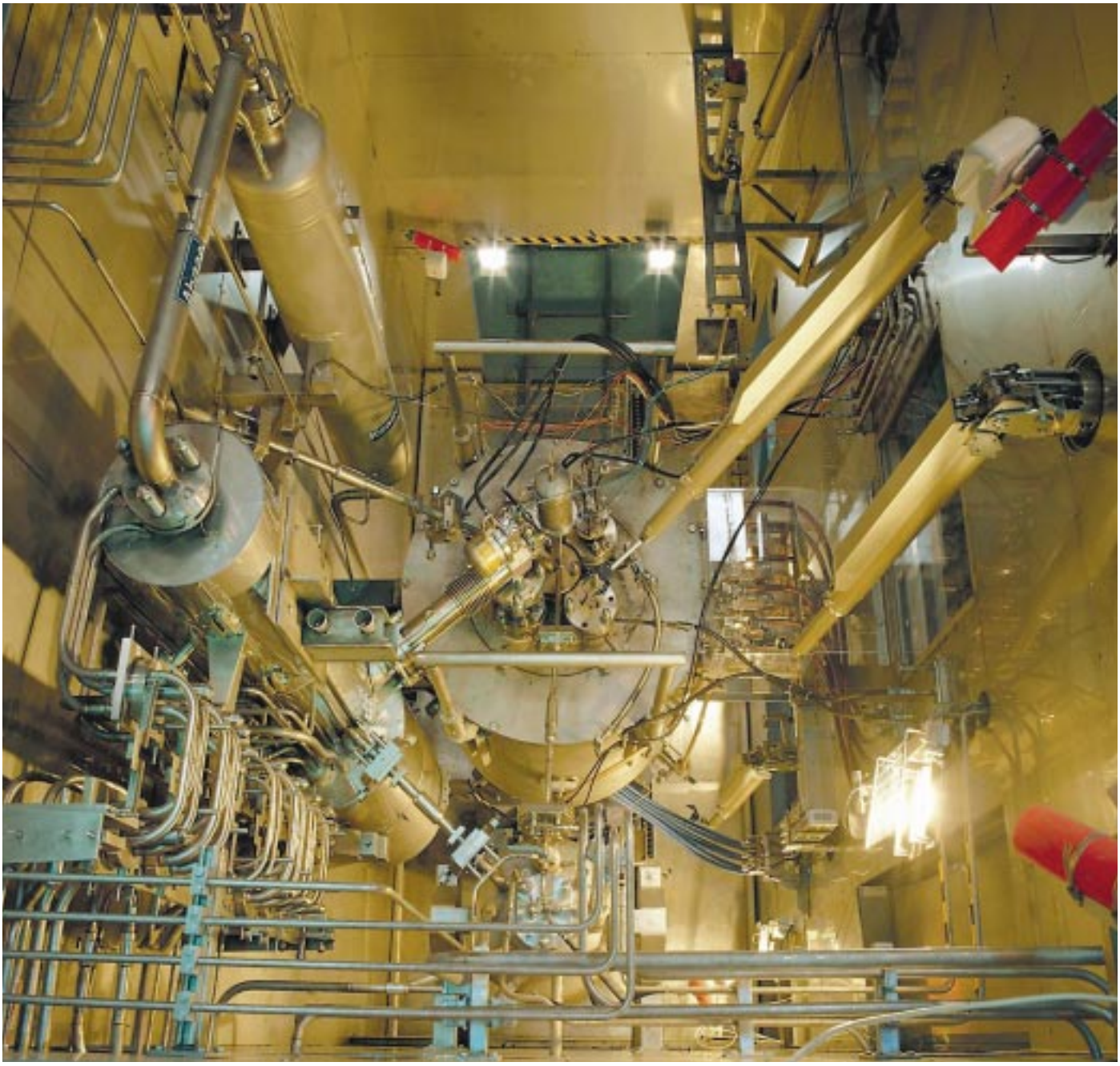

Volume 36 • 2/2004 • Special Edition in English

Nuclear Safety Research

Abbreviations used in the table of contents:

HS	Hauptabteilung Sicherheit (Central Safety Department)
IAI	Institut für Angewandte Informatik (Institute for Applied Computer Science)
IHM	Institut für Hochleistungsimpuls- und Mikrowellentechnik (Institute for Pulsed Power and Microwave Technology)
IKET	Institut für Kern- und Energietechnik (Institute for Nuclear and Energy Technologies)
IMF	Institut für Materialforschung (Institute for Materials Research)
INE	Institut für Nukleare Entsorgung (Institute for Nuclear Waste Disposal)
IRS	Institut für Reaktorsicherheit (Institute for Reactor Safety)
NUKLEAR	Nuclear Safety Research Program

Published by
Forschungszentrum Karlsruhe GmbH
Postfach 36 40 · D-76021 Karlsruhe, Germany,
phone ++49 (0)7247 82-0.

Editor:
Dr. Joachim Hoffmann.

Translated by
Ralf Friese.

Graphic design and typesetting by
Stolz Grafisches Atelier · Karlsruhe.

Layout by
Tassilo Schnitzer.

Printed by
Baur GmbH · Keltern.

Copies of NACHRICHTEN can be obtained free of charge from Hauptabteilung Bibliothek und Medien of the Karlsruhe Research Center.

Printed in the Federal Republic of Germany.

Printed on paper bleached without the use of chlorine.

Title photo:
View of the remotely operated melter cell of the non-radioactive prototype vitrification facility (PVA) of the Institute for Nuclear Waste Disposal (see contribution by G. Roth et al. on page 37).

ISSN 0948-0919

Contents

The Nuclear Safety Research Program of the Karlsruhe Research Center

J. U. Knebel, NUKLEAR

Irrespective of the decision about a continued use of nuclear power in Germany, very high demands will continue to be made on the safety of nuclear facilities operated in Germany, and on the disposal of radioactive waste.

The Nuclear Safety Research Program (NUKLEAR) of the Karlsruhe Research Center, which is an integral part of the Energy Research Area of the Hermann-von-Helmholtz Association of German Research Centers (HGF), is devoted to studies of scientific aspects of the safety of nuclear reactors and of nuclear waste disposal. The findings elaborated in this way are put into practice in the public interest so as to ensure that the high standard of safety of the nuclear installations operated in Germany will be preserved in the future, and will continue to meet the highest international requirements and standards.

Two program topics are covered within the Nuclear Safety Research Program:

- Safety Research for Nuclear Reactors:

  Studies and assessments of the nuclear reactors currently in operation with a view to design basis accidents, accidents beyond the design basis, and potential radiological consequences. This work is carried out on the basis of advanced research and development activities and serves to ensure safe operation of nuclear reactors and minimize any risks arising.

- Safety Research for Nuclear Waste Disposal:

  This program topic comprises research and development activities designed to reduce the radiotoxicity of high-level radioactive waste; research into the long-term safety of final storage; and the immobilization of high-level radioactive waste. The objective of these activities is the safe, permanent disposal of radioactive waste and, in this way, the protection of present and future generations.

In 2003, the NUKLEAR Program was reviewed by a group of international experts within the framework of program-oriented funding in the Helmholtz Association. The reviewers rated the work carried out at the Karlsruhe Research Center very good or excellent in scientific terms and emphasized that the Karlsruhe Research Center operated a unique science infrastructure.

An important purpose of the NUKLEAR Program is the preservation and further development of competence in the field of nuclear safety. Even after the decision by the federal government to

Nuclear Safety Research Program	
Program Topic 1 **Safety Research for Nuclear Reactors**	**Program Topic 2** **Safety Research for Nuclear Waste Disposal**
● Studies of the phenomena associated with design-basis and beyond-design-basis accidents. ● Description of the sequence of steps in beyond-design-basis accidents. ● Application to reactors currently in operation. ● Improvement of external emergency protection after potential nuclear accidents.	● Immobilization of high-level radioactive waste. ● Reduction of radiotoxicity (partitioning and transmutation). ● Safety research for final storage.

opt out of the peaceful uses of nuclear power, there will be a considerable need for young scientists and engineers for decades to come in order to ensure the highest scientific and technical level of know-how in the fields of reactor safety and nuclear waste disposal both in industry and with regulatory authorities and expert consultants. However, competence in nuclear safety research, and its application to national problems, can only be ensured through scientific and technical cooperation in international research programs and with groups and committees active in this field.

Studies of Severe Accident Phenomena in the Ex-vessel Phase

H. Alsmeyer, J. J. Foit, L. Meyer, IKET; W. Schütz, IRS

Introduction

In the course of a severe core meltdown accident it is possible, as a consequence of a long-term, highly improbable failure of the cooling system, that the molten fuel will penetrate the reactor pressure vessel (RPV), enter the reactor cavity and impinge on the concrete base mat. The important events occurring in this case were studied in large experimental facilities at the Karlsruhe Research Center already back in the eighties. Initially, those activities served to quantify the hazards associated with severe reactor accidents within the framework of safety studies conducted in Germany and in the United States [1]. Especially the Chernobyl reactor accident (1986), despite many grave deficits compared to the safety concepts of Western reactors, underlined the need for studies of this kind. The problems, to which answers had been elaborated at the Karlsruhe Research Center even before Chernobyl, include the attack on the concrete base mat by the melt, especially the penetration of the concrete base mat, and the pressure rise in the containment.

Although the probability of occurrence of accidents of that degree of severity is very low in German reactors, amounting to roughly 10^{-5} per reactor year, the safety criteria to be met under severe accident conditions were tightened up considerably against the background of increasing public sensitivity. Consequently, additional measures were taken for the reactors in operation in Germany which, on the one hand, improve the possibilities to intervene in an accident and, on the other hand, greatly reduce potential radioactivity releases to the outside [2]. This includes, for instance, filtered depressurization and early hydrogen recombination in the containment. These measures are also based on in-depth accident analyses in various test facilities of the Center, whose operation is continued to provide more knowledge about the sequence of accident events, and show possibilities of intervention.

The outline below follows the course of an accident, from the release of the hot core melt from the reactor pressure vessel to the long-term attack on the base mat and, potentially, cooling of the melt in the base mat area.

Melt Dispersion

The melt could leave the reactor pressure vessel (RPV) either in the center of the hemispherical bottom or, if there is a failure on the side of the RPV, roughly at the level of the surface of the melt. This depends on the details of the sequence of accident events, on any cooling measures initiated, and on the penetrations existing in the bottom of the pressure vessel.

Assuming successful depressurization of the primary system, i.e. that the pressure of the steam driving the melt has been reduced to a level clearly below 20 bar, it is possible for the reaction forces associated with an RPV failure to be accommodated by the RPV supports. However, depending on the existing geometry, a large part of the melt may be ejected from the reactor cavity and dispersed into adjacent compartments or into the containment. In this phase, most of it is fragmented into fine particles which can react very effectively, both thermally and chemically, with the steam and the atmosphere in the containment. These potential melt transport processes, and the thermal and chemical interactions, are being studied in order to detect potential hazards to the integrity of the reactor containment and reveal the countermeasures available.

On the basis of the DCH (Direct Containment Heating) experiments conducted by Sandia, USA, these events are being studied within the DISCO (DISpersion of COrium) experiments at IKET with the focus on the narrow caverns of typical European reactors. In a 1:18-scale geometry, the corium melt is simulated by cold model liquids or hot thermite melts (T>2000°C) (Fig. 1). In the course of these test series, the burst pressures, failure cross sections and failure locations, driving gases (nitrogen or steam), and the atmosphere in the containment (air or steam-air mixtures) were varied systematically.

If the RPV fails at the bottom, up to 75 % of the melt can be ejected from the reactor cavity at pressures close to 20 bar. At residual pressures below 5 bar, this fraction drops to less than 10 %. The melt volume dissipated is much smaller when the failure occurs in the RPV sidewall.

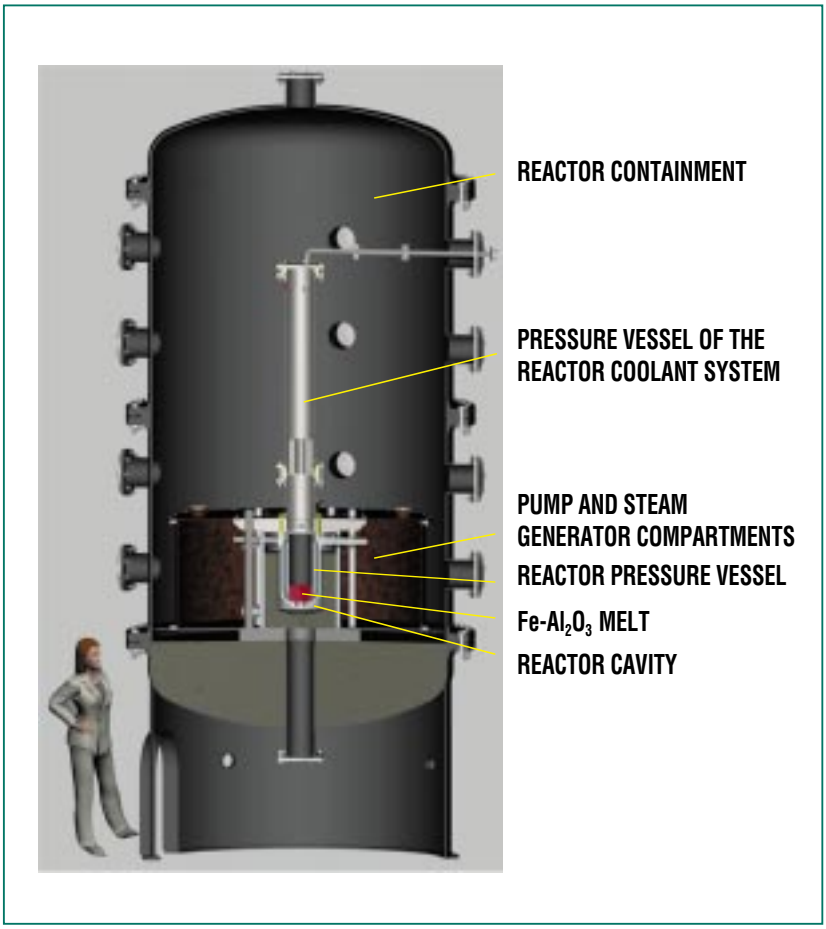

Fig. 1: The DISCO-H experimental facility models the main components and volumes of a pressurized water reactor.

Heat transfer from the small melt droplets to the containment atmosphere, and combustion of the hydrogen generated in the reaction of the metal part of the melt with the steam, may increase the pressure in the containment briefly by 2 to 4 bar. In case the direct way out of the reactor cavity into the containment is blocked, and there is only a connection to the relatively narrow pump and steam generator compartments, less hydrogen will be generated and burnt. As a consequence, also energy transfer to the atmosphere and the pressure rise will be reduced.

Any information above and beyond these findings requires plant-related experiments and careful extrapolation by computer codes. A powerful thermohydraulic code is used to analyze these experiments and improve the underlying models. The objective is to be able to extrapolate from small-scale experiments with model fluids to full-scale reactor conditions and prototype uranium oxide-steel melts.

Erosion by the Melt Jet

In case of local failure of the reactor pressure vessel, the pressure of the steam in the primary system may cause the melt to be ejected as a compact jet for a few seconds followed by a dispersed jet after gas penetration. The KA-JET experiments were performed to study the erosive action of this melt jet when this jet, driven by gas pressures of up to 2 MPa, impinges upon the concrete in the reactor cavity. The core melt in this case was simulated by a thermite melt at temperatures of approximately 2000°C.

The experiments were conducted to study erosion of the two types of concrete, structural concrete and borosilicate glass concrete. A total of seven experiments (KJ02 to KJ08) were run successfully. For independent studies of the effects of the two liquid corium phases, the metal and the oxide phases were allowed to separate in each experiment as a result of their different densities. The melt jets ejected one after the other hit two concrete specimens mounted to a drum which could be turned by 90°.

After the first specimen had been hit by the iron jet, the second specimen was moved into the path of the jet and impacted by the oxide jet. These specimens had been fitted thermocouples for detecting the erosion front as a function of time.

Here are some typical experimental parameters and findings for the KJ08 example, which involved structural concrete: mass of the melt, 75 kg of iron and 84.5 kg of oxide, respectively; melt temperature, 2050°C; driving pressure, 0.8 MPa; duration of in-

teraction, 5.8 s and 2.9 s, respectively; depth of erosion, 65 mm and 29 mm, respectively; eroded concrete volume, 180 ml and 95 ml, respectively (Fig. 2).

A database is now available which comprises two test series with driving pressures of 0.3 MPa to 0.8 MPa, namely KJ02-04 and KJ08 for structural concrete, and KJ05, 06, 07 for borosilicate glass concrete. The maximum downward erosion rates were around 11 mm/s. As a general finding, it is safe to say that the erosion rates are lower for oxide jets than for iron jets. Likewise, the rates are lower for borosilicate glass concrete than for structural concrete. As the driving pressure rises, so do the erosion rates.

The theoretical interpretation of the experiments was developed in cooperation with the Bochum Ruhr University. Melting of the concrete as a result of the heat transferred by the impinging melt jet was identified as the leading mechanism.

Melt Spreading

When the melt leaves the pressure vessel at a low release rate, e.g. after a complete pressure drop in the primary system, its propagation behavior on the concrete is of great interest as it influences the attack on the concrete and the possibility to cool the melt, if any. After earlier experiments conducted at the Karlsruhe Research Center and in European partner countries, the ECOKATS experiments supported by the European Union now serve to complete the database by large-scale experiments and are used for final validation of computer codes.

A new type of thermite melt was developed for these experiments which has a range of solidification between 1822 K and 1373 K, and exhibits the main properties of a core melt with respect to its spreading characteristics. It is especially the viscosity of the melt which is important for its spreading behavior; however, because of the high temperatures involved, it cannot be measured directly. Consequently, it was determined from an experiment in which 193 kg of melt at an initial temperature of 1893 K had been spread in an oblong duct whose bottom had been lined with a ceramic. The melt was fed for 55 s at an approximately constant volume flow of 1 l/s. The viscosity was estimated from the measured front positions as a function of time on the basis of approximate solutions developed for this purpose. This is possible, as oxide melts initially produce thin thermal boundary layers which hardly influence the movement of the front in the early phase of propagation. This phase lasted for 12 s. Afterwards, the crust formed in the environment of the front, which was carried along, reduced the propagation rate. Immediately after this crust had come to a standstill after

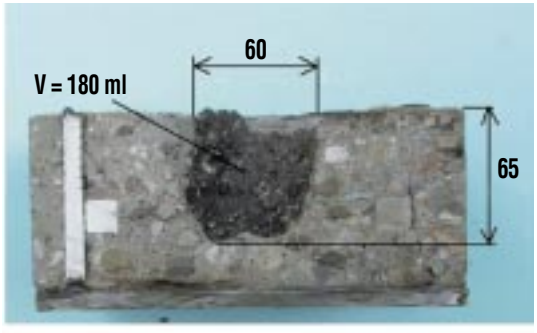

EROSION CAUSED BY IRON JET

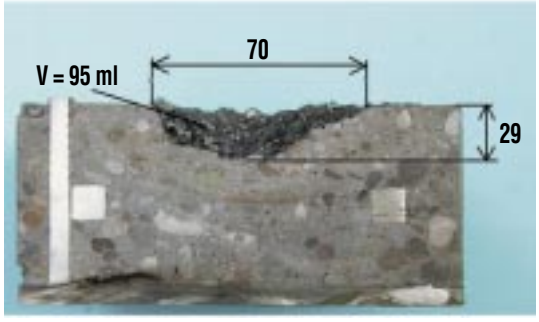

EROSION CAUSED BY OXIDE JET

Fig. 2: Cross section through the concrete test specimens (dimensions in mm).

Fig. 3: ECOKATS-1, end of propagation.

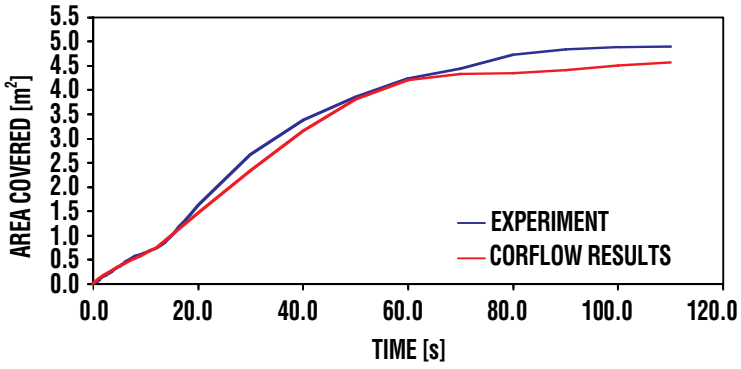

Fig. 4: Comparison between experiment and recalculation.

28 s, the hot melt underneath continued to flow on at a higher velocity. This process was repeated when another crust had become attached after 45 s. The end of movement of the front was reached when a third crust had come to a standstill after 74 s, which is 16 s after the end of feeding of the melt.

The ECOKATS-1 experiment is about propagation on a large plane concrete surface. The propagation geometry comprised a channel 2.6 m long and 0.29 m wide which converged into an area of 3 m x 4 m (Fig. 3). The large mass of oxide of 547 kg, which was released into the propagation area at an initial temperature of 1873 K and an approximately constant volume flow of 2 l/s, allowed the influence of melt cooling on three-dimensional propagation to be examined without feeding of the melt having stopped prior to the formation of thick crusts. The propagation of hot melts on concrete is influenced, on the one hand, by the gases released, because the voids contained in the melt change melt viscosity. The gas flow causes the viscosity to increase fourfold, which supports the findings made in earlier experiments. On the other hand, given the low discharge rates prevailing in this case, crust formation at the propagation front is very important, as it impedes undisturbed propagation like a dam and gives rise to a complex melt front.

It is not possible to model in detail all these processes in a computer code (CORFLOW). To assess the quality of the computed results, the area covered in the experiments is used as a yardstick. The agreement achieved (Fig. 4) documents the power of the computer code used. As far as application to reactor safety is concerned, it constitutes a tool allowing reliable information to be generated about the propagation behavior of a melt even under very adverse conditions, such as low discharge rates and slight overheating of the melt.

Base Mat Erosion and Coolability

When discharged from the pressure vessel, the core melt has an initial temperature of approx. 2000°C. Under these extreme conditions, the concrete in the reactor cavity is decomposed, which gives rise to gases released into the containment, while the melt, which is heated by the nuclear decay heat, penetrates into the base mat.

As has been shown by the use of the BETA experiments in the WECHSL computer code, penetration of the concrete base mat cannot be excluded unless effective cooling of the melt is started to extract the decay heat from the melt over long periods of time. Two concepts relating to this problem are currently pursued

within the framework program of the EU with the participation of other institutions, namely

(a) cooling by applying water to the surface of the melt,

(b) cooling by injecting water into the melt from below.

Experiments about cooling from the top need large propagation areas to prevent the sidewalls from atypically influencing surface crust formation, which would affect the cooling processes under study. To achieve a melt at least 20 cm high, 3200 kg of a simulated core melt consisting of a metal fraction and an oxide fraction were poured into a concrete cavity of 2 m x 2 m in the ECOKATS-2 experiment (Fig. 5a). The melt had spread evenly within 40 s and, as expected, caused pronounced erosion in the concrete. In this early phase, flooding of the top of the melt was initiated by applying 4 l of water / s from one side. Contact between the water and the surface of the melt was very smooth, without any violent interactions between the melt and the water. Below the thin initial layer of water, the melt first generated a bright, glowing, thin surface crust layer. This crust has holes through which the gases are discharged from the ongoing concrete erosion. The crust cools quickly and darkens, which is also characteristic of the transition from film boiling to nucleate boiling. This transition is shown in Fig. 5b, in which the surface cools progressively from right to left.

Except for the holes permeated by gas, the crust is closed and firmly anchored to the concrete sidewall. This prevents water from penetrating from the top and thus disrupting the melt, which would be a prerequisite for effective heat extraction from the bulk of the melt. As a consequence of the gas release from the concrete, the gas pressure generated lifts the crust in the inner region of the surface by up to 20 cm, thus generating a partly porous top structure. Moreover, the gases discharged through the holes in the crust transport lava-like melt into the top layer of water, which results in roughly 15 volcano-like cones being built up to 20 cm height. As is shown by the gradual temperature drop at the bottom of the melt, these processes contribute very little to improving the cooling situation. Consequently, cooling is mainly limited by thermal conductivity in the surface crust. In the course of the experiment, the bulk of the melt therefore solidified into a compact layer preventing cooling water from entering from above. Subsequent examination showed that merely the top 4 cm of the oxide melt layer had been transferred into a configuration capable of effective cooling. Under reactor conditions, base mat erosion cannot be expected to be stopped solely by flooding from above. These findings confirm experiments conducted at the Argonne National Laboratory, USA, which had been run on UO_2-based melts with decay heat simulation, though in a much smaller geometry.

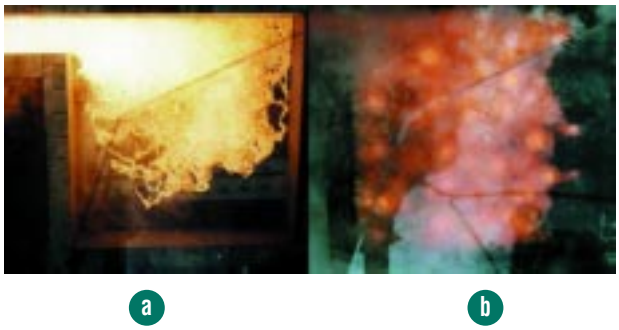

Fig. 5: Simulated core melt on a concrete area of 2 x 2 m^2; propagation (a) and cooling by water supplied from above (b).

The melt can be cooled more effectively by introducing water into the melt from below, which causes rapid evaporation and breaking up of the melt. This so-called COMET concept is being developed and optimized at the Karlsruhe Research Center. The COMET experimental facility is used for this purpose, which is a major extension of an earlier experimental setup and heating system used for the BETA experiments, and which allows continuous simulation of the decay heat over the duration of the experiment (Fig. 6).

After propagation on the plane COMET cooling facility, the melt initially erodes a sacrificial layer

Fig. 6: COMET experimental facility.

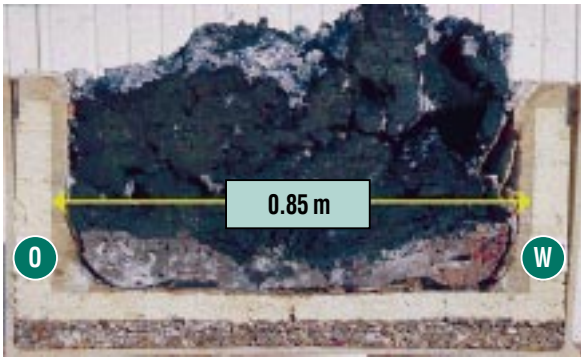

Fig. 7: Cross section through a coolable melt solidified into a porous configuration.

of concrete up to 10 cm high, and then opens up access pathways for the flooding water by melting. Depending on the design, water is supplied through a multitude of channels or a porous concrete layer at the bottom of the cooling system. The cooling water is kept at a slight overpressure relative to the melt, which makes for purely passive cooling.

The experiments show that the melt can be stopped and cooled reliably (Fig. 7). The cooling system is currently being optimized for use in reactors with respect to its installation height and to the coolable height of the melt.

Outlook

The experiments described above, and the associated development of computer codes, greatly add to our knowledge of the sequence of steps in severe accidents, but also to the possibilities of intervention to minimize the accident. In this way, these activities contribute to the continued safe operation of existing reactors. International participation, exchanges with important countries within and outside of Europe, and the support by the European Union thus assist in maintaining a high international level of safety of light water reactors.

Literature

[1] *Deutsche Risikostudie Kernkraftwerke, Phase B, Verlag TÜV Rheinland, Bonn 1989*

[2] *Fortschritte bei der Beherrschung und Begrenzung der Folgen auslegungsüberschreitender Ereignisse, Fachtagung der KTG-Fachgruppen Reaktorsicherheit und Thermo- und Fluiddynamik, Karlsruhe, 25. - 26. 9. 2003, FZKA 6935 (2004)*

Studies of Severe In-vessel Accident Phenomena

M. Steinbrück, L. Sepold, IMF; H. Jacobs, A. Miassoedov, IKET; W. Hering, R. Krieg, W. Schütz, IRS

Introduction

Most reactors currently in operation worldwide, and all reactors run in Germany, are light water reactors (LWR) using uranium oxide or uranium-plutonium mixed oxide (MOX) fuel contained in zirconium alloy cladding tubes permeable to neutrons. The coolant, and the moderator serving to slow down the fast neutrons released in a nuclear chain reaction, is ordinary "light" water (H_2O as distinguished from "heavy" water, D_2O, hence the name). Other important reactor components are the control rods for controlling the reactor power (the chain reaction) and for emergency shutdown (scramming) of a reactor. In most pressurized water reactors (PWR), the neutron absorber consists of a silver-indium-cadmium alloy (AIC), in most boiling water reactors (BWR), of boron carbide (B_4C).

Severe accidents are extremely improbable in this type of reactor. However, to raise the safety standards of nuclear power plants even higher, many research activities have been, and are being, carried out worldwide to understand the phenomena occurring under the extreme conditions of such an accident, determine upper bounds of load acting on the safety barriers, and find measures to reduce, terminate or even prevent the propagation of an accident. For this purpose, complex computer codes are used which are validated against experiments on various scales.

This article presents recent results of work performed within the Nuclear Safety Research Program at the Karlsruhe Research Center on phenomena up to failure of the reactor pressure vessel (RPV). These so called in-vessel phenomena determine the primary source term of fission products and hydrogen in the containment as well as the starting conditions, such as the temperature and composition of the melt, for the further course of an accident outside the pressure vessel (ex vessel) covered in the previous contribution (Alsmeyer et al.).

Early Core Degradation and Flooding of the Overheated Reactor Core

The early phase of core degradation is characterized by the initial formation of a melt of metal components and the preservation of most of the fuel element geometry. Both phenomenologically and with respect to modeling in the computer codes simulating severe accidents, this is well understood and has been described extensively. The accident of the Three-Mile-Island reactor (TMI-2) in the United States in 1979 initiated a host of national and international experimental work, including the CORA program (Karlsruhe, 1987 – 1993). One important result of these activities shows that eutectic interactions of different materials cause melts to form clearly below the melting temperatures of the individual components [1].

In the interest of timely termination of a severe reactor accident, flooding the overheated reactor core with water is one of the most important measures of accident protection. As a consequence of the exothermal chemical reactions between the steam generated and zircaloy cladding tubes of the fuel elements, this process may give rise to a temporary temperature escalation accompanied by the production of large amounts of hydrogen. The hydrogen generated in this way must not exceed safe levels. Consequently, it must either be bound chemically in recombiners in the reactor containment or burnt under controlled conditions in order to prevent oxyhydrogen gas detonations with immense consequential damage. To determine the so-called hydrogen source term (total quantity and rate), the QUENCH experimental facility (Fig. 1), which was commissioned in 1997, is used to run out-of-pile experiments, i.e. simulation experiments outside a reactor, under various conditions for PWR, BWR and Russian VVER fuel elements.

In these experiments, a simulation bundle equipped with an extensive set of instruments is heated to temperatures of 1500 to 2000°C in an oxidizing atmosphere to simulate various phases of an accident. Once the parameter settings, such as temperature and state of oxidation, have been reached, the bundle is quenched with water or steam [2]. Nine such integral experiments have been conducted so far. The most important test parameters included the temperature and degree of pre-oxidation at the time the quenching phase was initiated, and the quenching medium (water, steam) as well as

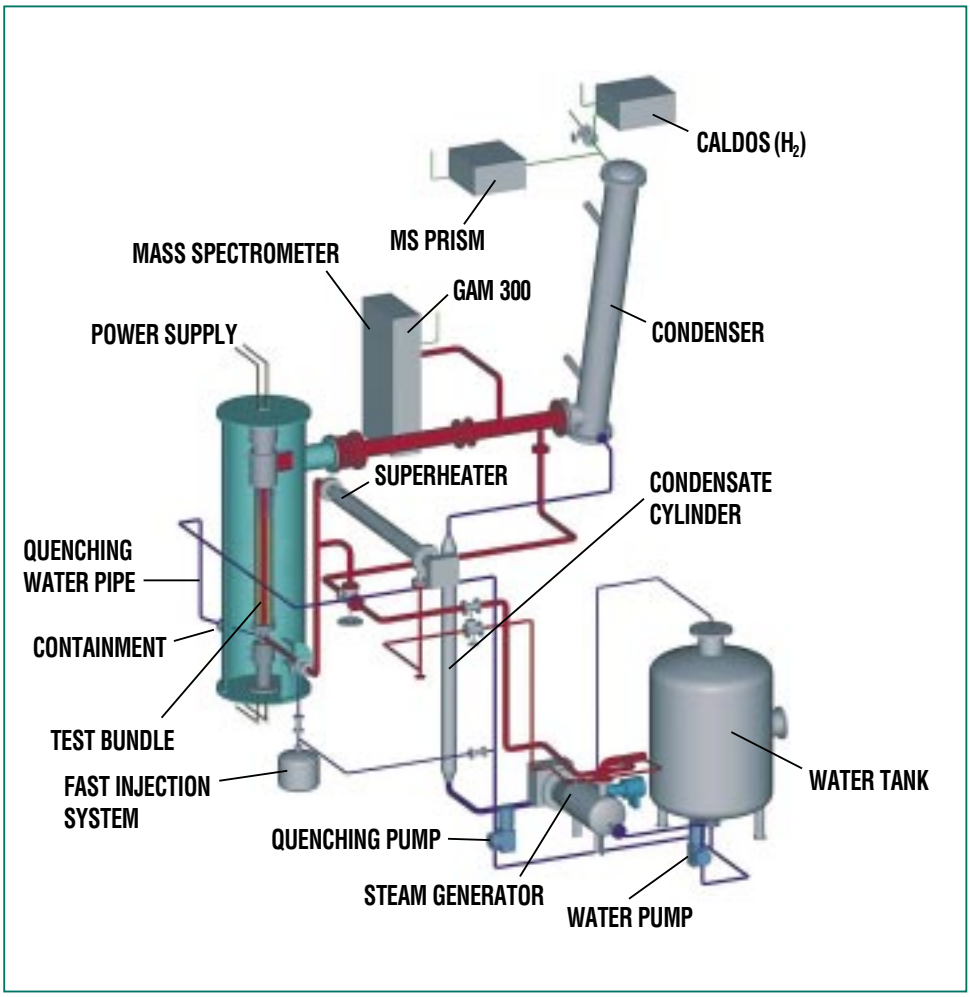

Fig. 1: QUENCH test facility for studies of the hydrogen source term and materials interactions arising when quenching a superheated reactor core.

studies of the influence of B_4C absorber materials and conditions of steam starvation. Steam starvation exists, e.g., when the steam supplied is consumed completely by the oxidation reaction in the lower bundle region, and reducing conditions prevail in the remaining upper region because of the generation of hydrogen.

In some of the experiments, flooding with water and quenching with steam, respectively, were successful, immediately causing a drop in temperature and thus only slight additional hydrogen production. In other experiments, however, temperature escalation combined with the release of large hydrogen volumes was observed at the beginning of the quenching phase. To understand what is happening, it must be realized that water and steam, respectively, act as coolants, as they should, but also as oxidants. The energy balance at the onset of the quenching process is a major criterion deciding whether the bundle will be cooled successfully or whether the increased supply of steam in this phase will lead to an escalation caused by the exothermal chemical reaction. Experimental work has shown that escalation is promoted by the impaired protective action of the surface oxide layers due to cracking, spalling, or dissolution under conditions of steam starvation and by the formation of metal melts, especially due to eutectic interactions far below the melting temperatures of individual components.

As the phenomena occurring under the extreme conditions of a hypothetical severe accident are very complex, the bundle tests are supported by small-scale single-effect studies and by using the appropriate computer codes. Various computer codes (SCDAP/RELAP5, CALUMO, SVECHA/Q), some of which were developed at the Karlsruhe Research Center, on the one hand, help prepare and analyze the experiments and, on the other hand, are validated and improved by experimental data. Within the QUENCH-06 experiment, various code systems were compared within the framework of the International Standard Problem (ISP) 45 [3] of OECD. It was seen that the codes had some problems in correctly computing the initial conditions in the bundle at the onset of flooding. Lack of experience of the users in handling such complex code systems, and difficulties in adequate modeling of the QUENCH facility, were the main causes of major deviations. The latter fact is indicative of the incipient loss of know-how in reactor safety, which may be coun-

teracted by including young scientists in further code comparisons.

Melt Relocation to the Lower Region of the Pressure Vessel

The LIVE (**L**ate **I**n-**v**essel Phase **E**xperiments) experiments are to be performed to study important phenomena in the late phase of core meltdown. These are the main objectives of the project, which is now in its buildup phase:

(1) Description of the late phase of core meltdown, core relocation, and the formation of a molten pool within the RPV.

(2) Studies of possible restoration of cooling and stabilization of the melt in the RPV by internal water supply and/or external flooding of the RPV.

The experimental program is arranged in various phases in which transient relocation of the core melt to the lower plenum, and the formation and behavior of molten pools will be studied. In that way, the main phases of the accident are to be determined and possibilities for intervention are to be detected for accident control.

The LIVE experimental facility consists of an experimental vessel, a furnace generating the melt, and a volumetric heater to simulate nuclear decay heat. The experimental vessel is an RPV of a typical German pressurized water reactor scaled down in a 1:5 ratio. It is equipped with a variety of measuring systems, such as heat flow sensors and thermocouples (Fig. 2). The internal instrumentation – thermocouples, viscosimeters, sampling systems, crust measurement systems, etc. – is introduced into the RPV from the top through the lid.

The experiments will be carried out with various simulated melts. In the first series, nitrate melts (KNO_3 and $NaNO_3$) will be heated to approx. 350°C. In this series of experiments, above all crust formation in the hemispherical bottom and heat flows into the vessel wall will be studied so that the loads and stresses affecting the vessel and possibilities of cooling can be indicated.

In a later series of experiments, oxide melts will be heated to approx. 1000°C. As the salt and oxide melts chosen are similar to core melts in their phase diagrams and in important materials properties, major findings can be translated into the accident situation. In the longer term, also metal melts will be used in combination with oxide melts.

Energetic Interaction of the Core Melt and Water (Steam Explosion)

Steam explosions can occur under adverse conditions when a hot melt is mixed with water in such a way that the heat transfer area abruptly increases by several orders of magnitude, leading to a sudden evaporation of water and a corresponding pressure buildup. Accidents caused by steam explosions can occur in practically all branches of industry in which large quantities of hot melts are handled. In connection with severe accidents in nuclear reactors, concern had been expressed about a steam explosion in the pressure vessel leading to early containment failure with catastrophic consequences. Most of these concerns were removed by probability analyses. In the light of our studies in three disciplines, we were able to prove also deterministically that a conservatively estimated maximum explosion energy will be accommodated by the pressure vessel [4]. These findings were generated in the following way:

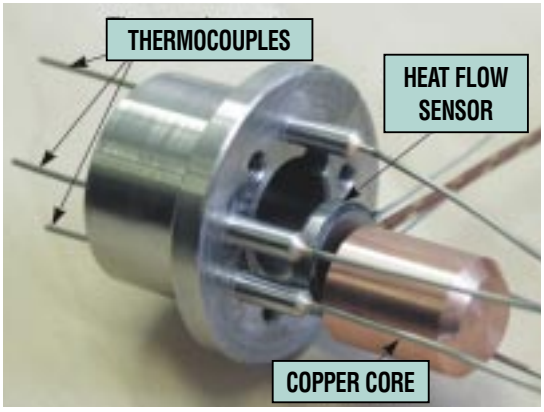

Fig. 2: Design of an instrumentation plug for measurements of temperature and heat flow in the LIVE facility.

(1) Determination of the states of RPV internals and the pathways open to the melt to relocate from the core region to the lower coolant plenum.

(2) Calculation by means of our computer codes of the mixed molten mass and its energy content.

(3) Conservative estimate of the explosion energy and the frac-

tion thereof affecting the RPV head.

(4) Experimental determination of the load transfer capability of the closure head system, i.e. the head and the bolts holding it in place.

There is still need to take into account the loads arising from these and other steam explosions when analyzing accident scenarios. For this purpose, they must be estimated as realistically as possible. This requires the development of the appropriate thermo-fluid dynamic computer codes and, for this purpose, a most comprehensive knowledge of the complex processes as well as informative and reliable experimental data against which to test the codes. For this reason, large-scale experiments have been, and will be, conducted: approximately up until 1999, the QUEOS and PREMIX experiments on premixing and, since 2000, the ECO (Energy COnversion) experiments about energy releases in explosions.

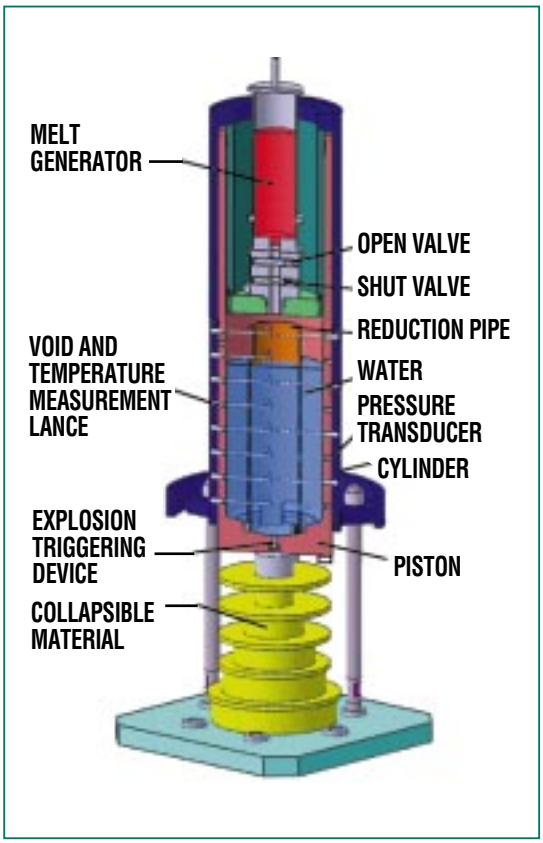

Fig. 3: The ECO facility consists of a cylinder firmly anchored to the baseplate, and a piston able to move only against the resistance offered by a special type of collapsible material so as to allow the mechanical energy to be determined. The core melt is replaced by molten aluminium oxide generated in a thermite reaction. The maximum quantity available is slightly less than 20 kg of Al_2O_3 at a temperature of approx. 2600 K.

A tool developed at the Research Center to describe melt-coolant interactions is the MATTINA computer code, a time-dependent fluid-dynamic multiphase multicomponent model, which allows the movements of the melt, water, and gas to be described separately. Heat and impulses are exchanged among the three fields, while mass is exchanged (by evaporation and condensation) between the water and the gas. The physical interactions among the fluids are described by arithmetic models from the literature, some of which were matched empirically. Except for cases involving high explosion pressures (above 10 MPa), recalculations of various experiments with MATTINA showed good results without individual parameter fitting. In addition, MATTINA was able to explain some phenomena which had consistently occurred during premixing in the ECO experiments and were difficult to understand initially.

The purpose of the ECO experiments (Fig. 3) is to measure directly the pressure during a steam explosion (for the first time for explosions of this magnitude) and the mechanical energy released [5]. Seven experiments have been conducted so far. In the ECO-05 experiment, 16.4 kg of melt were introduced into the water. The pressure of the explosion at several measuring points exceeded the range of 45 MPa for nearly 1 ms. The explosion energy amounted to approx. 2.35 % of the total thermal energy initially available in the 16.4 kg. When the experiment was repeated (ECO-06), the premixing phase was very similar (e.g., 15.2 kg were mixed). Still, pressures ranging up to approx. 100 MPa were measured, but prevailed only for shorter periods of time, and the explosion energy was only roughly one third of the previous level. The experiments showed that steam explosions are subject to pronounced statistical fluctuations.

Containment damage is influenced decisively by the closure head (head and bolts) of the RPV withstanding the impact of core melt ejected upward. For this reason, the maximum kinetic energy, E_{slug}, of the core melt propelled upward by the explosion was determined which can still be accommodated reliably by the head, as well as the release of mechanical energy (explosion energy) below the core support plate, E_{plate}, required for this purpose.

In this case, mechanical interaction with the relatively small and complex pressure vessel internals plays a major role. However, reliable description of the events in a computer code is nearly impossible. Interestingly enough, it was seen that this interaction and the resultant stress on the pressure vessel head can be simulated rather exactly in model experiments. Highly non-linear major plastic deformations are modeled correctly in this case [6].

For this reason, the studies were conducted with the support of the 1:10 scale BERDA model experiments. For this purpose, the IVAN impact test facility was built (Fig. 4). The core melt in this case is simulated by a low-melting lead alloy and accelerated upward by compressed-gas propulsion. Ductile pressure vessel internals were simulated as steel models, while embrittled internals were simulated in great detail by red brass models. Experiments were carried out without these models (upper internals molten down), with models only of the top grid, and with the complete models.

As was expected, the existence of internals has considerable consequences. They increase the permissible impact energy, E_{slug}, by a factor of 4 to 8, the permissible release of mechanical energy, E_{plate}, by a factor of 7 to 14 (Fig. 5).

In the light of our studies, it can thus be excluded on deterministic grounds that a steam explosion in a reactor pressure vessel will lead to early containment failure. Further theoretical and experimental work serves to achieve more realistic estimates of pressures and explosion energies.

Outlook

Over the past few years, important contributions to the phenomenology and to modeling of

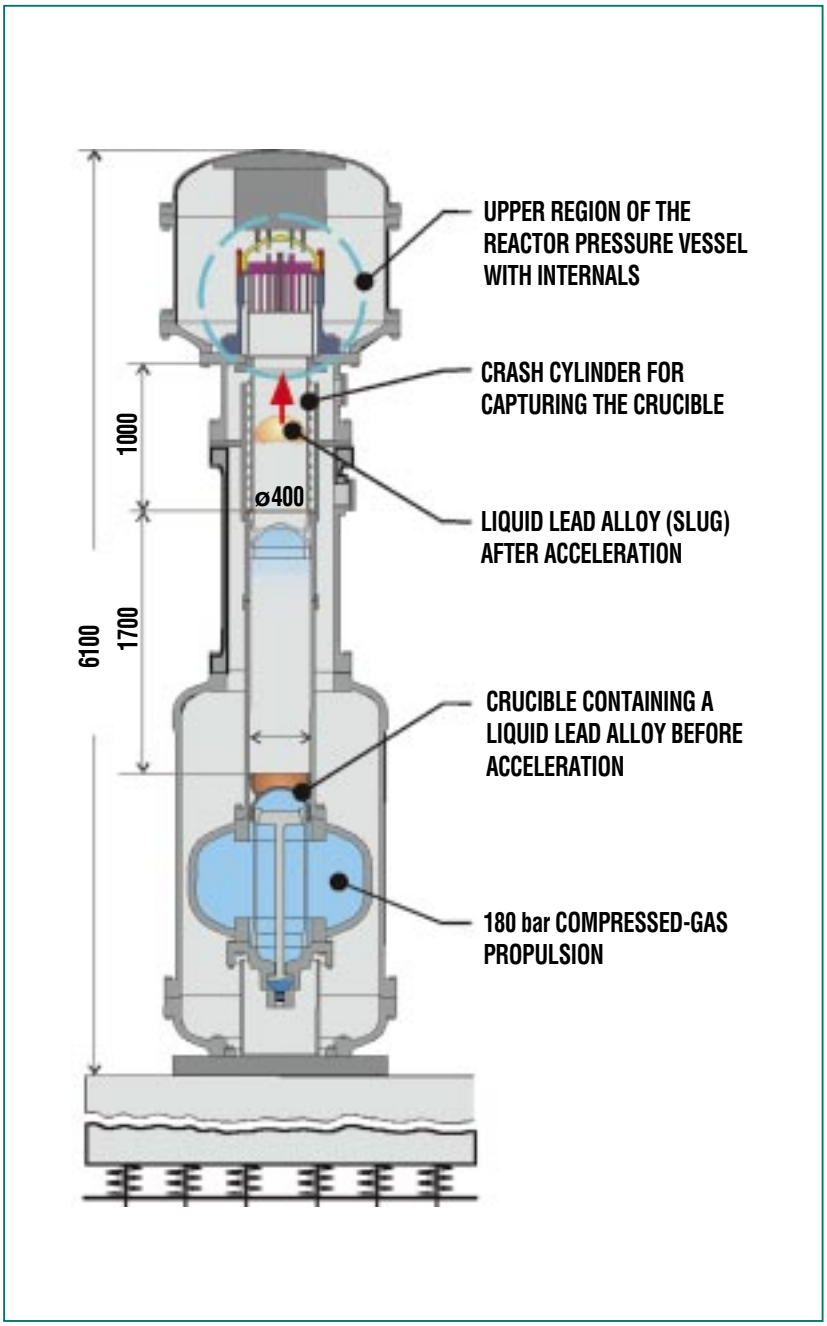

Fig. 4: IVAN impact tester to study the load acting on the RPV head as a result of core melt propelled upward after an energetic interaction between the melt and the coolant.

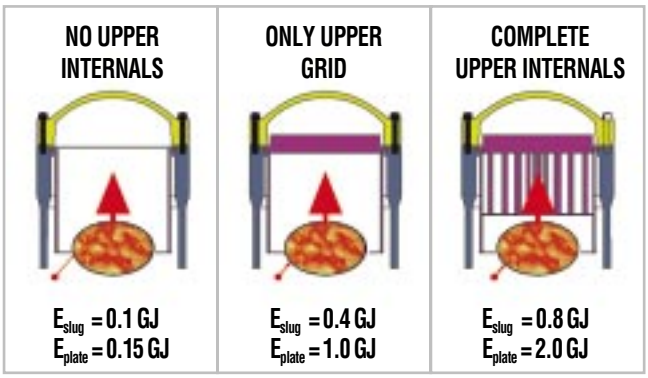

Fig. 5: Maximum permissible impact energies, E_{slug}, and the associated energy releases, E_{plate}. The closure head of the reactor pressure vessel will withstand these energies. Some rather conservative assumptions were used as a basis of these assessments.

the events occurring in a reactor pressure vessel have been made at the Karlsruhe Research Center. They have been incorporated, among other things, in the engineered safeguards design of the new European Pressurized Water Reactor (EPR), which will soon be built in Finland by the French-German Framatome company.

Despite the politically motivated restriction of our present activities to reactors currently in operation, there are a number of important new problems to be solved. In addition to the work described above about the late in-vessel phase in the LIVE test facility, which has hardly been studied so far, new problems arise from the use in reactors of advanced materials optimized so far only for operation. Thus, proof must be generated for new cladding tube alloys optimized with respect to burnup to show that they will behave similar to, or better than, the classical zircaloy-4 in severe accidents. Moreover, the enlargement of the European Union entails the obligation to include also Russian VVER reactors in European safety research.

Many of the activities presented in this article are part of, and acknowledged in, international programs run within the framework of the EU, OECD, and other bilateral and multilateral schemes of cooperation.

Literature

[1] P. Hofmann,
J. Nucl. Materials, 270, 1999, 194-211

[2] L. Sepold, P. Hofmann, W. Leiling, A. Miassoedov, D. Piel, L. Schmidt, M. Steinbrück,
Nucl. Eng. Des., 204, 2001, 205-20

[3] W. Hering, Ch. Homann, J.-L. Lamy, A. Miassoedov, G. Schanz, L. Sepold, M. Steinbrück,
FZKA 6722, July 2002

[4] D. Struwe, H. Jacobs, U. Imke, R. Krieg, W. Hering, M. Böttcher, M. Lummer, T. Malmberg, G. Messemer, Ph. Schmuck, B. Göller, G. Vorberg,
FZKA 6316, July 1999

[5] W. Cherdron, U. Imke, H. Jacobs, A. Kaiser, W. Schütz,
NURETH-10 : The 10th Internat. Topical Meeting on Nuclear Reactor Thermal Hydraulics, Seoul, Korea, October 5-11, 2003, Paper G00103

[6] R. Krieg, B. Dolensky, B. Göller, G. Hailfinger, O. Jonatzke, T. Malmberg, G. Messemer, E. Stratmanns, G. Vorberg, H. Benz, W. Ratajczak,
Nucl. Eng. Des., 202, 2000, 179-96

Studies of Design Basis Accidents and Severe Accidents in Light Water Reactors

D. G. Cacuci, D. Struwe, W. Hering, Ch. Homann, M. Ionescu-Bujor, X. Jin, V. Sanchez-Espinoza, W. Sengpiel, IRS

Introduction

Reactor safety research is carried on to improve the evaluation of risks associated with the operation of light water reactors, and to diminish these risks where necessary. For this purpose, both deterministic approaches to analyze potential accident scenarios and probabilistic methods of risk and reliability analysis are used. At the present time, increasing use is made of an approach attempting to couple probabilistic analyses with a deterministic approach and, in this way, generate more precise information.

In accordance with the advanced state of the art, the consequences of severe accidents are now included in the evaluation of design basis measures. In Germany, this extension of the evaluation base was required for future facilities under the omnibus law of 1994 (amendment to the Atomic Energy Act).

Initially, accident sequences are determined mainly by what goes on in the reactor pressure vessel, the “in-vessel” phenomena. They establish the primary source term for fission products and hydrogen in the containment as well as the starting conditions, such as the temperature and composition of the melt, affecting the further course of an accident outside the pressure vessel, the “ex-vessel” phase. However, this has been dealt with in earlier contributions to this journal.

Detailed thermohydraulic mechanistic codes, such as ATHLET-CD, ICARE/CATHARE, SCDAP/RELAP5, SCDAPSIM, are used to develop in-plant accident management measures (AMM) for the primary system of a nuclear power reactor. The same codes are used to study measures seeking to improve the economic performance of existing plants with respect to their impact on plant safety.

The general purpose of all analytical codes, which is to provide reliable analyses of plant transients and accidents, can be achieved by proper modeling of important phenomena and processes and their interactions in the reactor core and the primary system. Suitable experiments are analyzed to validate and update these codes; the extrapolability to reactor conditions is verified on the basis of international comparative studies, so-called benchmarks. This contribution presents the current status of this development and validation for the design basis area as well as the beyond-design-basis regime.

Validation of Accident Codes

In recent years, a number of advanced code systems describing thermohydraulics were coupled with three-dimensional neutron kinetics models. Such coupled code systems are being used increasingly in research, industry, and by regulatory authorities to study complex accidents (such as reactivity transients, deboration transients or subcooling transients) with pronounced spatial differences in power distribution inside the core. In this way, safety-related local parameters can be determined in the light of various factors, such as enrichment, burnup, etc., and the safety margins of core configurations can be assessed with greater precision.

In addition to real data from power reactors, also numerical benchmarks are used for further development and validation of these coupled code systems. These include the international benchmarks of OECD/NEA and of the Code Assessment and Maintenance Program (CAMP) of USNRC.

The NUKLEAR Program of the Karlsruhe Research Center, in a cooperative venture with Framatom/ANP, Erlangen, successfully participated in the international benchmarking exercise on the main steam line break with their RELAP5/PANBOX code system [1]. The progress achieved is apparent from a comparison of the reactor power (Fig. 1) calculated by point kinetics and 3D kinetics. The important feature is the lower power rise after a reactor scram as determined by 3D kinetics as compared to the level determined by point kinetics (up to 600 MW).

In addition, more detailed information is obtained about the change in time of axial and radial power distributions. The power distortion visible in Fig. 2 is due to asymmetrical core cooling and assumed blockage of an absorber rod bundle (“stuck rod”). These pronounced spatial modifications highlight the problems inherent in the point kinetics approach which is based on the as-

sumption of a constant axial power profile function.

The RELAP5/PARCS code system is currently being qualified within the framework of the international VVER-1000 coolant transient (V1000-CT) benchmarking exercise. Experimental data measured in the Kozloduy nuclear power station are available for this purpose.

Adjoint Sensitivity Analysis Procedure

The Adjoint Sensitivity Analysis Procedure (ASAP) [2] is a method of determining the sensitivities of the results of thermohydraulic models as a function of all systems parameters, α, to a systems result, R.

(Definition: $\frac{\partial R}{\partial \alpha} \cdot \frac{\alpha}{R}$)

The relative sensitivities allow the importance of the respective parameter to the overall systems result to be determined.

The implementation of this method in RELAP5/MOD3.2 has been completed successfully and tested on the basis of the QUENCH-04 experiment [3]. Figure 3 shows the example of time-dependent behavior of the eight highest relative sensitivities of the temperature of the outside wall of the heated rod at a level of 1.3 m.

The parameters shown have this physical significance: nominal power factor (α1), nominal power up to 121 s (α2), nominal power up to 2088.6 s (α3), nominal pow-

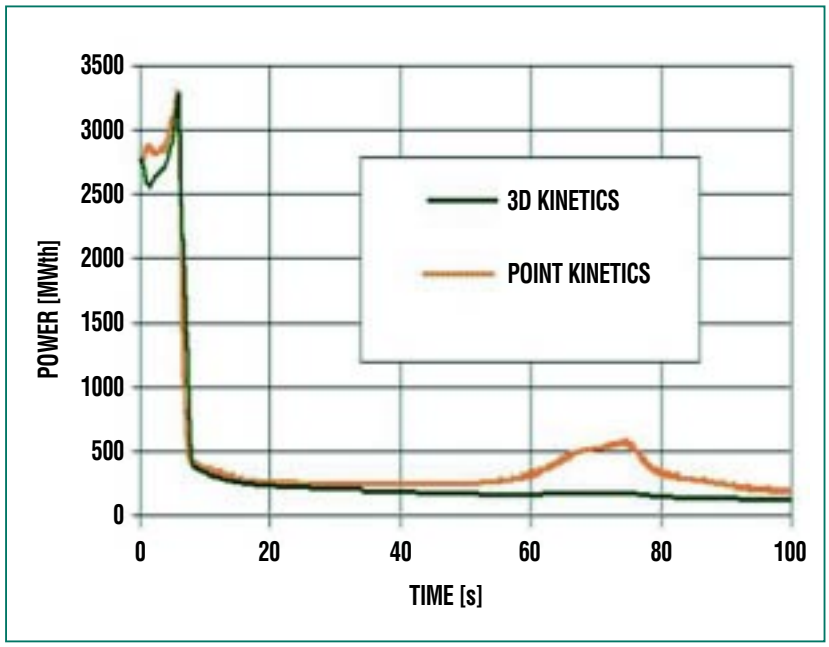

Fig. 1: Comparison of the reactor power computed by point kinetics and 3D kinetics for the TMI-1 reactor for the steam line break scenario.

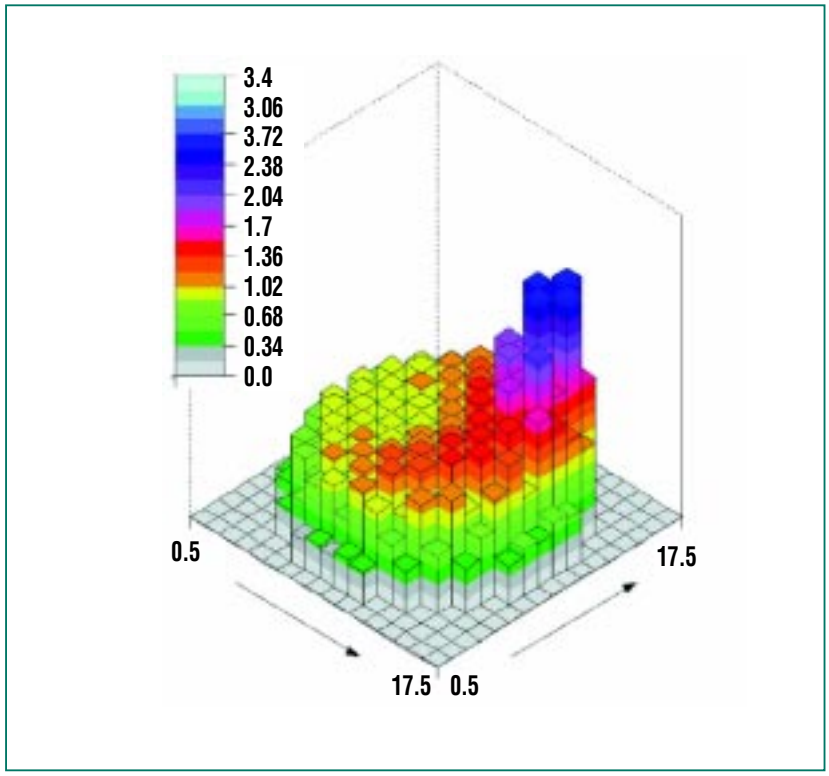

Fig. 2.: Radial distribution of the power profile as computed by the 3D kinetic model.

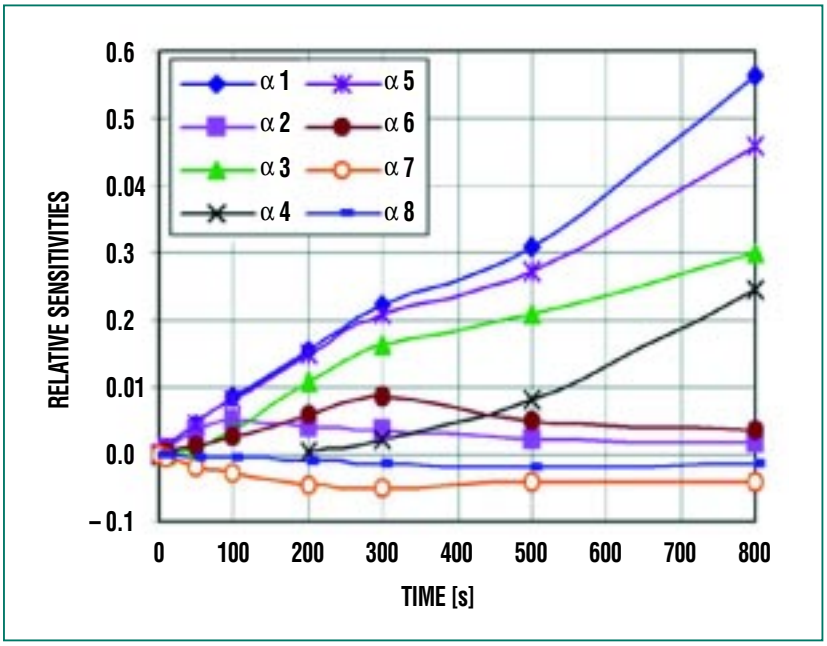

Fig. 3: Time-dependent relative sensitivities of the temperature of the outside wall of the heated rod at 1.3 m.

er up to 2103 s (α4), nominal multifactor of the internal source (α5), nominal surface temperature at 1.3 m (α6), nominal volumetric heat capacity of the ZrO_2 pellet (α7), and nominal volumetric heat capacity of zircaloy (α8).

The sensitivities of the α1, α4, α3, and α5 parameters are positive, i.e. their values increase with time. The sensitivities of parameters α7 and α8 are negative, i.e. their values decrease with time. Above all, the relative sensitivity of the temperature of the outside wall after 800 s reaches approx. 56 % with respect to the nominal power factor, i.e., a 10 % change in the nominal power factor results in a 5.6 % change in the temperature of the outside wall. The other relative sensitivities are comparatively low.

Flooding a Superheated Reactor Core

Improving predictions of the response of a superheated reactor core to a flooding event is a problem under study worldwide. One contribution to this topic by the Nuclear Safety Research Program (NUKLEAR) of the Karlsruhe Research Center was the QUENCH-06 experiment [3], which OECD/NEA selected as the International Standard Problem (ISP) No. 45, and which was run under the responsibility of the Research Center. It includes studies of core behavior in nuclear power plants during heating and delayed flooding in an assumed loss-of-coolant accident.

In order to be able to assess the status of core meltdown codes for simulating core heating and quenching with water at temperatures above 2000 K, the so-called blind phase of the ISP was given only the initial conditions and boundary conditions necessary for recalculating the experiment; no other experimental details were provided. 21 organizations from 15 countries participated in this phase with eight different code systems (ATHLET-CD, ICARE/CATHARE, IMPACT/SAMPSON, GENFLO, MAAP, MELCOR, SCDAPSIM, SCDAP-3D), and IRS was involved with a version of its own, SCDAP/RELAP5 mod3.2.irs (S/R5).

Up to and including the second heating phase (t = 7 …s, Fig. 4), most of the results did not differ greatly other than as a consequence of obvious user errors; this allowed a “main field” of results to be defined. For the quenching phase (t > 7…s), modeling of thermohydraulics was found to be insufficient: some participants were not able to model the cooling rates observed experimentally, while others had to use a very fine grid to balance out inadequacies in nodalization of the computer code.

In the experiment, a sufficiently thick oxide layer prevented failure of the cladding tube below ~ 2200 K and thus the release of molten metal. In most computer codes, this behavior was described by the standard oxidation models, unless spalling of the oxide layer is assumed arbitrarily. In the main field, variation of the H_2 masses released as calculated increased from approx. ± 15% before flooding to approx. ± 40 % after flooding (Fig. 5).

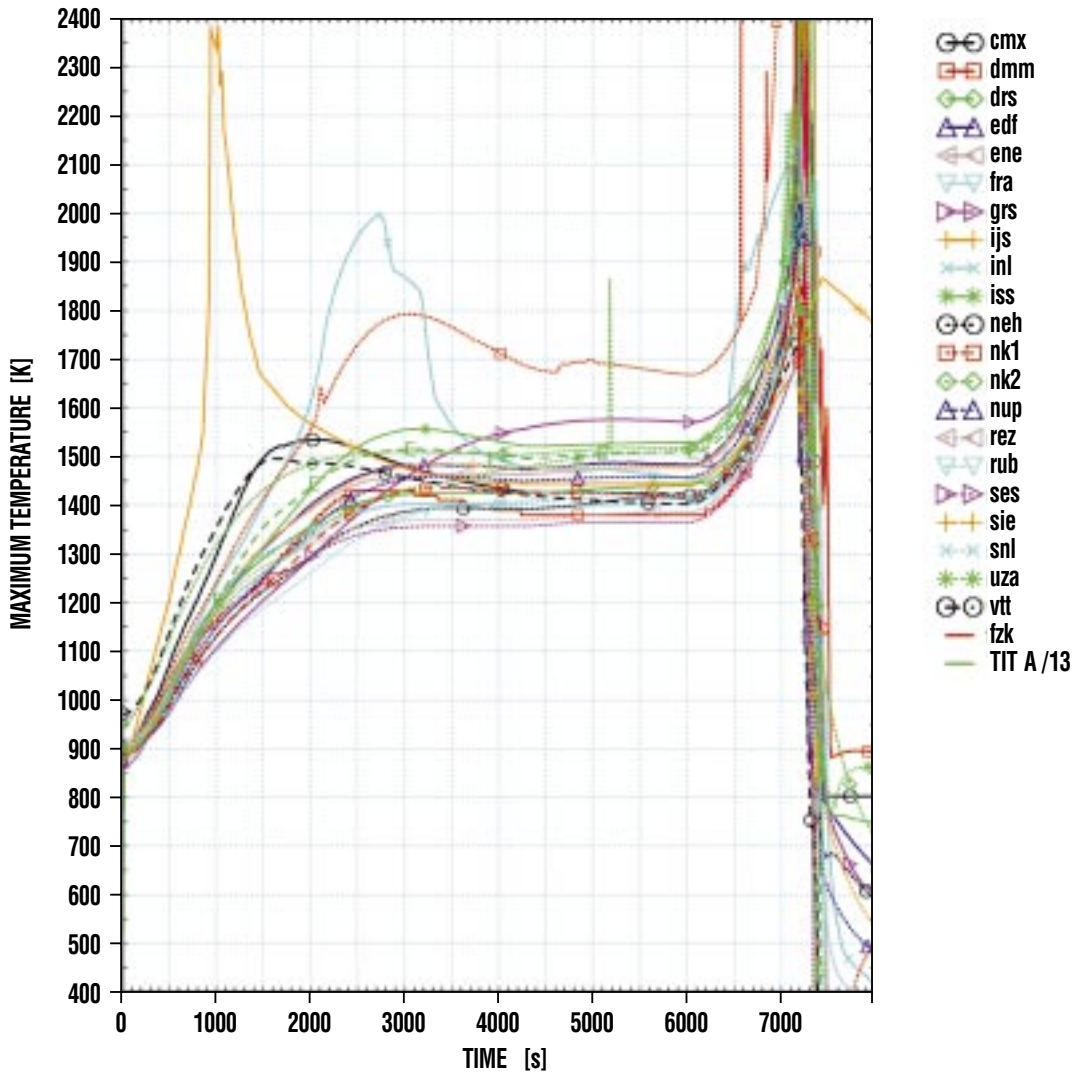

Fig. 4: Maximum temperatures at the cladding tube as calculated in the blind phase of ISP-45 and measured in the experiment.

The outliers among the calculated temperatures and hydrogen masses released are based on the assumption of the protective oxide layer spalling. In the main field of results, most participants correctly calculated that there would be no destruction of the bundle. Detailed examination also showed that the codes still have problems in correctly calculating the initial conditions in the bundle at the onset of flooding.

Another surprising result is this: The energy balance needs to be checked carefully before interpreting any findings. Lack of experience among the code users, and difficulties in adequately modeling the QUENCH facility, were the main causes of major deviations.

The results of the open phase show that the codes are able to analyze the experiment satisfactorily by parameter fitting. Some participants corrected errors or improved modeling of the code. Variance in the findings, e.g. in

the total H_2 mass calculated, was clearly reduced (Fig. 5).

The validation of ASTEC V1 on the basis of QUENCH-06, which was begun last year, indicated deficits which are to be repaired in SARNET within the 6th EU Framework Program.

The database about core behavior in delayed flooding was clearly expanded in the QUENCH program, but there is still need to examine conditions at low flooding rates and extensive damage conditions, such as a local bed of debris.

Final Phase of a Severe Core Meltdown Accident

The experimental Phebus-FP (fission product) Program is carried out by international partners at Cadarache, France, for prototype studies of fuel rod behavior up to the late phase of a core meltdown accident.

The Phebus-FP series of experiments serve to study the thermomechanical and physico-chemical phenomena in an LWR core meltdown accident, especially the release of fission products, and make these findings available for code validation.

The series comprises six experiments, four of which have already been conducted: three experiments with fuel elements containing 20 fuel rods each and one central absorber rod; one experiment with a predefined bed of fuel and oxidized cladding tube fragments [6].

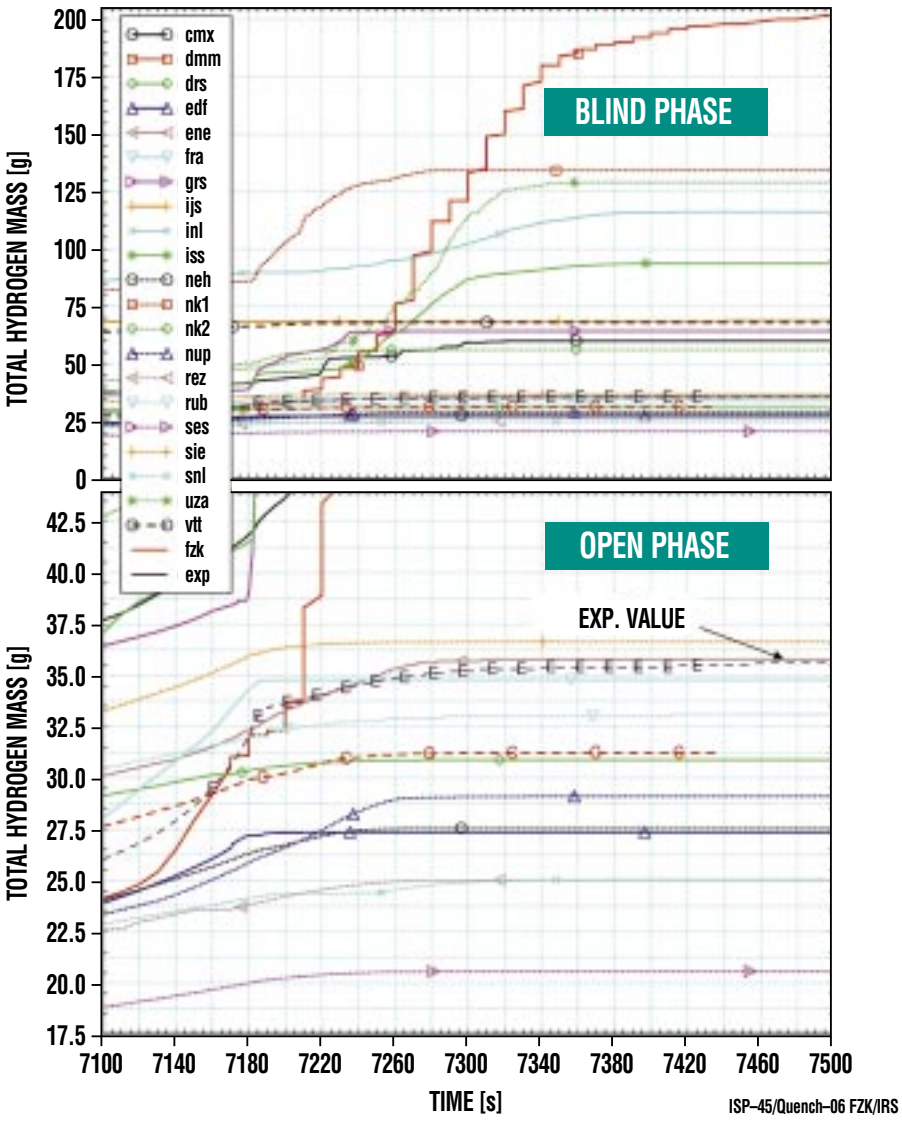

Fig. 5: Hydrogen masses calculated in the blind and open phases of ISP-45.

In the FPT1 Phebus experiment, the fuel element (approx. 1 m long) consisted of 18 irradiated fuel rods (burnup ~ 23 GWd/tU) and two fresh fuel rods as well as one central control rod with silver-indium-cadmium as the absorber material, a stainless steel cladding tube, and a zircaloy guide tube. Heating of the fuel rod bundle was controlled by the rising nuclear power and the steam mass flow (0.5 – 2 g/s); an excess supply of oxygen was provided for zircaloy oxidation.

The experiment has been analyzed and interpreted in detail as ISP-46 of OECD. IRS participated in this effort by recalculating

the first phase of the experiment, i.e. fuel rod failure and fuel rod meltdown, melt relocation and molten pool formation, hydrogen generation due to zirconium oxidation [7]. The ICARE2 and SCDAP/RELAP5 mod 3.2.irs (S/R5) computer codes were used for this purpose.

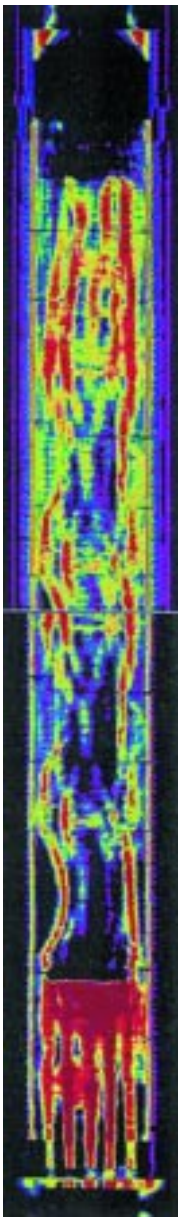

Fig. 6: Radiograph of the FPT1 test section [6].

Figure 6 shows a radiograph of the final state of the bundle with a central region largely free from fuel and a molten pool at the bottom end. Figure 7 shows that the calculated fuel rod temperatures are in good agreement, both qualitatively and quantitatively, with the systemically induced lower levels of the ultrasonic thermocouples; in the best-estimate case at the axial position of 0.3 m, ICARE2 calculates fuel superheating to approx. 3000 K, which is due to a local blockage caused by dislocated fuel. One parameter very important in assessing the consequences of an accident is the cumulated volume of hydrogen released as a result of zirconium oxidation. The calculated hydrogen mass (Fig. 8) is within the uncertainty band of the measured results of approx. 20 %.

These and other analyses of the Phebus-FP experiments demonstrate that both ICARE2 and SCDAP/RELAP5 are able to describe with good accuracy the key phenomena of an LWR core meltdown accident up to fuel dislocation and molten pool formation. However, the experiments indicate that massive core degradation can occur even some 250 K below the melting temperature of $(Zr,U)O_2$, with burnup and, thus, the fuel structure exerting a major influence. In both computer codes, these influences of burnup on the onset and development of fuel dislocation are taken into account only in a greatly simplified way, which

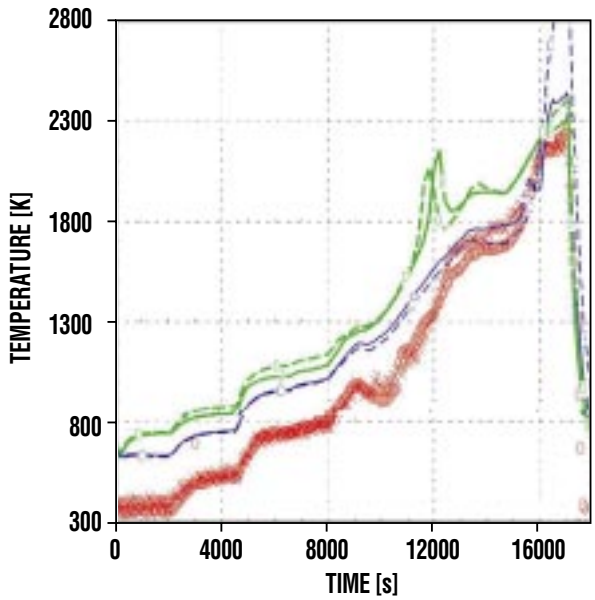

Fig. 7: Fuel rod temperatures at 0.3 m. Red: data measured by ultrasonic thermometers; blue/green curves: ICARE2 and S/R5 results, respectively.

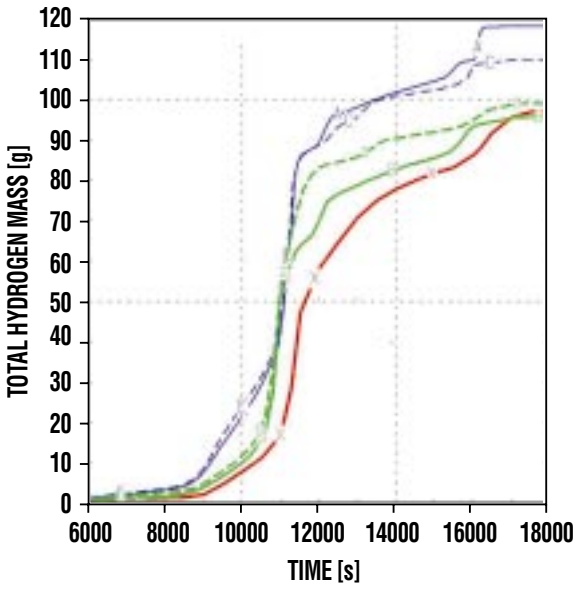

Fig. 8: Comparison of hydrogen volumes. Red: measured data; blue/green: ICARE2 and S/R5 results, respectively, for the reference and best-estimate cases.

means that quantitative statements about the origin and propagation of the resultant molten pool in the late accident phase are still subject to major uncertainties.

Outlook

Future work will concentrate on qualifying the TRACE/PARCS code system, the successor to the RELAP5/PARCS system, for application to light water reactors and ADS systems.

The new versions of the integral French-German ASTEC accident code will continue to be validated on the basis of the QUENCH experiments.

Preparation of the two QUENCH experiments in the LACOMERA EU program will be backed by advance calculations and analyses. As for QUENCH, analytical support will be continued for the integral experiments, such as Phebus STLOC (to study the influence of burnup).

Experimental findings about core reflooding as an accident measure will be systematized with respect to the parameters influencing them, such as core degradation state, flooding rate, systems pressure, feeding location, burnup, etc., and prepared for probabilistic applications.

Literature

[1] V. Sanchez, W. Hering, A. Knoll, R. Böer, *FZKA-6518, July 2002*

[2] D. G. Cacuci, M. Ionescu-Bujor, X. Jin, *IAEA Technical Meeting on Progress in Development and Use of Coupled Codes for Accident Analysis, Vienna, Austria, November 26-28, 2003*

[3] *QUENCH code, see contribution to this publication*

[4] L. Sepold et al., *Nucl. Eng. Des., 204, 2001, 205-20*

[5] W. Hering et al., *FZKA-6722, July 2002*

[6] *PHEBUS P.F. – FPT1 Final Report, IPSN/DRS Cadarache, France, December 2002*

[7] W. Hering, W. Sengpiel, *ISP-46 Progress Meeting, Aix-en-Provence, October 21-23, 2002*

Studies of the Control of Radiolysis Gas Detonations in German Boiling Water Reactors (BWR)

W. Breitung, A. Kotchourko, M. Kuznetsov, R. Redlinger, IKET;
A. Friedrich, J. Grune, G. Stern, A. Veser, K. Sempert, ProScience GmbH

Introduction

IKET is conducting extensive studies of hydrogen behavior in pressurized water and boiling water reactors within the framework of nuclear safety research. Last year, a number of third-party-funded projects were carried out (Table 1).

This article focuses on work seeking to improve the control of radiolysis gas in German boiling water reactors (BWR) currently in operation. The general objective of these studies is to create a database for fundamental understanding of the gas dynamics and structural dynamics impacts of radiolysis gas chemical reactions so that effective countermeasures may be derived for BWR plants currently in operation.

In boiling water reactors, normal operation gives rise to considerable volumes of radiolysis gas ($2H_2$ + O_2) due to radiation-induced splitting of water. In a 900 MWe plant, for instance, some 180 std. m^3/h are produced. Although gas concentrations in the main steam line are very low (22 vol. ppm H_2 + 11 vol. ppm O_2), steam may condense in pipes connected to the primary system in which there is no permanent flow, and the remaining non-condensable radiolysis gas may be enriched to high partial pressures (up to 70 bar) over weeks and months. Despite careful monitoring of potentially endangered plant components, radiolysis gas detonations with local pipe failure and considerable consequential costs occurred in the German Brunsbüttel nuclear power plant and the Japanese Hamoaka-1 plant in late 2001. The German BWR op-

Client	Plant/type	Activity
German BWR operators (VGB)	German BWRs	Experiments on the detonation stability of small pipes connected to the primary system
EnBW	Philippsburg-1 BWR, 920 MWe	3D simulation of radiolysis gas detonations in the annulus of blowdown pipes
HEW, Vattenfall Europe	Brunsbüttel BWR, 800 MWe	Modeling radiolysis gas detonations in safety valves and relief valves
HEW, Vattenfall Europe	Brunsbüttel BWR, 800 MWe	Origin and combustion of radiolysis gas (RG) in measurement pots
Krümmel GmbH	Krümmel BWR, 1310 MWe	3D distribution calculations for a new concept of RG reduction in blowdown pipes
KKW Leibstadt AG, Switzerland	Leibstadt, General Electric BWR, 990 MWe	3D modeling of RG compression and combustion in a blowdown pipe after opening of the safety + relief valve
Austrian Federal Office of the Environment, Vienna	Temelin Nuclear Power Plant, Czech Republic, VVER 1000	Hydrogen situation in a LOCA core meltdown accident and recommended countermeasures
Framatome (FANP), Erlangen	EPR PWR, 1600 MWe	Development of additional models for the GASFLOW (distribution) and COM3D (combustion) FZK codes used by FANP
KAERI South Korea	APR-1400 PWR, 1400 MWe	Analysis of a containment LOCA by GASFLOW. Implementation of the GASFLOW code by various Korean organizations

Table 1: Third-party-funded IKET projects in 2003 on hydrogen behavior in pressurized water and boiling water reactors (PWR and BWR).

erators thereupon commissioned IKET to conduct a variety of experimental and theoretical studies, two of which will be described below.

3D Analysis of Gas Dynamic Detonation Loads

The detonation of radiolysis gas in the head spray line of the Brunsbüttel nuclear power plant (KKB) was simulated by the COM3D 3D code [1] developed at IKET so as to compute local pressure developments, gas dynamic impulses, and temperature transients in the environment of the failing line. The head spray line is not used in normal operation. Only when refueling is prepared, the line is used to spray water from the inside on the reactor pressure vessel head to achieve a faster temperature drop. At KKB, leakage of an upstream valve had caused elevated steam condensation and an accumulation of radiolysis gas over prolonged periods of time. These complex processes are described in detail in [2].

Before restarting the plant, the operator had to demonstrate that secondary damage to safety-related components could be excluded. For this purpose, the near field of the damaged head spray line was modeled in great detail (5 million cubic computation cells of 4 cm length of the edges). Figure 1 shows a semi-transparent "glass model" of the containment region of interest. As the initial conditions of the gas detonation are not known exactly, various calculations were performed with different initial states of the gas in the head spray line. The most probable sequence of steps in radiolysis gas detonation is shown in Fig. 2 [3].

In this case, a fully fledged detonation in the entire gas volume of the head spray line was simulated. The pipe section destroyed in the accident was described by a dynamic wall model in which the pipe wall failed 10 cm behind the leading detonation front. Figure 2 shows computed schlieren images, i.e. the gradient of gas density, for three orthogonal sectional planes through the 3D geometry at different points in time. The two pictures at the top, each taken at a fixed point in time, repre-

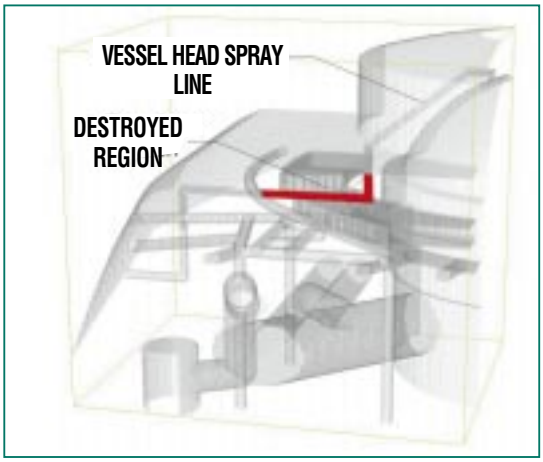

Fig. 1: "Glass model" of the upper part of the KKB containment close to the vessel head spray line damaged by a radiolysis gas detonation. Geometry model for COM3D simulation with 5 million cubic computation cells of 4 cm length of the edges each.

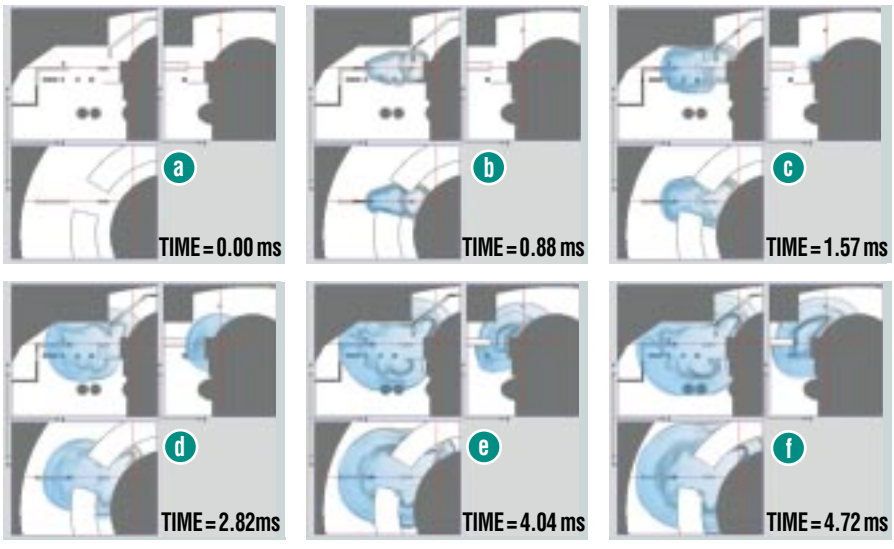

Fig. 2: "Schlieren" images computed with COM3D to represent the detonation pressure wave in the near field of the failing head spray line of the Brunsbüttel nuclear power plant. The gradient of gas density is shown. For each fixed point in time, three orthogonal sections through the 3D geometry are shown; top = vertical sections, bottom = horizontal section. The outermost dark blue zone characterizes the leading pressure shock propagating in the containment atmosphere. The following second dark blue zone corresponds to the edge of the expanding hot combustion gases (= steam).

sent vertical sections, while the third picture is a horizontal section. The large structure on the right in each picture represents the reactor pressure vessel. Above it, there is the upper containment border. In the pictures, the first dark blue zone represents the leading shock propagating in the ambient atmosphere. The second dark blue zone behind it (= high gradient of the gas density) characterizes the boundary of the hot expanding combustion gases. A total combustion energy of 14.5 MJ was released.

Figure 3 shows examples of calculated pressure loads in the environment of the failing head spray line. The following conclusions can be drawn from these data:

- The gas dynamic loads drop very rapidly with increasing distance from the site of the explosion because of the low ratio of the radius of the head spray line (0.05 m) to the characteristic distance of other internals (meters).
- Structural dynamic damage is restricted to thin internals (≤ 1 mm wall thickness) close to the point of failure (≤ 1 m).
- The temperature transients in the gas are limited to short times (< 1 s) and a few meters' distance from the failure point.
- The damage pattern observed is dominated not by the expanding detonation pressure wave, but by the projectile effects associated with pipe failure.

On the basis of these findings, it was possible to exclude undetected secondary damage to safety-related cables, measuring systems, and pipes due to pressure or temperature impacts. The calculations described above furnished important data for the renewal of the operating permit of KKB.

Detonation Experiments with Radiolysis Gas in DN-15 Pipes

In German boiling water reactors, many measurement pipes of the primary system are so-called DN-15 pipes made of austenitic steel with an inner diameter of 15 mm and a relatively large wall thickness of 2.9 mm. In extreme cases, such measurement pipes, which do not permanently carry liquids, could be filled with radiolysis gas at 70 bar. Some simple estimates show that DN-15 lines, because of their large wall thickness, could withstand even radiolysis gas detonations at 70 bar initial pressure. One special factor of uncertainty was the complicated structural mechanics behavior of pipe bends, of which there are large numbers in the plant. Under a contract from the German BWR operators, IKET therefore conducted detonation experiments with radiolysis gas in a U-shaped DN-15 test pipe from the Gundremmingen nuclear power plant [4].

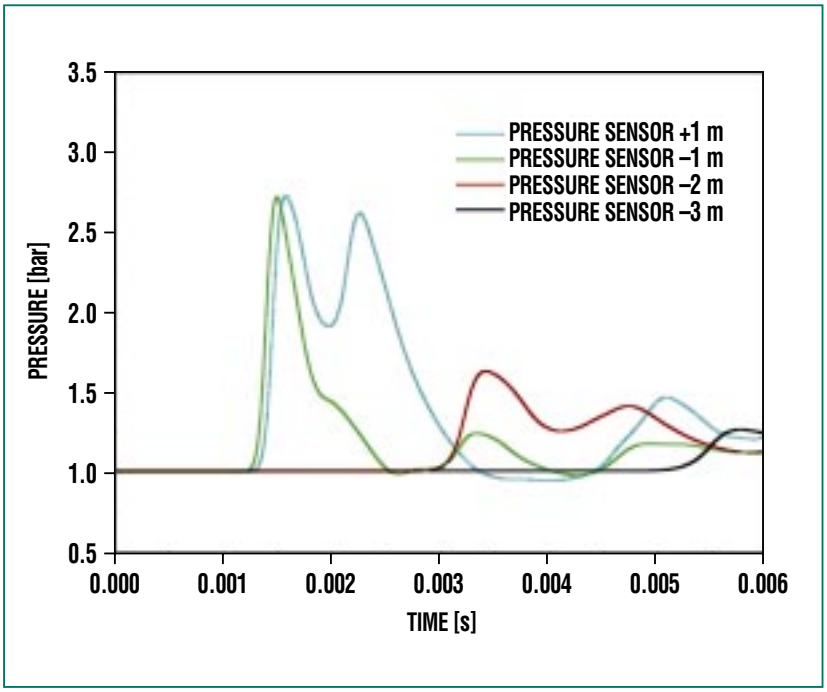

Fig. 3: Calculated local pressure loads in the environment of the failing head spray line. The overpressures decay quickly with increasing distance from the line. On the basis of these data and others, undetected secondary damage to safety-related installations was excluded. The calculation supported the reissue of an operating permit to the Brunsbüttel nuclear power plant.

Figure 4 shows a schematic set-up of the experimental facility. All components containing radiolysis gas in the course of the experiment were enclosed in a safety vessel (22 m^3 volume, 40 bar rated pressure). This vessel was equipped with sensors for hydrogen and oxygen, a safety venting system, and other protective devices. Valves were actuated pneumatically, not electrically, so as to minimize potential ignition sources. The H_2/O_2 ratio of the gas mix fill was set by two mass flow controllers. The most important experimental parameter was the initial pressure of the radiolysis gas in the U-shaped test pipe. The initial temperature corresponded to the ambient temperature of approx. 293 K. The pipe was equipped with five fast pressure sensors, two thermocouples, and 16 strain gauges. A total of 31 radiolysis gas experiments were run with initial pressures ranging from 0.5 to 70 bar. Despite careful conditioning of the test facility by various chemical cleaning techniques, previous burning at low radiolysis gas pressures, avoidance of particle entrainment, and deliberately slow filling procedures, there were occasional cases of spontaneous ignition during filling which damaged the experimental set-up.

Figure 5 shows an example of the pressures measured as plotted in a so-called x-t diagram in which the pressure signals are arranged along the vertical x-axis. The x-coordinate corresponds to the distance of the respective pressure sensor from the point of ig-

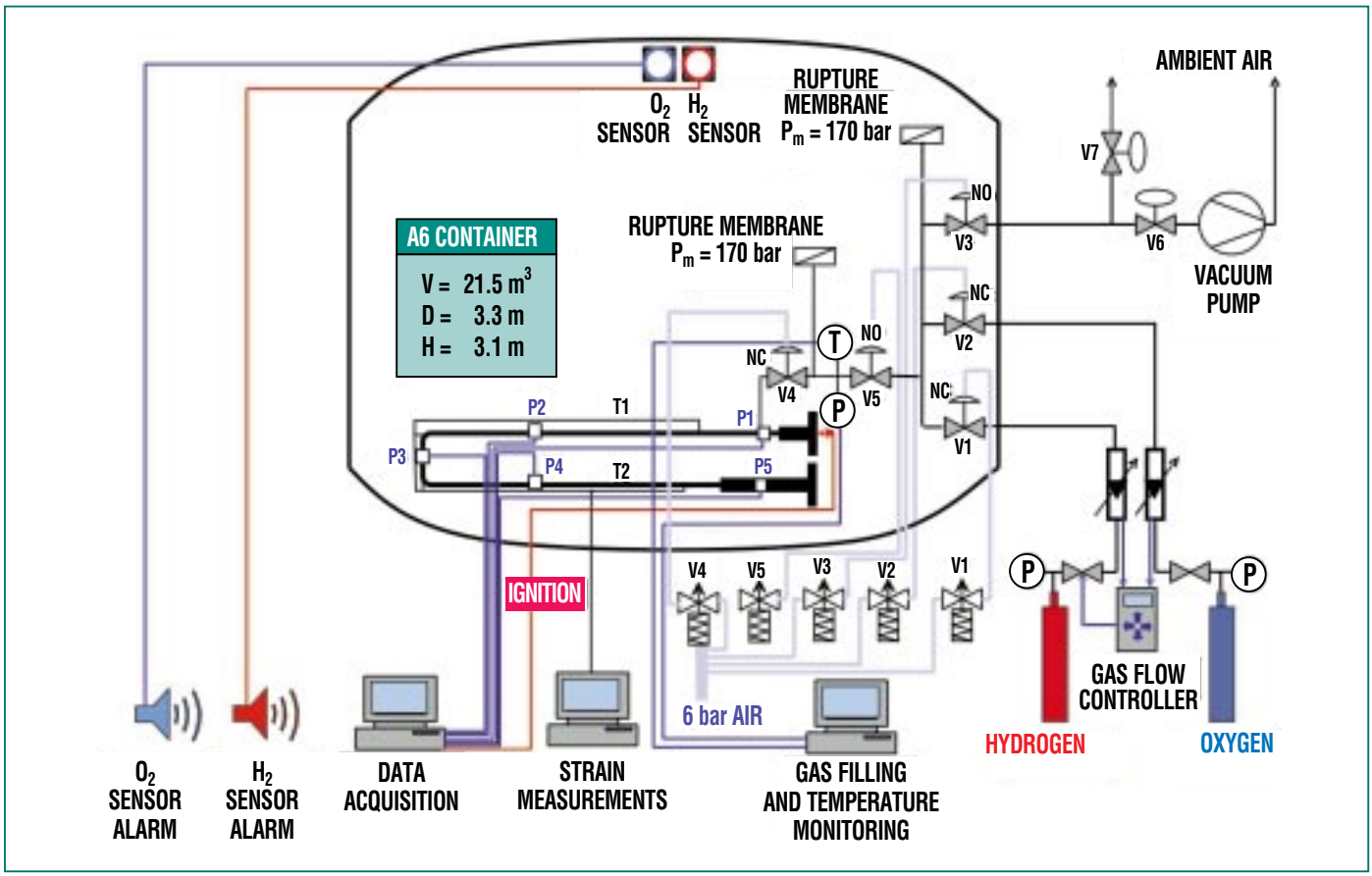

Fig. 4: Facility for detonation experiments with radiolysis gas in a U-shaped D-15 test pipe from the Gundremmingen nuclear power plant. All components containing radiolysis gas are enclosed in a vessel for protection and safety. The test pipe was instrumented with pressure sensors, strain gauges, and thermocouples. The initial pressure of the radiolysis gas was varied between 0.5 and 70 bar, while peak pressures in the pipe varied between 9 and 1540 bar.

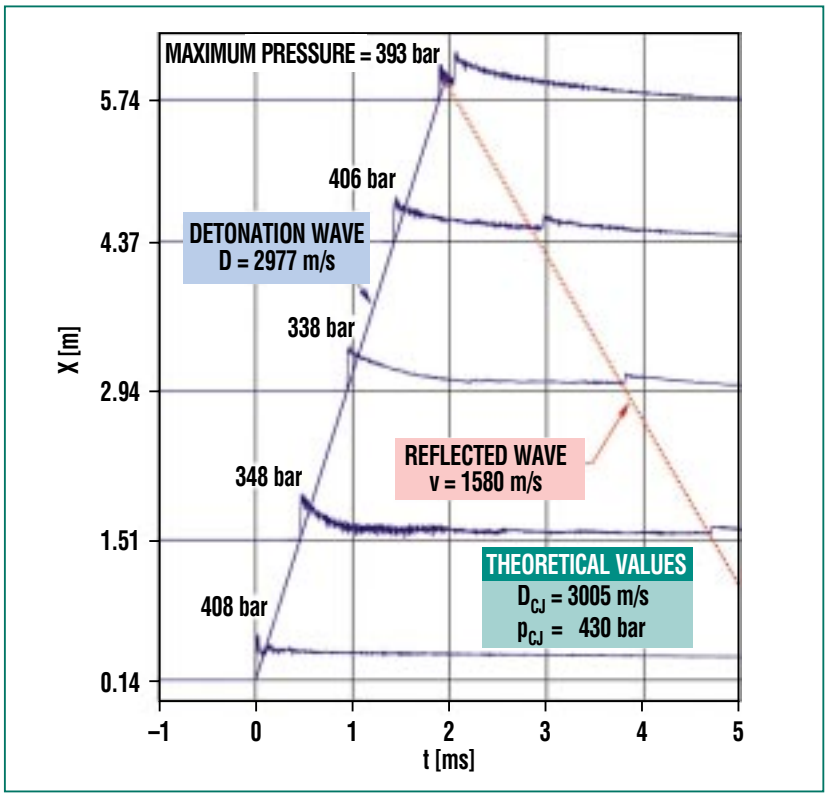

Fig 5: Measured pressure data for the experiment with radiolysis gas at 20 bar initial pressure. In this so-called x-t diagram, the velocity of the detonation wave can be taken from the slope of the connecting straight line (blue). From the pipe end, a reflected pressure wave runs back into the burnt gas (red).

nition (x=0). In this representation, the speed of the detonation wave results from the slope of the blue straight connecting line (D=dx/dt). Surprisingly, the two 90° bends of the U-shaped test pipe had no measurable influence on the detonation velocity. The detonation wave is reflected at the pipe end at x = 5.9 m, thus giving rise to a shock wave which now returns in the burnt gas (= steam) to the ignition point at x=0 (red line in Fig. 5).

Figure 6 summarizes all measured detonation velocities and peak detonation pressures. The measured data are in excellent agreement with zero-dimensional calculations for the so-called Chapman-Jouguet (CJ) model [5]. In this simplified model, the conservation of mass, energy, and momentum over the detonation front is considered, supplemented by the assumption of the burnt gases flowing out behind the front at the local velocity of

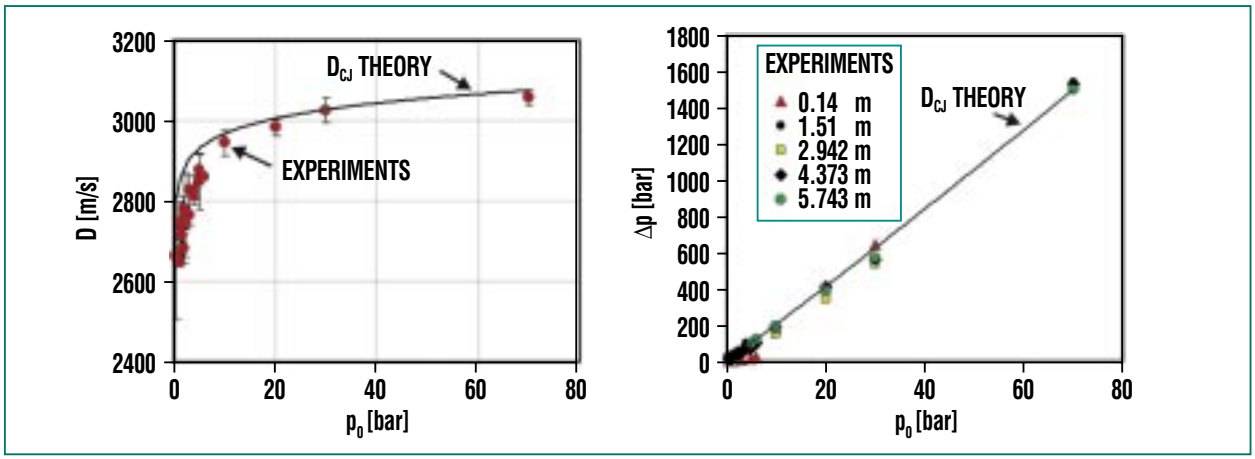

Fig. 6: Measured detonation velocities and peak pressures of all experiments. The measured data are in excellent agreement with the zero-dimensional Chapman-Jouguet (CJ) model. Even in the bounding case of radiolysis gas at 70 bar, there was no pipe failure. DN-15 pipes in BWR plants therefore may be considered detonation-proof under certain boundary conditions, which allows major cost savings to be made.

sound (so-called CJ condition). At 70 bar initial pressure, the CJ pressure is 1504 bar, the CJ velocity, 3064 m/s, and the CJ temperature, 4570 K.

The main result of the experiments is that the DN-15 experimental pipe withstood unreflected detonation loads at initial pressures of up to 70 bar. This proves experimentally that this type of pipe would not fail even in the extreme case of a stable detonation. Consequently, DN-15 lines may be released from the monitoring programs in German BWR facilities if they discharge into an open system (no reflection), and if ignition is assumed to occur at the pipe end, the most likely location. Moreover, it is no longer necessary, whenever there are signs of radiolysis gas accumulating in such lines, to stop power operation as a matter of precaution in order to initiate countermeasures. Both amendments to the operating instructions can give rise to major cost savings while not detracting from the uniformly high safety level of plant operation.

Literature

[1] A. Kotchourko, W. Breitung, *Nachrichten, 32, 3/2000, p. 22*

[2] W. Hartel, U. Kleen, *atw (2002), 7, July 2002*

[3] A. Kotchourko, W. Breitung, S. Dorofeev, A. Veser, H. Ohlmeyer, *Jahrestagung Kerntechnik, 2003, Berlin, May 22-23, 2003, p. 153*

[4] M. Kuznetsov, R.K. Singh, S. Dorofeev, G. Stern, W. Breitung, *Jahrestagung Kerntechnik 2004, Düsseldorf, May 25-27, 2004*

[5] B. Lewis, G. von Elbe, *Combustion, Flames and Explosions of Gases, Academic Press, Inc. ISBN 0-12-446751-2, 1987, p. 532*

Improvements in Off-site Emergency Management after Nuclear and Radiological Accidents

J. Ehrhardt, IKET

Introduction

The Chernobyl accident had a profound effect on emergency preparedness and post-accident management worldwide and, in particular, in Europe. Deficiencies in arrangements dealing with an accident of this magnitude, at both national and international levels (e.g., in world food trade), led to many problems of a practical and political nature. Many lessons have been learnt, and considerable resources have since been committed to improve emergency preparedness and post-accident management in order to avoid similar problems in future. Improvements have been made at national, regional and international levels and have been diverse in nature. However, more needs to be done to ensure a timely and effective response to any future accident.

Emergency management more generally has received increased attention following the tragic events in the U.S. in September 2001. Attacks with radiological dispersal devices (RDD), which spread radioactive material by aerosolizing or dissolution in water reservoirs, are currently under intense discussion.

A number of requirements emerge from these considerations; they include

- the need for a more coherent and harmonized response in Europe and during different stages of an accident (in particular, to limit the loss of public confidence in the measures taken by the authorities for their protection);
- exchanges of information and data in an emergency so as to enable neighboring countries to take more timely and effective action; and
- the need to make better use of limited technical resources and avoid duplication.

The RODOS project was established to respond to these needs. It was launched in 1989 and increased in size through the European Commission's 3rd, 4th and 5th Framework Programs. Significant additional funds have been provided by many national R&D programs, research institutions and industrial collaborators. In particular, the German Federal Ministry for the Environment, Nature Conservation and Nuclear Safety (BMU) contributed to the project financially with a special focus on early emergency response. Up to 40 institutes from some 20 countries in the EU, CEE, and FSU were actively involved in the project [1] (http://www.rodos.fzk.de).

The RODOS Project: Strategic Achievements

As a result of these collaborative actions, a comprehensive decision support system (RODOS) has been developed which can be applied generally within and across Europe [2, 3]. It can be used in national or regional nuclear emergency centers, providing coherent support at all stages of an accident (i.e., before, during and after a release), including the long-term management and restoration of contaminated areas. The system is able to support decisions about the introduction of a wide range of potentially useful countermeasures (e.g., sheltering and evacuation of people, distribution of iodine tablets, food restrictions, agricultural countermeasures, relocation, decontamination, restoration, etc.) mitigating the consequences of an accident with respect to health, the environment, and the economy. It can be applied to accidental releases into the atmosphere and into various aquatic environments. Appropriate interfaces exist with local and national radiological monitoring data, meteorological measurements and forecasts, and for adaptation to local, regional and national conditions in Europe.

The current version of the system (RODOS version PV 6.0) has been, or is being, installed in national emergency centers in several European countries for (preoperational) use (Germany, Finland, Spain, Portugal, Austria, the Netherlands, Poland, Hungary, Slovakia, Ukraine, Slovenia, and the Czech Republic). Installation is foreseen or under consideration in Switzerland, Greece, Romania, Bulgaria, and Russia within the next few years. Installation in the CEE and FSU has been achieved with support from the European Commission's ECHO, PHARE and TACIS programs, respectively.

Installation is most advanced in Germany [4] (see Fig. 1). A RO-

DOS Center has been established at BfS/ZdB, Neuherberg, and has been coupled to the nuclear reactor remote monitoring systems (KFÜ), the German Integrated Measurement and Information System (IMIS), and the German Weather Service (DWD). In the current configuration, ten main users actively access the RODOS Center as A- and B-users; seven of these are responsible for emergency management in their respective federal states, and three of them act at a national level. Five federal states are passive C-users.

Installation of the system for (pre-operational) use in many national emergency centers is indicative of the success of the system and its potential for achieving more coherent and effective responses to future accidents which may affect Europe.

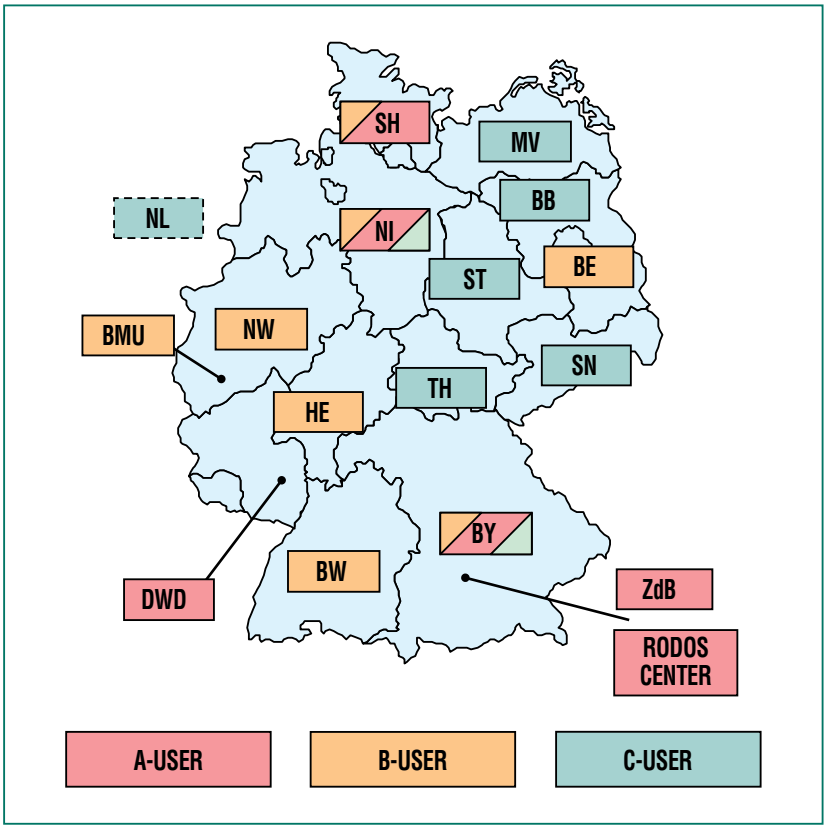

Fig. 1: RODOS users in Germany.

The RODOS System: Technical Performance

The RODOS Concept of Decision Support, Data Assimilation, and Uncertainty Handling

The RODOS system provides coherent decision support at all levels, ranging from largely descriptive reports, such as maps of the predicted, possible and, later, actual contamination patterns and dose distributions, to a detailed evaluation of the benefits and disadvantages of various countermeasure strategies and their ranking according to the societal preferences as perceived by the decisionmakers (see Fig. 2).

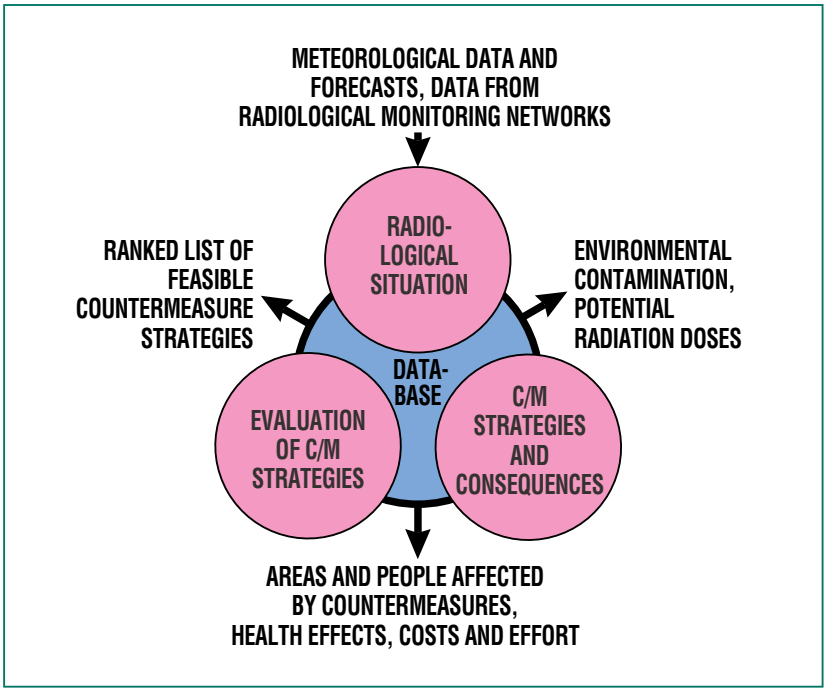

Fig. 2: Information processing in RODOS.

It is also able to perform 'what-if' calculations, allowing investigations of how a situation could develop in different scenarios. Its modern decision analysis techniques (MAV/UT – multi-attribute value and utility models) support emergency managers in evaluating the overall efficacy of possible countermeasure strategies. Data assimilation techniques combine model predictions and monitoring data for smooth transition from pure model predictions (in the pre-release phase) to a real situation (in the post-release phases). The Bayes decision analysis approach addresses all issues of uncertainty and data assimilation in a manner coherent with the decision analysis techniques used in evaluation. No decision support system on this scale has ever achieved this broad functionality in other contexts, much less so in an area as demanding as a nuclear emergency.

Interfaces with Plant Safety and Environmental Monitoring

The RODOS system provides appropriate interfaces to meteorological and radiological monitoring data and numerical weather prognoses from national weather services broadly used in Europe (see Fig 3). Customization guidelines help users adapt the system to regional and national conditions.

Prototype software tools have been developed within the STEPS/ASTRID and STERPS projects [1] which, in the event of an emergency situation in a light water reactor, allow monitoring of the progression of an accident from the moment it is detected to forecasting the future behavior of the reactor and estimating ongoing and potential releases as a function of time. The source term, thus evaluated faster than in real time, can be used to predict and/or assess the potential and/or real radiological consequences. A uniform interface exists which allows direct transfer of source term data to the RODOS system. On the basis of the results of its prognostic calculations, decisions about precautionary emergency action can be initiated in a timely manner.

User Interfaces

Three user interfaces are adapted to the needs of different users. The first one is based on X-Windows for UNIX and is intended for qualified operators and systems developers (User Category A). This interface offers full access to all systems functions, model parameters and

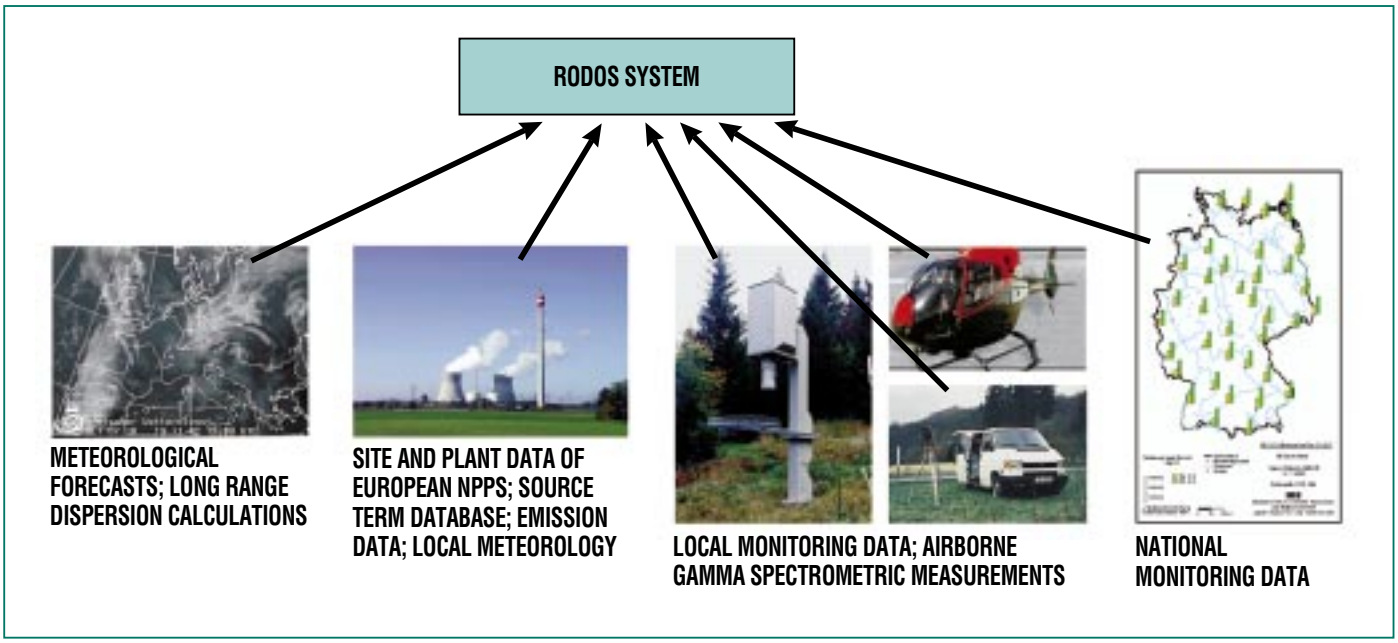

Fig. 3: Coupling RODOS to meteorological and radiological monitoring data.

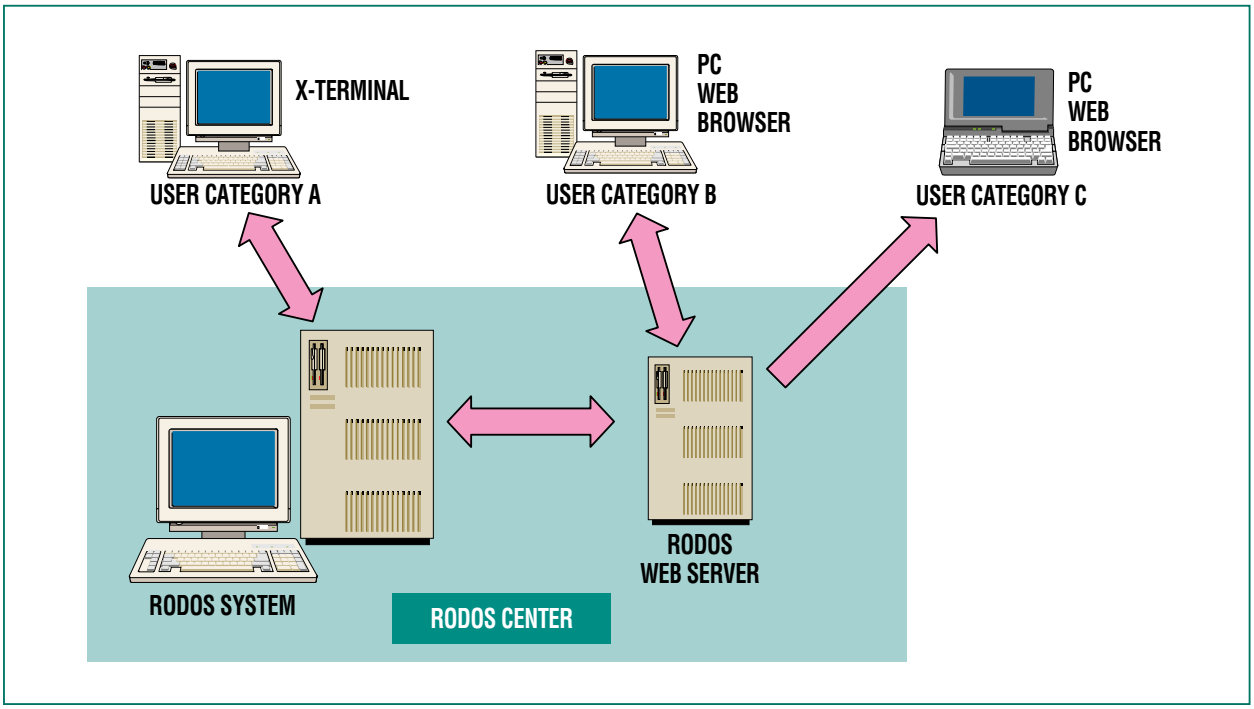

Fig. 4: User categories of the RODOS system.

stored data. The second interface (User Category B) is based on the design of Internet sites using well-established WWW technology. It is intended for users (User Category B) not needing permanent access to the system (e.g., only during an emergency or in drills), such as radiological advisers, decision-makers, etc. The third user interface for User Category C is identical with Category B, but is limited to receiving results of RODOS calculations only (see Fig. 4).

With increasing power of personal computers and the extended functions of their operating systems it is now possible to migrate the RODOS system to one of the most advanced operating systems running on personal computers, the LINUX operating system. The possibility to use powerful PCs and LINUX servers will greatly reduce installation and maintenance costs. In that way, dependence on one hardware provider (Hewlett Packard) will cease to exist, and platform-independent installations of RODOS will become possible. The first LINUX-based RODOS version will be available in summer 2005.

Data Exchange Between Neighboring Countries

As past experience clearly demonstrates, the consequences of nuclear emergencies do not stop at national borders. It is essential in good emergency management that dose assessments and decisions be co-ordinated and harmonized among the countries affected. Countermeasures, recommendations, and information of the public and the media must be consistent. Discrepancies in assessments by different emergency centers and decisionmakers in different countries must be avoided or, at least, must be well understood. Consequently, there is great need for thorough, rapid, reliable exchanges of all kinds of information.

Given the fact that computer-based decision support systems for nuclear emergencies have become a reality in Europe, the most effective way of achieving this goal is by ensuring timely and direct data and information exchanges among those systems. Accomplishing this objective will guarantee that, regardless of the operating system and hardware platform, decision support systems will be able not on-

ly to run and serve their purpose, but also to communicate with each other and share all necessary information and data associated with an accidental release of radioactivity, thus ensuring prompt and adequate emergency management.

With the MODEM Project [1, 5], a Web server technology based data exchange tool using the XML format has been developed which allows for direct communication among decision support systems, such as RODOS (push-pull concept). The tools have already been tested successfully in a number of European-wide emergency drills. Their application in international data exchange between the U.S. and Japan is currently under investigation.

The EURANOS Project

Despite the considerable resources devoted to improving the management of consequences of nuclear emergencies and, in particular, the progress achieved in the RODOS project, the situation in Europe continues to be characterized by national solutions in the technical as well as the administrative/political areas. The EURANOS Project, which integrates 17 national emergency management organizations with 33 research institutions, combines best practice, knowledge and technology to further preparedness for Europe's response to any nuclear or radiological emergency (see Fig. 5). The five-year multinational project, which started in April 2004, combines all EC-funded activities in nuclear and radiological emergency management and rehabilitation strategies in one integrated project (http://www.euranos.fzk.de).

Nature and Scope of the Project

European countries are prepared to respond to radiation emergencies to various degrees. Emergencies of this kind can occur within a country or outside its borders, as a result of an accident or of a deliberate terrorist attack, at a site for which emergency plans exist, or at an unexpected location. Whatever the cause, an emergency in one country in Europe to some extent will affect all others. By sharing expertise, data and technology among member states, Europe is

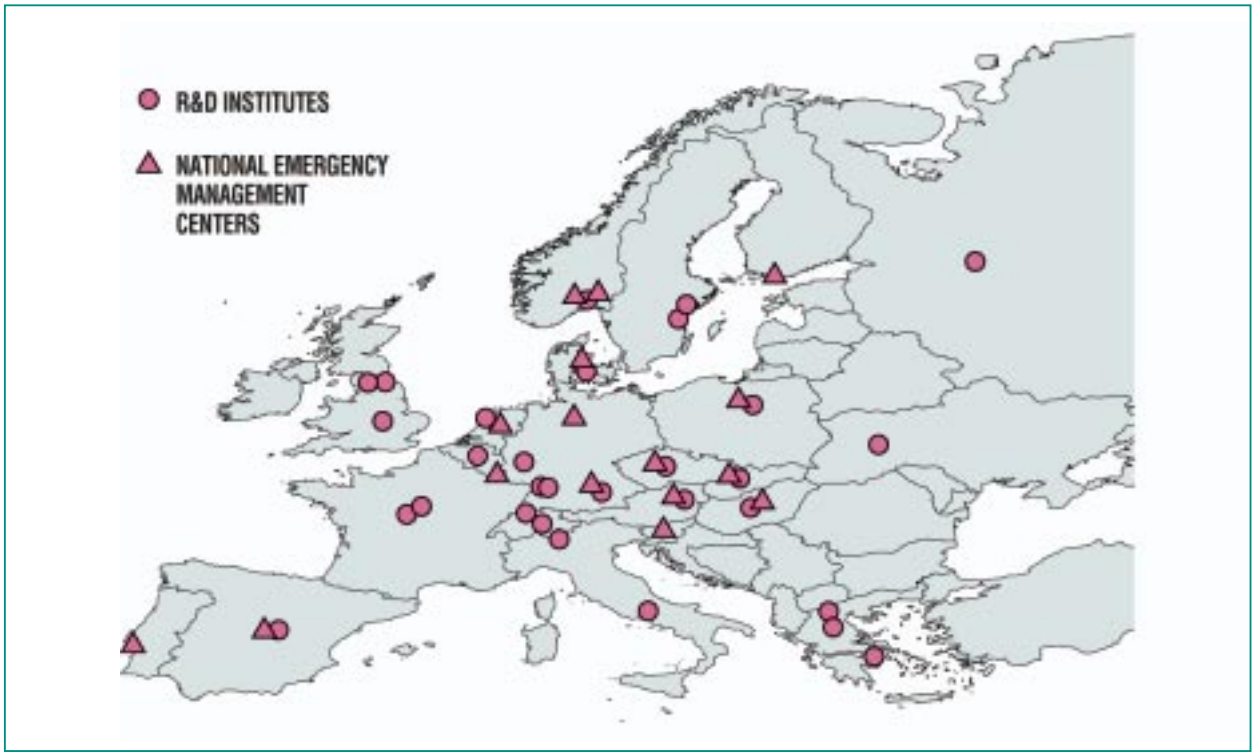

Fig. 5: European extension of the EURANOS project.

getting ready to respond to a radiation emergency appropriately and effectively.

Here are the main objectives of the project:

- Collate information about the likely effectiveness and the consequences of a wide range of countermeasures.
- Provide guidance to emergency management organizations and decisionmakers in establishing an appropriate response strategy.
- Further enhance advanced decision support systems, in particular RODOS, through feedback from their use in the field.
- Create regional initiatives to achieve information exchanges based on state-of-the-art information technologies.
- Develop guidance to assist member states in developing a framework for the sustainable restoration of living conditions in contaminated areas.
- Maintain and enhance knowledge and competence through emergency drills, training and education, thus fostering best practice in emergency response.

Activities and Impact

The project is divided into three R&D 'Categories' and a set of 'Demonstration' activities. The project is subdivided into a first and a second phase lasting two and three years, respectively.

The R&D 'Categories' address specific issues previously identified by users or by earlier research in the area. They are focused on

- emergency actions and countermeasures,
- enhancement of decision support systems for field use,
- rehabilitation strategies and guidance.

Demonstrations practice the methods and tools developed in their real field environments. In Phase 1, they will focus on methods and IT tools developed within previous EC Framework Programs. In parallel, the R&D activities requested by end users will be performed. The results of these R&D activities will be demonstrated in Phase 2. Throughout the work program, training activities are planned to ensure broad dissemination of the project results.

At the end of Phase 1, the project will be reviewed on the basis of feedback from demonstrations and training activities, R&D results, and recommendations from users. As a result of that evaluation, the strategic orientation and the key elements of the work program for the remaining three years will be defined.

Integration in one common project of R&D institutions with agencies responsible for radiation emergency management and rehabilitation allows project resources to be focused on the practical needs of decisionmakers. This collaborative iteration process ultimately will lead to a shared and integrated technical, methodological, and strategic approach in national and cross-border emergency management and rehabilitation in Europe. A well-conceived approach like this can progressively lead to the development of a European policy of emergency management and rehabilitation strategies.

Acknowledgment

The work described in this publication has been carried out with the support, *inter alia,* of the European Commission under the EURATOM Research and Training Program on Nuclear Energy (2002-2006), EURANOS Project, contract No. FI6R-CT-2004-508843. The views expressed in this paper are those of the author and do not necessarily reflect those of the EURANOS Project.

The Accident Consequence Group of the Institute for Nuclear and Energy Technologies at the Karlsruhe Research Center bears the main responsibility for developing and installing the RODOS system, has acted as principal co-ordinator of the RODOS activities for the past fifteen years, and is now co-ordinator of the EURANOS project. All current Group members have contributed to the work described in this publication: G. Benz, F. Fischer, E. Munz, C. Haller, I. Hasemann, C. Landman, A. Müller, J. Päsler-Sauer, M. Rafat, W. Raskob, T. Schichtel, A. Weis.

References

[1] E.-H. Schulte, G.N. Kelly, C.A. Jackson, *Decision Support for Emergency Management and Environmental Restoration, European Commission, Luxemburg, Report EUR 19793, 2002*

[2] J. Ehrhardt, A. Weis (eds.), *RODOS: Decision Support System for Off-site Nuclear Emergency Management in Europe, European Commission, Brussels, Report EUR 19144, 2000*

[3] J. Ehrhardt (ed.), *Migration of RODOS to Practical Applicability, Forschungszentrum Karlsruhe, Report FZKA-7015, 2004*

[4] J. Ehrhardt, M. Rafat, W. Raskob, *Errichtung und Betrieb des RODOS Systems an zentraler Stelle (RODOS Zentrale), Forschungszentrum Karlsruhe, Report FZKA-6765, 2002*

[5] T.J. Sullivan, M. Chino, J. Ehrhardt, V. Shershakov, *International Exchange of Emergency Phase Information and Assessments: an Aid to National/International Decisionmakers. Rad., Prot. Dos. vol. 109, No. 1-2, p. 133, 2004*

INE's Melter Technology for Vitrification of High-level Liquid Waste

W. Grünewald, G. Roth, W. Tobie, S. Weisenburger, INE

Introduction

High-level radioactive fission product solutions arising in reprocessing of nuclear fuels must be stored safely over long periods of time in order to protect the biosphere from the extremely persistent effects of radiation. The concepts pursued worldwide in the management of such waste include immobilization in a glass matrix and subsequent final storage in a geologic formation shown to work for this purpose. Borosilicate glass meets the requirements of repository storage in terms of chemical and radiological stability. The process of immobilization in glass is called vitrification.

Vitrification of high-level radioactive liquid waste on an industrial scale has been conducted since the late seventies. The most widely used vitrification technology is based on ceramic-lined melters employing direct electric heating of the glass melt. Glass melting systems for high-level radioactive waste must meet the very special requirements of nuclear technology. To protect the operating personnel from the intense ionizing radiation, the melters are enclosed in shielded hot cells not accessible for manual intervention. Running this high-temperature process in the environment of a hot cell takes a robust, reliable melter technology and sophisticated remote handling techniques.

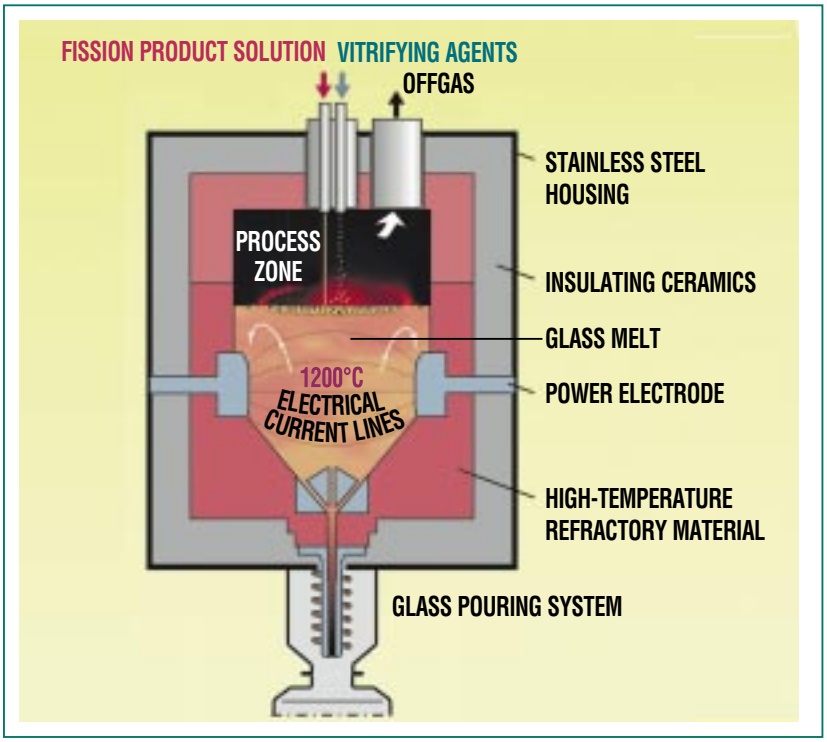

Fig. 1: Schematic design and operating principle of a liquid-fed ceramic melter for vitrification of high-level radioactive fission product solutions.

Structure and Operating Principle of a Liquid-fed Ceramic Melter

Ceramic melters are attractive for use in nuclear technology because they allow fission product solutions to be vitrified in a single-stage continuous process without any preparatory treatment. The schematic diagram in Fig. 1 shows the design and the operating principle of a variant developed at the Institute for Nuclear Waste Disposal (INE) of the Karlsruhe Research Center. In this design, liquid waste and vitrifying agents are fed to the melter in separate streams. Feeding liquid waste gives rise to a cool, stationary process zone on the surface of the hot glass melt, out of which the liquid waste components evaporate while the dry residues, following thermal decomposition and transformation into oxides, react with the glass frit and melt. The offgases in the melter generated in this process must be cleaned thoroughly.

Design of the Ceramic Structure of the Melter

The melter system is composed of a number of different, yet compatible, ceramic materials. The region in contact with glass consists of a fused cast refractory ceramic referred to as ER 2161 (main constituents, approx. 27% each of Al_2O_3, Cr_2O_3, Zr_2O_3, and approx. 15% of SiO_2). The walls of the glass tank are made up of blocks precision-ground so as to seal the unit against penetration of the melt into the layers behind. Figure 2 shows a schematic view

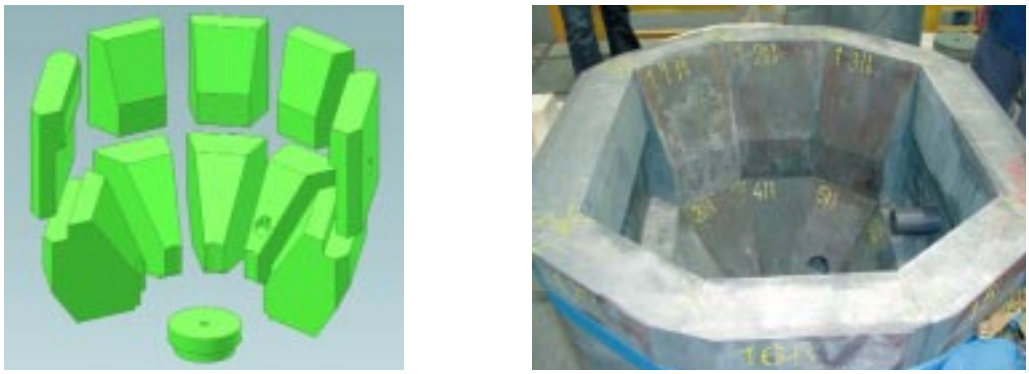

Fig. 2: Walls of the melt tank made out of a refractory fused cast ceramic. Schematic representation (left) and the assembled tank structure (right).

of the design of the glass tank (left) and a photograph of the component blocks assembled for acceptance at the manufacturer's works (right). More structural details can be seen in Fig. 3, which offers a view of the brick lining of a melter (left picture) and the layers making up the wall (picture on the right). The ceramic blocks making up the glass tank are followed by a barrier layer of refractory ceramics arranged in such a way as to cover all joints. Towards the outside, this is followed by a ceramic insulation consisting of various layers of stone of different qualities. Their thermal conductivity decreases towards the outside in the direction of the outer stainless steel housing. The choice of materials is made so that any glass which could penetrate through joints of the glass tank ceramics would solidify on its way out while still in the area of the ceramics resistant to glass. This special design of a thermal insulation allows the melter to reach temperatures of

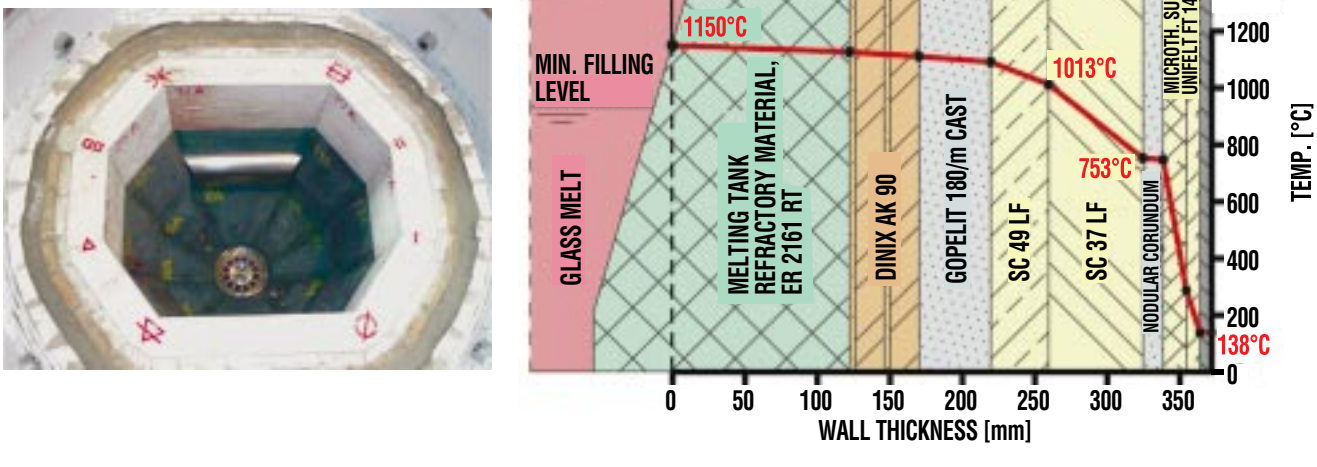

Fig. 3: Wall structure of a ceramic glass melter. The photograph shows the brick assembly, top view (left picture), and the layers making up the wall plus the calculated temperature curve (right).

approx. 100°C at its stainless steel outside wall. In this way, there is no need for forced cooling of the stainless steel outside wall.

Heating

The glass melter is heated to a maximum temperature of approx. 1200°C by the Joule principle: Application of an alternating voltage (50 Hz) between two or more paired opposite metal power electrodes embedded in the wall causes a three-dimensional electrical potential field to develop in the glass melt and the pool areas immediately around it. The local release of energy is determined by the prevailing intensity of the electric field and the local electric resistivity of the material. The total power is the sum total of all local contributions to this power level.

The electric resistivity of the ceramic structure is approximately two orders of magnitude higher than that of the glass melt. As a consequence, the energy released outside the melt is negligible. Usual levels of electric resistivity of the melt are between approx. 4 and 20 Ω cm, dependent on temperature.

The electrode material is a high-temperature resistant chrome-nickel alloy (Ni > 58%, Cr 27-31%) commercially available under the trade name of Inconel 690®. The melting temperature of this alloy is around 1365°C. At temperatures above approx. 1100°C, materials wear increases markedly. In the interest of a sufficiently long service life, the electrodes therefore are kept at a glass contact temperature of approx. 1000°C by means of air cooling.

The number and arrangement of electrodes in the melt tank are the result of criteria, such as the highest possible energy release in the glass pool, pronounced thermal convection for homogeneous mixing of the melt, and sufficient energy transport to the process zone on the surface of the molten pool, which requires a large amount of energy (evaporation, melting).

The melt is heated at a constant electric current. This type of power supply helps to limit the power transferred to the melt in case of excessive temperatures of the molten pool because of the electric resistivity decreasing with temperature; in this way, temperature peaks are avoided. This approach also ensures that the permissible power density load of the electrode surfaces will not be exceeded.

Geometry of the Melt Tank

The size and shape of the melt tank is determined by the throughput which, in the case of liquid feeding, depends largely on the surface of the molten pool, the desired mean residence time of the melt (refining), and the amount and type of glass extracted. Also specific properties of the melt can affect the tank geometry. Melting waste with high contents of platinum metals (ruthenium, palladium, rhodium) which, because of their lack of chemical affinity to the glass network structure in the borosilicate glass normally used, gives rise to particle sedimentation and to viscous, electrically highly conductive bottom layers, requires a special design of the glass tank in order to prevent accumulations which could endanger the system. Waste with high contents of platinum metal arises mainly in reprocessing nuclear fuels with high burnup for commercial power production.

Because of the minimal solubility of platinum metals in the borosilicate glass melt, glass chemistry approaches will not remove the platinum metal problem. Technical solutions either try to avoid particle sedimentation by mechanical homogenizing measures or seek to remove from the system as quickly as possible any deposits forming. Experience in the vitrification of this type of waste has shown that the flow properties of bottom sediments and, hence, the discharge probability, clearly deteriorate in the course of prolonged residence in the system. Homogenization of the melt by mechanical agitation (e.g. air sparging by means of submerged air lances) will work only within certain limits and can be employed successfully only if platinum metal concentrations in the melt are low. The concept developed at INE is based on minimizing residence time by enforcing sediment discharge by design measures. For this purpose, the sedimenting platinum metal particles are made to slide down oblique walls in the bottom region of the melt tank (> 50°) where they are moved to the lowest part of the tank and their concentrate is

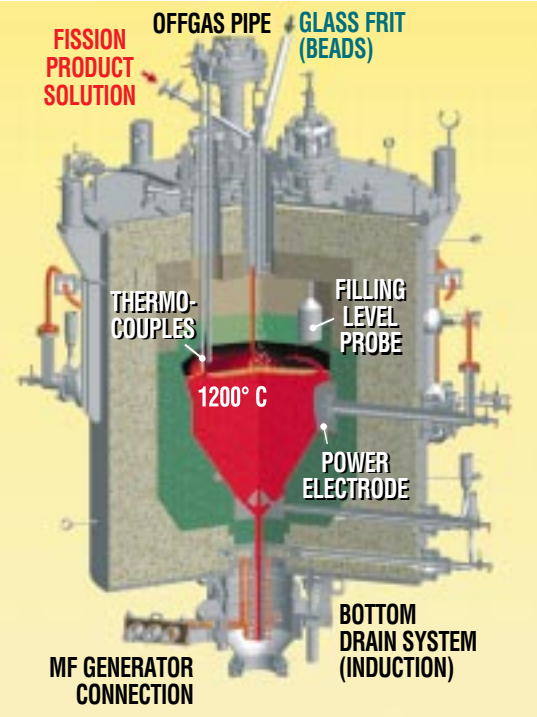

Fig. 4: 3D representation of a glass melter with a steeply inclined melt tank bottom to vitrify fission product solutions with high contents of platinum metals.

Fig. 5: Photograph of a liquid-fed ceramic glass melter.

collected. In the course of periodic glass pouring, they then flow out through the glass discharge duct located right underneath. Figure 4 shows the design of a melter able to handle also platinum metals. Figure 5 shows the outside view of the melter ready for installation.

Glass Pouring

The liquid glass is poured in batches through a bottom drain system through which only part of the melt is discharged at a time. The melter is emptied only to such an extent that the electrodes will stay completely immersed in the melt. The glass discharge system in the central bottom part of the glass tank, whose design is shown in Fig. 6, operates by the principle of a thermal valve (freeze seal). The glass discharge duct consists of an upper ceramic part and a lower metal part (thick-walled tubular duct made out of Inconel 690®). To discharge the glass melt into stainless steel containers (canisters), the glass discharge duct must be heated until the glass is molten. The metal duct integrated into the ceramics of the bottom of the melter is heated by a 10 kHz medium-frequency (MF) induction heater. To support the MF heater up to the point of fluidity of the glass, the glass is heated by applying electricity directly to the upper ceramic duct for a limited period of time. Glass flow (approx. 120 kg/h) into the canister is controlled through the inductive power applied to the Inconel 690® tube. To terminate the glass flow by solidification, the heating power is throttled over a number of steps and turned off. The flow of the melt is stopped in this way, and the glass solidifies in the discharge duct.

The transition area between the glass discharge duct and the glass tank contains a metal insert protecting the main discharge duct from blockages caused by foreign bodies, such as ceramic fragments (see Fig. 6). To ensure unobstructed discharge of the precious metal sediments, this blockage protection has twelve openings along the sides and one central opening. Passage through the openings has been optimized in terms of the flow pattern so as to provide an unobstructed entry for the melt into the glass discharge duct. In addition to its protective function, this insert also serves as an electrode for Joule heating of the glass in the region of the ceramic duct. The flange of the metal discharge duct constitutes the counter-electrode.

To protect the cell against contamination by volatile components of the hot glass flow (such as cesium as one of the main sources of radioactivity), gases are extracted from the housing of the bottom discharge section during pouring, and fed to the gas compartment of the melter. In this step, air from the cell flows into the housing connected to the canister by means of a labyrinth seal.

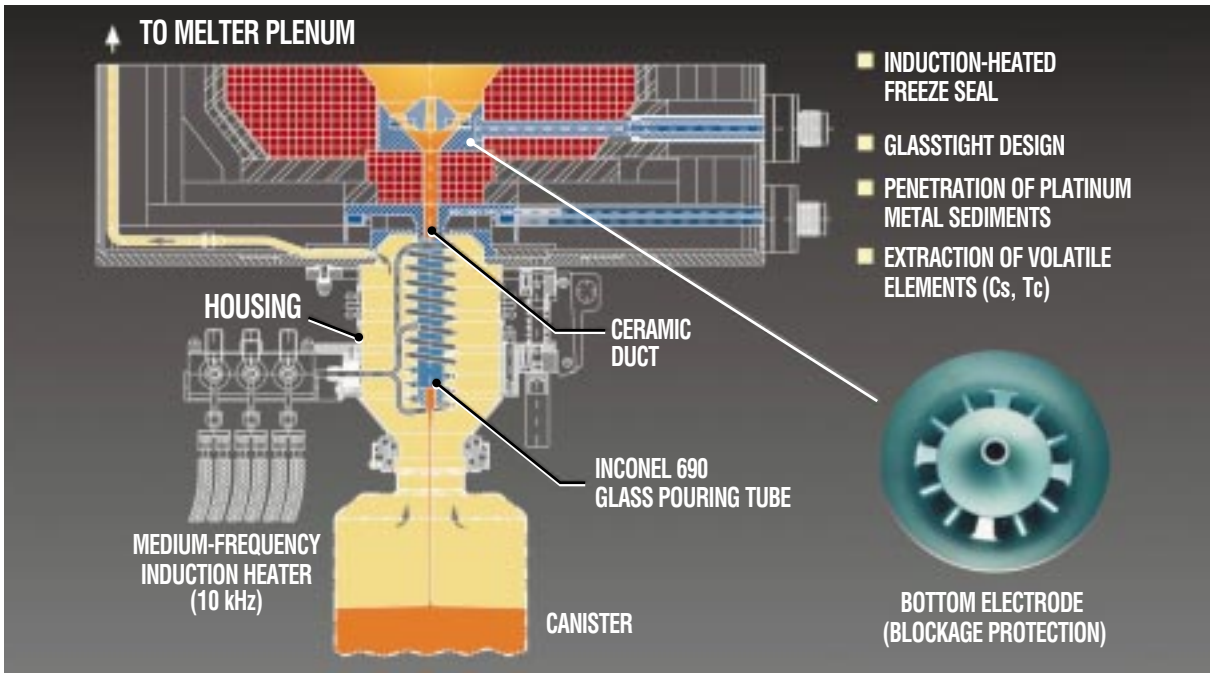

Fig. 6: Design of the bottom discharge system for pouring glass batches.

Measurement

For monitoring the high-temperature process, the melter is equipped with systems for temperature measurement (thermocouples) and a filling level probe. Several temperature measurements ensure that temperature conditions are met in various regions of the ceramic structure, in the electrodes, and in the glass pouring system. The four thermocouples staggered in the upper compartment of the melter as shown in Fig. 4 are used for process control. They provide information about the extension of the process zone on the surface of the molten pool, the glass filling level, and the glass melting temperature. The glass filling level probe indicates when glass has to be discharged. Pressure measurement in the gas compartment above the melt serves to monitor the negative pressure in the melter necessary for extraction of melter offgases into the offgas cleanup train. Maintaining the negative pressure prevents emissions into the environment of the cell. The electric power supplied to the melt is controlled by voltage and current measurements.

Melter Temperature Treatment

Prior to their first commissioning, ceramic glass melters must be subjected to a temperature treatment. In this process, the empty melter is heated to a tank temperature of approx. 1000°C over a temperature-controlled gradual heating phase of approximately three weeks. This heating serves the purpose, among other things, of driving residual moisture out of the melter walls and, in particular, of driving water of crystallization out of the fused cast ceramic and obtaining temperature conditions in the structure which are close to operating conditions. This heat treatment is achieved by several external SiC radiative heating elements introduced into the interior through openings in the melter top. When the set temperature has been reached, the heating element positioned in the center is removed and replaced by the feeding system. Afterwards, glass frit is added step by step in small batches at intervals so as to allow the frit to be molten in the meantime by the remaining heating elements. When the level of the melt reaches the electrode level, the system can be switched to electrode heating. After removal of the remaining heating

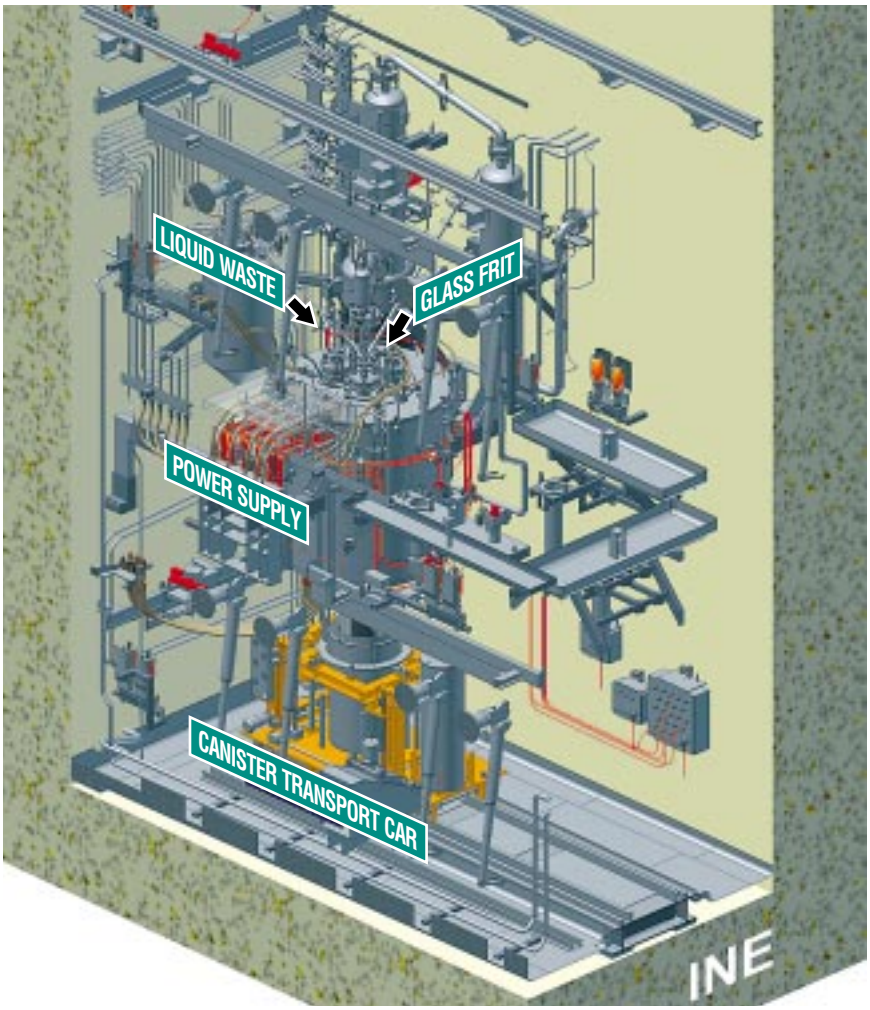

Fig. 7: 3D representation of a melter cell equipped with remote handling facilities.

elements and installation of the other melter components (offgas pipe, thermocouple nozzles, etc.) and connection to the process periphery, the melter is ready for vitrification.

Remote Handling

Because of the intense radiation, high-level radioactive fission product solutions must be vitrified in hot cells. For the melter design, this implies the need to carry out maintenance and repair work and replace components or the entire assembly from outside the cell. For this purpose, the melter is equipped with special connections which can be disengaged and assembled remotely by the appropriate manipulator tools. Figure 7 shows the as-installed situation of the melter cell equipped with remote handling systems as shown in a 3D view. Figure 8 is a view from the top into a comparable melter cell with remote handling capability of the non-radioactive prototype vitrification plant (PVA) of INE.

Fig. 8: View of a melter cell with remote handling capability of the non-radioactive prototype vitrification facility (PVA) of INE.

Literature

G. Roth,
atw 40 (1995, 3)

G. Roth, S. Weisenburger
Nuclear Engineering and Design 202 (2000), pp. 197-207

S. Weisenburger
NUCEF'98, Ibaraki, Japan, Nov. 16-17, 1998; Proceedings pp. 241-51

Reducing Spent Nuclear Fuel Radiotoxicity by Actinide Separation and Transmutation: Partitioning

A. Geist, K. Gompper, M. Weigl, T. Fanghänel, INE

Introduction

Some 16% of the electricity generated worldwide comes from nuclear power. Compared to electricity generation from fossil fuels, this avoids the emission of approx. 2 billion t of carbon dioxide annually. 10,500 t of spent nuclear fuels annually are unloaded from nuclear power plants and have to be managed and disposed of safely [1]. Safe management is to ensure that present and future generations are protected sustainably from the damaging impacts of ionizing radiation. In this respect, special attention needs to be paid to the radionuclides with long halflives and high radiotoxicity levels. These are the transuranium elements, above all plutonium, but also the so-called minor actinides (MA), i.e. neptunium, americium, and curium, as well as some particularly longlived fission products, such as technetium and iodine. Projects are being pursued worldwide to store spent fuel elements and high-level radioactive waste in deep geologic formations and, in this way, remove them from the biosphere. However, at the present time, no repository for high-level radioactive waste is in operation.

Given the long life of some radionuclides and the related question whether it can be ensured over very long periods of time that there will be no release of radioactive substances from a repository, alternatives to the repository storage of longlived radionuclides are being studied internationally. One possibility would be to separate (partition) these nuclides from the spent nuclear fuel by suitable processes and then convert (transmute) them into stable fission products or those with comparatively short halflives by neutron reactions in special facilities. This partitioning and transmutation strategy (P+T) is to ensure that, after some hundred years, the radiotoxicity of the waste held in final storage has decayed to a level, for instance, of that of natural uranium, which clearly reduces the long-term hazard potential of that waste.

Contributions to Radiotoxicity by Actinides and Fission Products

Figure 1a shows the radiotoxicity of one ton of spent nuclear fuel plotted as a function of the time after discharge from a reactor. Moreover, the development of radiotoxicity of the fission products, minor actinides, and plutonium contained in this fuel is shown [2]. It is obvious that, in the first one hundred years, the fission products will make the largest contribution; next, up to approximately one thousand years, it is the minor actinides,

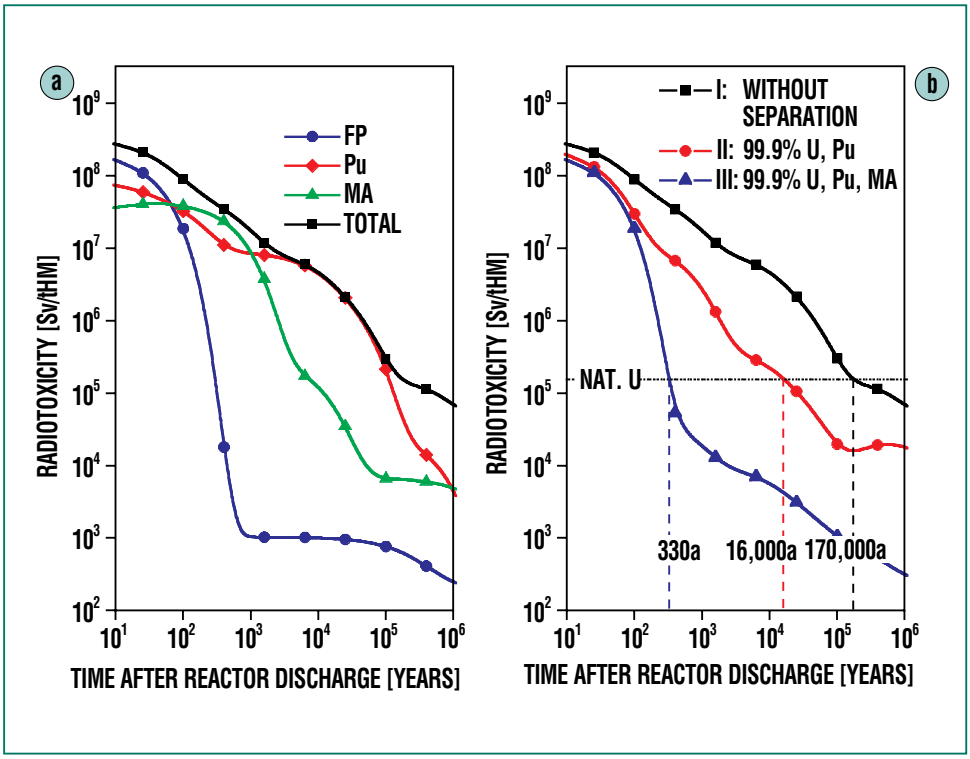

Fig. 1: Radiotoxicity inventory of one ton of spent nuclear fuel (t HM = ton of heavy metal) from a pressurized water reactor (enrichment 4.2% ^{235}U, burnup 50 GWd/t, radiotoxicity based on ingestion [2]). (a) Contributions to radiotoxicity by plutonium (Pu), the minor actinides (MA), and the fission products (FP). (b) Influence of actinide separation on the development of radiotoxicity. The reference is the amount of natural uranium needed to manufacture one ton of fuel.

mainly americium, and afterwards, for more than 100,000 years, plutonium will dominate the scene. As a consequence, partitioning and transmutation of plutonium and the MA would lead to a clear long-term reduction of radiotoxicity, while the longlived fission products are of less interest because of their small share (flat part of the fission product curve after approx. 1000 years). There are plans to develop a P+T strategy also for the longlived fission products [3]. However, this article focuses on actinide partitioning.

Effectiveness of P+T

The consequences upon radiotoxicity of partitioning of plutonium and the MA are shown in Fig. 1b, in which three scenarios are indicated. For reference, the radiotoxicity of that amount of natural uranium is indicated which is needed to manufacture one ton of fresh nuclear fuel. Curve I describes the development of radiotoxicity in the absence of partitioning. This applies to the direct final storage of spent nuclear fuels which, in the future, will be the only waste management pathway permitted in Germany [4]. The radiotoxicity level of natural uranium will be reached after some 170,000 years. Curve II shows the development of radiotoxicity if 99.9% of the plutonium and uranium are partitioned, as is the case now in a modern reprocessing plant, such as La Hague in France. In this case, radiotoxicity will drop to the level of natural uranium after approximately 16,000 years. However, if also 99.9% of the MA are partitioned, radiotoxicity (curve III) drops sharply, and the radiotoxicity of natural uranium will be reached after only slightly more than 300 years which, historically, is a foreseeable period of time.

However, partitioning is only the first step. The effectiveness of the following transmutation step also affects the assessment of E_{PT}, the effectiveness of P+T. In the following example, which is explained in detail by Magill et al. in [5], the effectiveness of actinide partitioning is E_P = 0.999 (99.9% partitioning, curve III in Fig. 1b), and the effectiveness of transmutation is E_T = 0.2 (20% of the actinides are transmuted). This implies the need for multiple recycling. In each cycle, 99.9% of the actinides remaining after transmutation would be partitioned. The overall effectiveness of P+T over all cycles can be calculated, according to [5], to be

$$E_{PT} = \frac{E_P E_T}{1-(1-E_T)E_P}$$

resulting in E_{PT} = 0.995 or 99.5%. Despite the highly effective partitioning of 99.9% of the actinides, overall P+T effectiveness is only 99.5% because of the necessary recycling steps and the associated, minor, losses in separation. This means that the radiotoxicity of the waste remaining after P+T treatment will not decay as fast as in Fig. 1b, Curve III, in which only partitioning was taken into account. Hence, the objective is to ensure the highest possible separation efficiencies in order to offset the losses incurred in the necessary recycling steps. It will be shown below that partitioning can achieve almost complete separation of the actinides. For transmutation, reference is made to an article elsewhere in this publication.

Separation Processes

Radionuclides can be separated by hydrometallurgical techniques, i.e. from aqueous solutions, or by pyrometallurgy from salt melts. Pyrometallurgical techniques by far have not reached the level of development of hydrometallurgical processes, some of which have been applied for several decades, e.g. the PUREX process (Plutonium and Uranium Recovery by EXtraction). However, pyrometallurgy is expected to offer processes which can be run in very compact facilities and include the possibility to reprocess fuels with high burnups and short cooling times, as there will be no problems, such as radiolysis of aqueous and organic solvents. Future P+T scenarios could quite well include a combination of hydrometallurgical and pyrometallurgical separation processes. This contribution, however, will refer only to actinide separation out of aqueous systems.

Actinide Separation

Figure 2 shows a simplified process flowsheet of an advanced concept [6] of separating plutonium and the other actinides. Uranium and plutonium and, after process modifications, neptunium (Np) are separated in the so-called PUREX process.

The next step is the separation of americium (Am) and curium (Cm) from the high-level radioactive PUREX product. Because of their almost identical chemical behavior, this is possible only together with the lanthanides (fission products). As there is an excess of lanthanides, and some of the lanthanides have high neutron capture cross sections which would aggravate effective transmutation of the MA, subsequent lanthanide-actinide separation is indispensable. Moreover, it makes sense to separate americium from curium, as the neutron dose rate of curium renders fuel fabrication difficult. The curium separated can be stored and, after having decayed to plutonium, passed on to transmutation.

Step 1:
Separation of Uranium, Plutonium, and Neptunium in the PUREX Process

The separation of uranium and plutonium from spent fuel elements in the PUREX process has been employed in reprocessing spent nuclear fuels for many years to recover the unspent valuable uranium and plutonium. Reprocessing is performed on a commercial scale in Europe at La Hague in France and Sellafield in the United Kingdom. The fuel is dissolved in nitric acid, out of which uranyl nitrate and plutonium nitrate are extracted into a solution of tributyl phosphate (TBP) in kerosene. Subsequently, uranium and plutonium are separated and purified. The residual actinides and the fission products remain in the PUREX raffinate. Neptunium occurs in the fuel solution in its pentavalent and hexavalent forms. While Np(V) is not extracted by TBP in the PUREX process, it may be separated in a modified PUREX process by quantitative oxidation to Np(VI).

Step 2:
Separation of Americium and Curium together with the Lanthanides

A number of processes have been developed worldwide (see [3]) to separate the MA together with the lanthanides from the remaining fission products in the PUREX raffinate. European cooperation favors the DIAMEX process (DIAMide EXtraction) [7], one advantage of which lies in the fact that the alkylated malonamides used, such as DMDOHEMA (see Fig. 3), consist only of carbon, hydrogen, oxygen, and nitrogen. Once they have been consumed, they can be burnt to gaseous products, thus minimizing the arisings of solid secondary waste. The DIAMEX

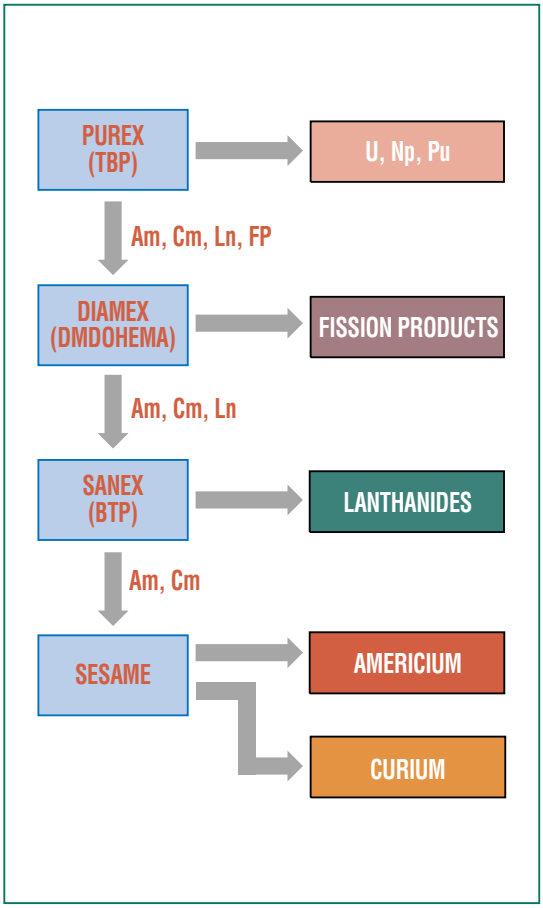

Fig. 2: Simplified process flowsheet for the separation of plutonium and minor actinides from spent nuclear fuel.

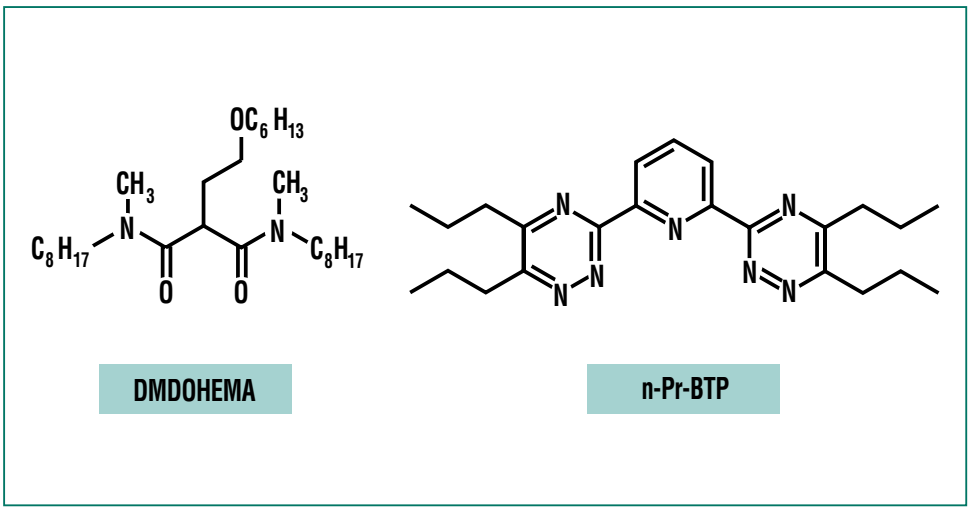

Fig. 3: Extraction agents for separating minor actinides: on the left, for the DIAMEX process; on the right, for the SANEX process.

process has been tested successfully on a laboratory scale with a real PUREX raffinate at the Karlsruhe Institute for Transuranium Elements [8] and in France [6].

Step 3:
Separation of Americium and Curium from the Lanthanides

Because of the chemical similarities between the trivalent actinides and the lanthanides, this separation poses an extreme challenge. The usual extractants, which coordinate via oxygen atoms, are practically unable to achieve the necessary selectivity. Only the use of so-called soft donor ligands, which coordinate preferably actinides (III) via nitrogen or sulfur atoms, makes it a successful proposition.

A large number of such N-donor extractants have been synthesized and tested; for instance, cf. [9, 10]. However, none of them extracts from nitric acid solutions which arise in Step 2. A very promising extractant, 2,6-di(5,6-dipropyl-1,2,4-triazine-3-yl)pyridine (n-pr-BTP), has been developed at the Karlsruhe Research Center and met with immense international response. It is able to extract from 0.5 – 2 M nitric acid americium(III) and curium(III) with a separation factor of >100 relative to europium(III) [10, 11].

Step 4:
Separation of Americium and Curium

Americium can be oxidized to Am(IV) and Am(VI), respectively, in a nitric acid solution, which is practically impossible for curium. Separation can then be achieved by various extractants. This is the principle underlying the SESAME process [12] developed in France. The difficulty in this process is stabilization of the higher oxidation levels of americium. If multiple-stage separation processes are accepted, also the existing, though not very high, separation factors between Am(III) and Cm(III) of some extractants could be used [6].

Work at the Research Center

The separation of Am and Cm by liquid-liquid extraction is being studied at the Institute for Nuclear Waste Disposal (INE) of the Karlsruhe Research Center within the framework of European research programs (PARTNEW, EUROPART). This work covers the co-extraction of actinides(III) and lanthanides in the DIAMEX process, and the separation of actinides(III) from lanthanides in the SANEX process (Selective ActiNide EXtraction). The main focus is on the synthesis of selective extractants of high stability, and on studies and tests of continuous extraction processes, more details of which will be outlined below.

Extraction Processes in Hollow Fiber Modules

In studies and tests of continuous extraction processes at INE, the usual phase contactors (such as mixer-settlers, centrifugal extractors) are replaced by so-called hollow fiber modules (HFM). In the simplest version, these consist of a bundle of microporous hollow fibers in a shell tube. One phase flows inside the hollow fibers, the other on the shell side. The phase boundary is immobilized in the pores of the membrane (see Fig. 4a). Dense packing of the hollow fibers (approx. 700 fibers/cm^2) results in a large exchange area. The main advantage of this process is that, unlike with classical extraction units, throughput within wide limits is not determined by hydrodynamics.

A number of very successful experiments have been run with commercially available HFM [13]; because of their design for technical applications, however, they required relatively large feed volumes. For this reason, miniature HFM were developed which consist of approximately 100 hollow fibers (Fig. 4b). They can achieve throughputs in the ml/h range, with the feed volumes required being around several 10 ml. Effective DIAMEX and SANEX experiments [14, 15] have been run with these miniature HFM, initially with separate extraction and stripping steps. One example shown is the result of a SANEX test using n-pr-BTP as extractant (see Fig. 5). For an aqueous flow rate of 0.7 ml/h, the residual americium content of the raffinate is less than 0.1% (> 99.9% separation), while merely approx. 1% of the lanthanide inventory is co-extracted.

A “microplant” has been developed, manufactured, and tested to implement HFM in hot cells. Four miniaturized HFM modules

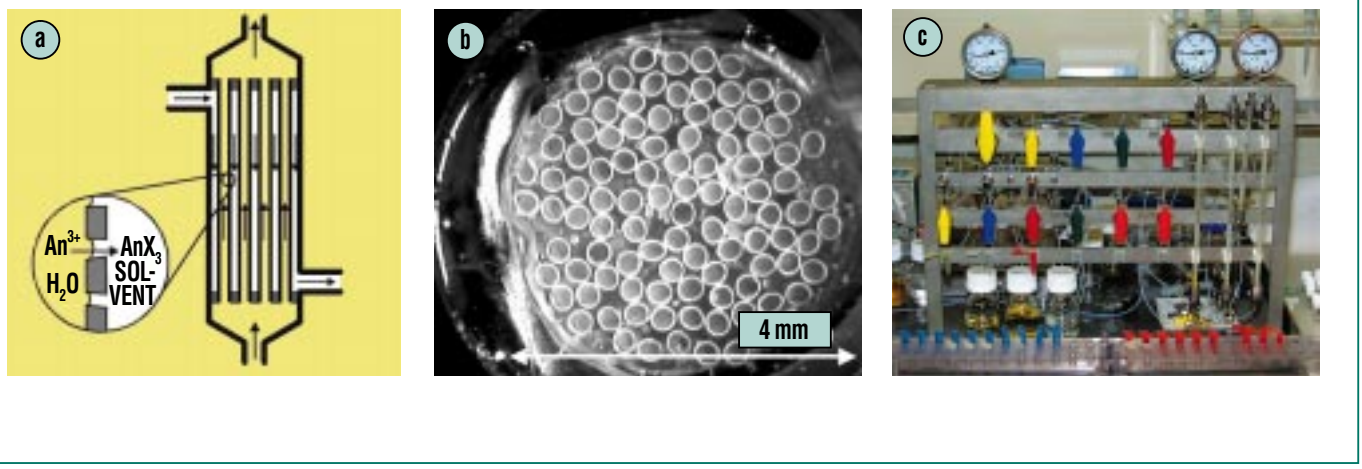

Fig. 4: (a) Schematic representation of the mode of operation of a hollow fiber module; (b) hollow fiber bundle (bundle diameter 4 mm) in a miniature HFM; (c) microplant for testing extraction in hot cells; on the right, the miniature HFMs for extraction, two scrubbing steps, and stripping.

were coupled (see Fig. 4c) for the extraction, lanthanide scrubbing, acid scrubbing, and stripping steps. This system allowed more than 99.9% of Am to be separated by means of the DIAMEX process from a simulated PUREX raffinate doped with Am. The product solution obtained can be used directly as a feed solution for the SANEX process for actinide/lanthanide separation. A version of the HFM microplant developed further for use in hot cells is currently under construction. It will be used for extraction experiments with a real high-level radioactive PUREX product in the hot cells of the European Institute for Transuranium Elements in close cooperation with that Institute.

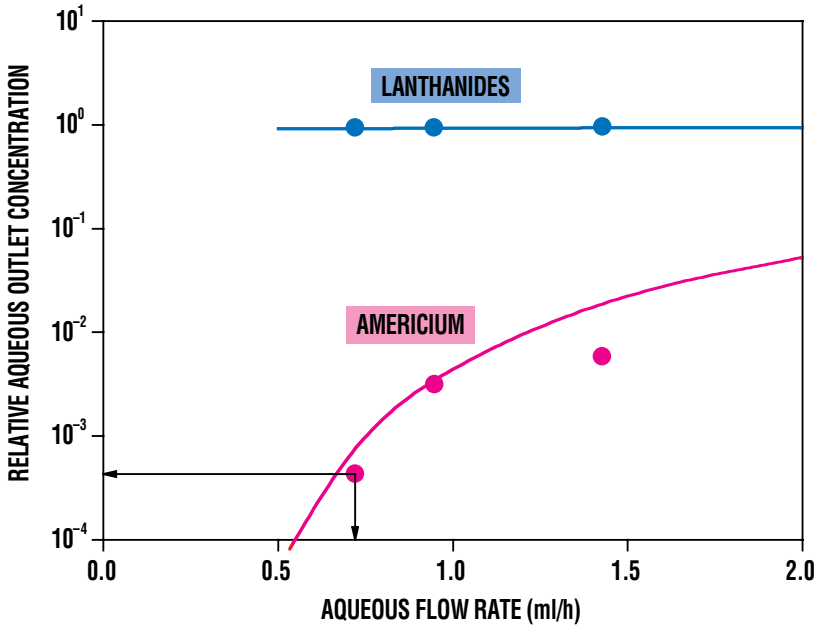

Fig. 5: Am(III)/lanthanide separation by n-pr-BTP in a miniature HFM. Relative aqueous discharge concentrations as a function of the aqueous volume flow rate. Symbols: experiment; lines: calculations (mass transfer calculations on the basis of equilibrium data and kinetic data with hydrodynamics taken into account).

Summary

The actinides, especially plutonium, are the cause of radiotoxicity in high-level radioactive waste

over very long periods of time. Transmutation of the actinides into stable, or at least shortlived, products is one possible alternative to final storage in repositories. One prerequisite for this to happen is selective and nearly complete separation from the other radionuclides, which is now felt to be feasible. However, even with very high effectiveness, partitioning and transmutation cannot replace geologic repository storage, which would remain necessary for the residual high-level, though shorter-lived, waste.

Literature

[1] K. Fukuda, W. Danker, J.S. Lee, A. Bonne, M.J. Crijas, *Proc. Int. Conf. Storage of Spent Fuel from Power Reactors, June 2 – 6, 2003, Vienna (IAEA)*

[2] *International Commission on Radiological Protection, Annals of the ICRP, Publication 68, Pergamon Press (1994)*

[3] *Status and Assessment Report on Actinide and Fission Product Partitioning and Transmutation, OECD-NEA (1999)*

[4] *Atomgesetznovelle vom 22. April 2002 (amendment to the German Atomic Energy Act dated April 22, 2002)*

[5] J. Magill, V. Berthou, D. Haas, J. Galy, R. Schenkel, H.-W. Wiese, G. Heusener, J. Thommasi, G. Youinou, *Nuclear Energy, 42(5), 263, 2003*

[6] P. Baron, M. Lecomte, B. Boullis, N. Simon, D. Warin, *Proc. GLOBAL 2003, November 16 – 20, 2003, New Orleans, USA, p. 508*

[7] C. Musikas, *5th Symp. Sep. Sci. Technol. for Energy Applications, October 26 – 29, 1987, Knoxville, USA*

[8] D. Serrano-Purroy, B. Christiansen, R. Malmbeck, J.-P. Glatz, P. Baron, *Proc. GLOBAL 2003, November 16 – 20, 2003, New Orleans, USA, p. 1920*

[9] Z. Kolarik, R. Schuler, U. Müllich, *Partitioning of High-level Radioactive Wastes, EUR 16958 EN, 1996*

[10] C. Madic, M.J. Hudson, J.O. Liljenzin, J.-P. Glatz, R. Nannicini, A. Facchini, Z. Kolarik, R. Odoj, *New Partitioning Techniques for Minor Actinides, EUR 19149 EN, 2000*

[11] Z. Kolarik, U. Müller, F. Gassner, *Solvent Extr. Ion Exch., 17(5), 1155, 1999*

[12] J.M. Adnet, P. Brossard, J. Bourges, *Proc. GLOBAL '93, September 12 – 17, 1993, Seattle, USA*

[13] A. Geist, M. Weigl, K. Gompper, *Sep. Sci. Technol., 37, 15, 3369, 2002*

[14] A. Geist, M. Weigl, K. Gompper, *Proc. Int. Workshop on P&T and ADS Development, SCK-CEN, Mol, Belgium, October 6 – 8, 2003*

[15] A. Geist, M. Weigl, K. Gompper, *In: Actinide and Fission Product Partitioning and Transmutation, 7th OECD/NEA Information Exchange Meeting, October 14 – 16, 2002, Jeju, Korea. EUR 20618 EN, 2003, pp. 421 – 30 (on CD)*

Partitioning and Transmutation: A New Perspective for Nuclear Waste Treatment?

W. Maschek, X. Cheng, A. Rineijski, R. Stieglitz, IKET; J. Konys, IMF; G. Müller, IHM;
C. Broeders, M. Schikorr, D. Struwe, IRS

Introduction

Transmutation is to convert into shortlived or stable nuclei the radiotoxic isotopes produced by reactors, especially plutonium and the minor actinides (neptunium, americium, and curium). In this way, transmutation opens up a perspective of clearly reducing the arisings and radiotoxicity of the residual waste left over in the end. Nuclear transmutation is a term which can encompass both conversion by neutron capture, (n, xn)-processes, radioactive decay, and the most efficient form of conversion, fission.

In the early nineties, accelerator-driven subcritical systems (ADS) were proposed as a system potentially suitable for transmutation [1, 2, 3]. In April 2001, the European Technical Working Group on ADS, whose members include staff of the Karlsruhe Research Center, published the European Roadmap for Developing Accelerator Driven Systems (ADS) for Nuclear Waste Incineration [4]. This roadmap constituted the basis of the work discussed below on various projects within the 5th EU Framework Program.

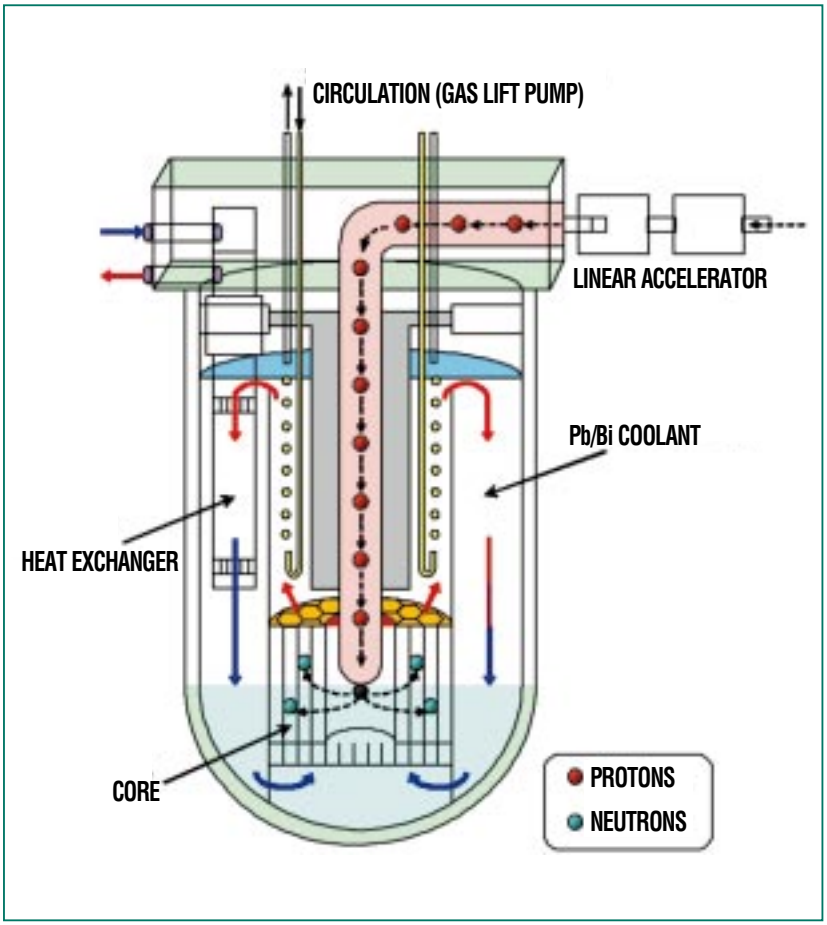

Fig. 1: Schematic representation of an accelerator-driven system.

The Conceptual Design of Accelerator-driven Systems (ADS)

An ADS consists of three main components: an arrangement of fuel elements which is subcritical in terms of neutron physics, an accelerator, and a spallation target representing the external neutron source [5]. An accelerator (linear accelerator or cyclotron) is used to shoot high-energy protons through an evacuated beam tube onto a spallation target consisting of a heavy element (e.g. a lead-bismuth (Pb-Bi) alloy), and free neutrons are generated in spallation reactions. The so-called source neutrons produced in this way initiate and maintain a chain reaction in the subcritical assembly. Figure 1 shows the basic setup of the system. This system uses the liquid Pb-Bi heavy metal alloy as a spallation medium and coolant. Actually, a variety of target variants are being studied, from solids to the liquid Pb-Bi referred to above. In addition to Pb-Bi, lead, and helium, also sodium is being considered as a coolant for ADS.

Neutron Physics Properties

In ADS facilities, waste is destroyed mainly in reactions involving neutrons. Effective destruction of transuranium elements is achieved mainly through fission, while other capture processes mainly shift the composition of transuranium elements. Figure 2 shows the number of fissions per neutron capture in selected fuel isotopes as

a function of neutron energy. It is seen that the fission probability in general increases for higher neutron energies roughly above 100 keV. In a number of higher transuranium elements, as shown in the illustration for Np^{237}, Am^{242}, and Cm^{244}, fission probability is very low below approx. 1 MeV.

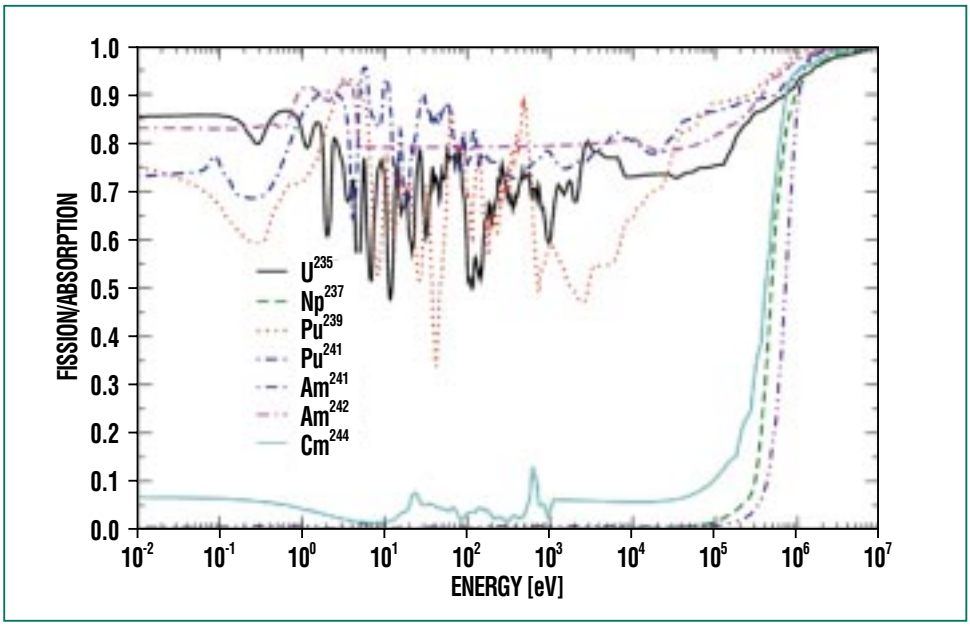

Fig. 2: Comparison of the fission fraction relative to total capture for some selected isotopes.

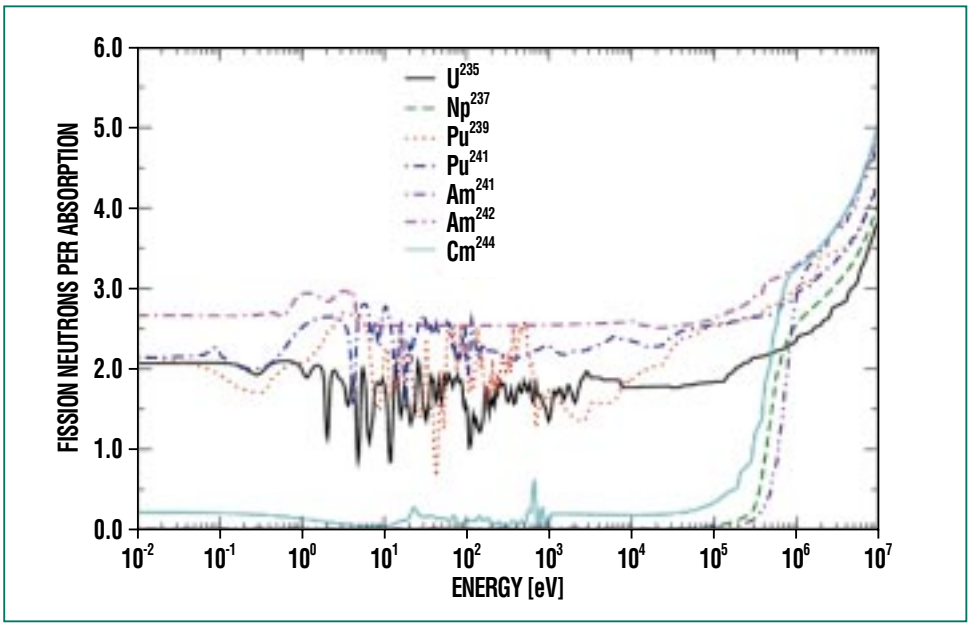

Fig. 3: Comparison of the number of fission neutrons per capture for some selected isotopes.

In these facilities, also the number of neutrons produced in the fission reaction is important, as surplus neutrons are available for additional captures for waste destruction. Figure 3 shows the fission neutrons generated per neutron capture as a function of neutron energy. Also this comparison indicates a positive yield approximately above 1 MeV, which increases as the mass number rises.

The MCNPX (Los Alamos) Monte Carlo code has become the standard code to determine static reference solutions in neutron physics calculations of accelerator-driven subcritical reactor systems. For very complex geometric fuel element arrays, MCNPX allows all necessary systems parameters to be determined reliably on the basis of the specifications of the proton beam. As Monte Carlo methods take very long computation times, also deterministic multigroup computation methods are used for a number of problems, such as burnup calculations and safety studies. The KAPROS code system [6] developed at the Karlsruhe Research Center over a long period of time now offers a number of special procedures in support of development work on accelerator-driven systems.

Conducting the appropriate experiments is absolutely imperative if the database is to be improved. These experiments are run with international partners in EU projects, thus allowing competence to be preserved and fast access to new findings to be achieved. Examples to be men-

tioned are participation in the MUSE project, or cooperation in ISTC projects as a "collaborator." The International Scientific Technology Center (ISTC) in Moscow organizes financial support of scientific projects in Eastern Europe by Western countries, such as the United States and Japan, and institutions, such as the European Union. These projects involve both integral measurements of subcritical facilities with powerful neutron sources and measurements of differential cross sections.

In an accelerator-driven subcritical system, the spallation target area hit by the high-energy proton beam is one of the components sustaining the highest loads and stresses. In addition to the high energy densities and energy density gradients occurring at these points, also spallation products are generated in proton reactions with the target material. These spallation products can greatly influence the chemical and mechanical properties of the target components. As the rates at which spallation products are generated have not yet been backed experimentally with sufficient accuracy, a number of experiments are currently being performed in an effort to improve the database supporting the computer codes.

Fuel for an ADS

To achieve the highest possible transmutation and incineration rates, special fuels must be developed for an ADS [7]. These fuels may not contain U-238, as new plutonium would be bred by way of U-238. Fuels therefore must be produced as pure plutonium/MA fuels (americium and curium) imbedded in an inert matrix. The fraction of minor actinides should be as high as possible. At present, three different types of fuels are investigated which have emerged as the most suitable varieties in a preliminary selection phase:

- Solid solution fuels of the (Pu, Am, Cm, Zr)O_{2-x} type.
- CERCER fuels of the (Pu, Am, Cm)O_{2-x}+MgO type.
- CERMET fuels of the (Pu, Am, Cm)O_{2-x}+Mo-92 type.

The following aspects were studied in greater detail in the selection of a fuel suitable for use in an ADS [8]:

- Fabrication/use potentials.
- Margin relative to fuel melting at nominal power.
- Reactivity worth in coolant displacement.
- Burnup and reactivity loss during a loading cycle.
- Fission probability.

The buildup of higher minor actinides, especially curium, is to be minimized in a hard neutron spectrum. For the transmuters under study, the americium incineration rate in the first reactor cycle is around 120 kg/TWhe, plutonium reduction is around 20 kg/TWhe, accompanied by the simultaneous Cm buildup of 12 kg/TWhe.

On the basis of these criteria, a MgO matrix is currently favored for the CERCER fuels. For CERMET, the choice has been in favor of Mo-92. On the whole, it was shown that fuel development is one of the main cornerstones in ADS development.

Thermohydraulic Problems of an ADS

Heavy liquid metals are favored worldwide as coolants for the fuel element array and the spallation target. Their ability to be employed as coolant and spallation material allows the use of simple spallation target or window geometries.

Spallation reactions in the fluid release large quantities of heat on the order of 1000 W/cm^3. Reliable heat transfer from the spallation region of the target at all times in plant operation poses one of the biggest technical challenges in spallation target design. In addition, the design of a complete ADS, with all its accessory components, requires detailed knowledge of the thermohydraulic behavior of heavy liquid metals in all nominal and disturbed plant states. It is therefore of fundamental importance in thermohydraulic design of plant components to make available numerical tools and experimental platforms by which to determine reliably the velocity and temperature distributions of the heavy liquid metal flow within the components.

The main subject of thermohydraulic activities at the Karlsruhe Research Center therefore consists in providing an experimental database and reliable analytical tools by means of which to design the ADS components.

The basic physics experiments as well as component experiments are carried out at the KALLA Heavy Liquid Metal Laboratory of the Karlsruhe Research Center. The KALLA laboratory is a modular structure consisting of three liquid metal loops of different sizes and for different purposes: THESYS, THEADES, and CORRIDA (see also http://www.kalla.fzk.de).

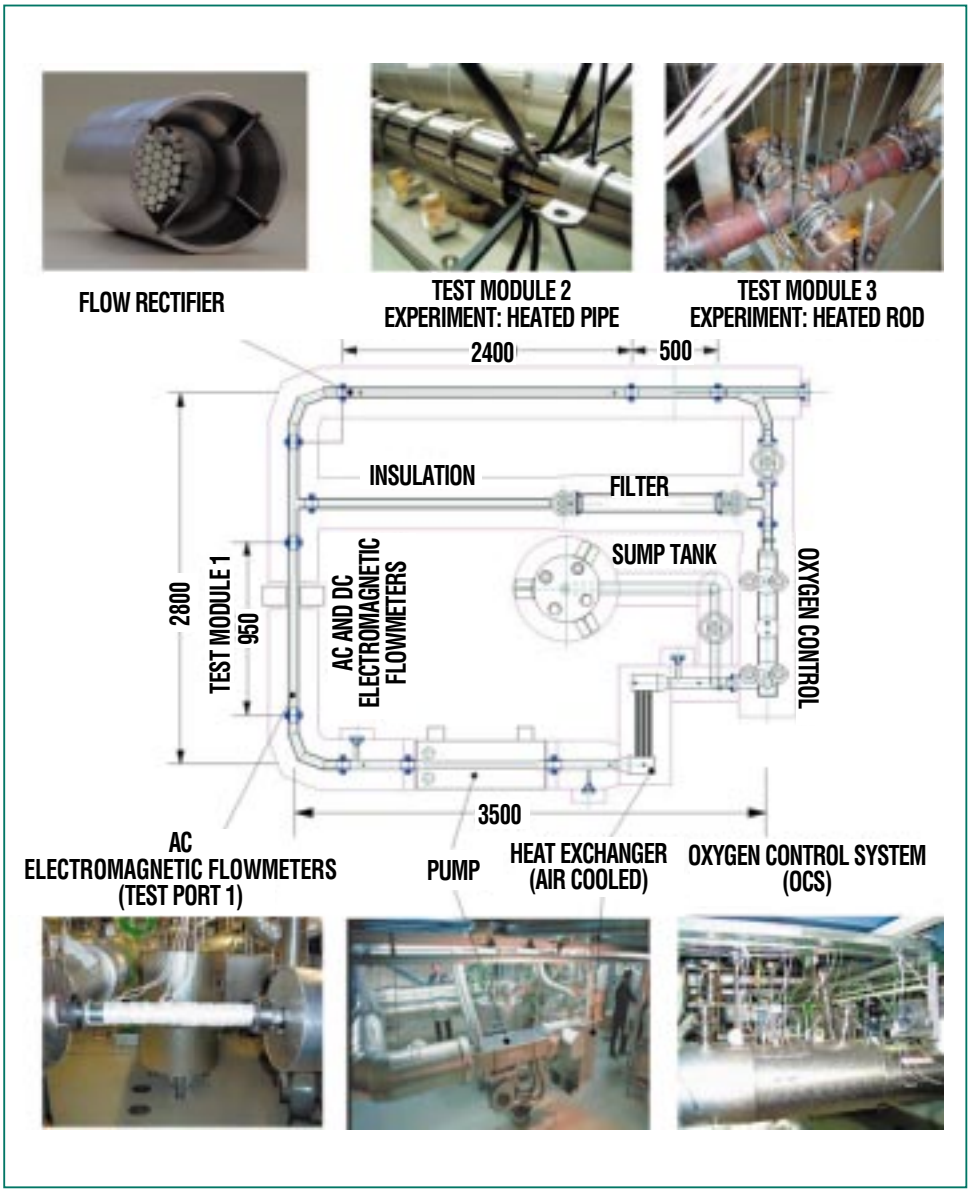

Fig. 4: Semitechnical view and photographs of the THESYS liquid-metal loop of the KALLA laboratory of the Karlsruhe Research Center.

A semi-technical sketch of the THESYS loop is shown in Fig. 4. Over 20,000 hours of operation, this unit has demonstrated the reliable, failsafe feasibility of a loop operated on a heavy liquid metal.

The large THEADES (THErmal-hydraulics and ADS DESign) liquid metal loop is used for thermohydraulic studies of complete components of an ADS on a geometrical scale of 1:1. The findings generated within a specific geometry, on the one hand, serve to verify numerical simulations and, on the other hand, to support individual subsegments of systems design.

The research activities of the technology experiments performed in the THEADES loop lie in the following main areas of interest:

(1) Coolability of a beam window in different geometric configurations.

(2) ADS-related fuel element development.

(3) Preparation of a thermohydraulics database.

(4) Development of physics models and verification of numerical computation methods.

The THEADES loop, whose performance characteristics and schematic layout are shown in Fig. 5, was commissioned first in November 2002 and has since proven its merits in the execution

of two large-scale experiments on the MEGAPIE spallation target.

Behavior of Structural Materials in Lead-Bismuth Loops

The design, construction, and planned demonstration phase of ADS facilities require detailed studies of the suitability of structural materials in a eutectic Pb-Bi flow at high plant temperatures of approximately 550°C. Earlier studies have shown that Pb-Bi can be very corrosive to austenitic and also ferritic-martensitic steel grades [9]. Especially because of the high solubility of iron, chromium and, above all, nickel in Pb-Bi, any solution attack on these steel grades must be avoided absolutely. This corrosive attack could lead to a complete loss of structural integrity and, thus, component failure.

Protective oxide coatings can prevent dissolution attack on steel to such an extent that corrosion is reduced to a level ensuring a sufficiently long life of structures [10]. Preconditions for persistent protective action of these oxide coatings are both sufficient density and inhibition of the diffusion of metal ions, and stability of these layers and adhesion to the structural material. These characteristics are determined largely by the composition of the alloy making up the active surface coating. Long-term stability of the oxide coatings can be ensured only if the oxygen potential in the liquid Pb-Bi is in a range in which the oxides on the steel surface will not be decomposed. On the other hand, it must not be so high as to cause lead oxide to be precipitated and deposited in the loop. This requires continuous monitoring of the oxygen concentration in Pb-Bi [11, 12].

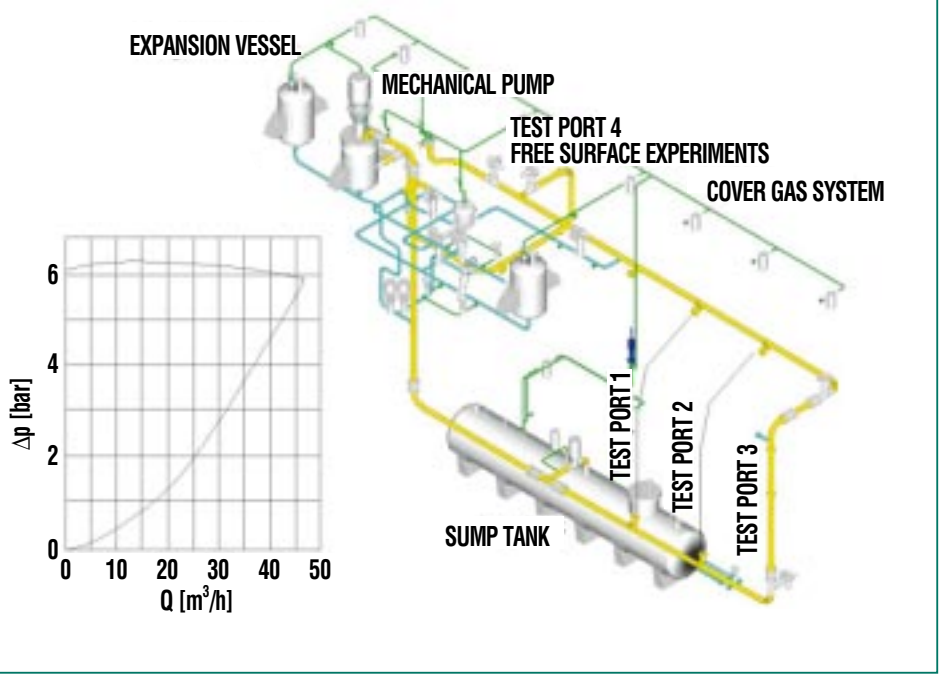

Fig. 5: Performance characteristics of the THEADES loop in the KALLA laboratory (left), and schematic representation of the associated piping system with the test ports 1 – 4 run in parallel (right).

Intensified formation of protective coatings is achieved by incorporating into the surface stable oxide forming substances, such as aluminium, Al. They ensure that dense, slowly growing oxide coatings of Al_2O_3 are generated which remain stable even at temperatures above 550°C and thus protect components under high loads and stresses. The incorporation of Al in the materials surface is achieved preferably by the GESA process [13]. In this case the Al, which had been precipitated on the surface first, is alloyed to a depth of 10 – 15 µm by remelting the surface with a pulsed electron beam.

Test Facilities

The CORRIDA loop for studies of the behavior of structural materials contains approximately 100 l of liquid Pb-Bi circulated by an electromagnetic pump at 3.5 m^3/h (see Fig. 6). In the loop extending over two stories, the liquid Pb-Bi is circulated continuously over a total pipe length of approximately 36 m at temperatures between 400 and 550°C at a rate of 3.5 m^3/h, in which operation several temperature gradi-

ents are passed as preset by the loop components.

In the direction of flow, the melt at 400°C is first heated to 510°C in the countercurrent flow heat exchanger. In the two series-connected superheaters heated electrically, the melt is then raised by 20 K each to the maximum loop temperature of 550°C. After having passed the two test sections at 2 m/s, the Pb-Bi reaches the oxygen control box. At this point, it is brought into an equilibrium at 550°C with a flow of Ar containing H_2 and H_2O in an 0.4:1 ratio. A device developed at the Karlsruhe Research Center is used to condition the gas [14]. Afterwards, the oxygen concentration in Pb-Bi amounts to 10^{-6} wt.%. Oxygen activity in the melt is measured by probes using YSZ (yttria-stabilized zirconia) as the electrolyte [6]. At the present time, test specimens covering a period of 2000 h are available from this loop which do not differ greatly from the results so far obtained from experiments with stagnant Pb-Bi. Because of their Ni content, austenites can be used only up to temperatures below 500°C even under the most favorable conditions with respect to oxygen activity in the liquid metal and a period of use of >10,000 h. Martensitic steel grades show a slightly more favorable behavior and can be used up to somewhat higher temperatures of 550°C. All steel grades alloyed with Al in their surfaces by means of the GESA surface remelting process developed at the Karlsruhe Research Center exhibit excellent behavior over the entire temperature range.

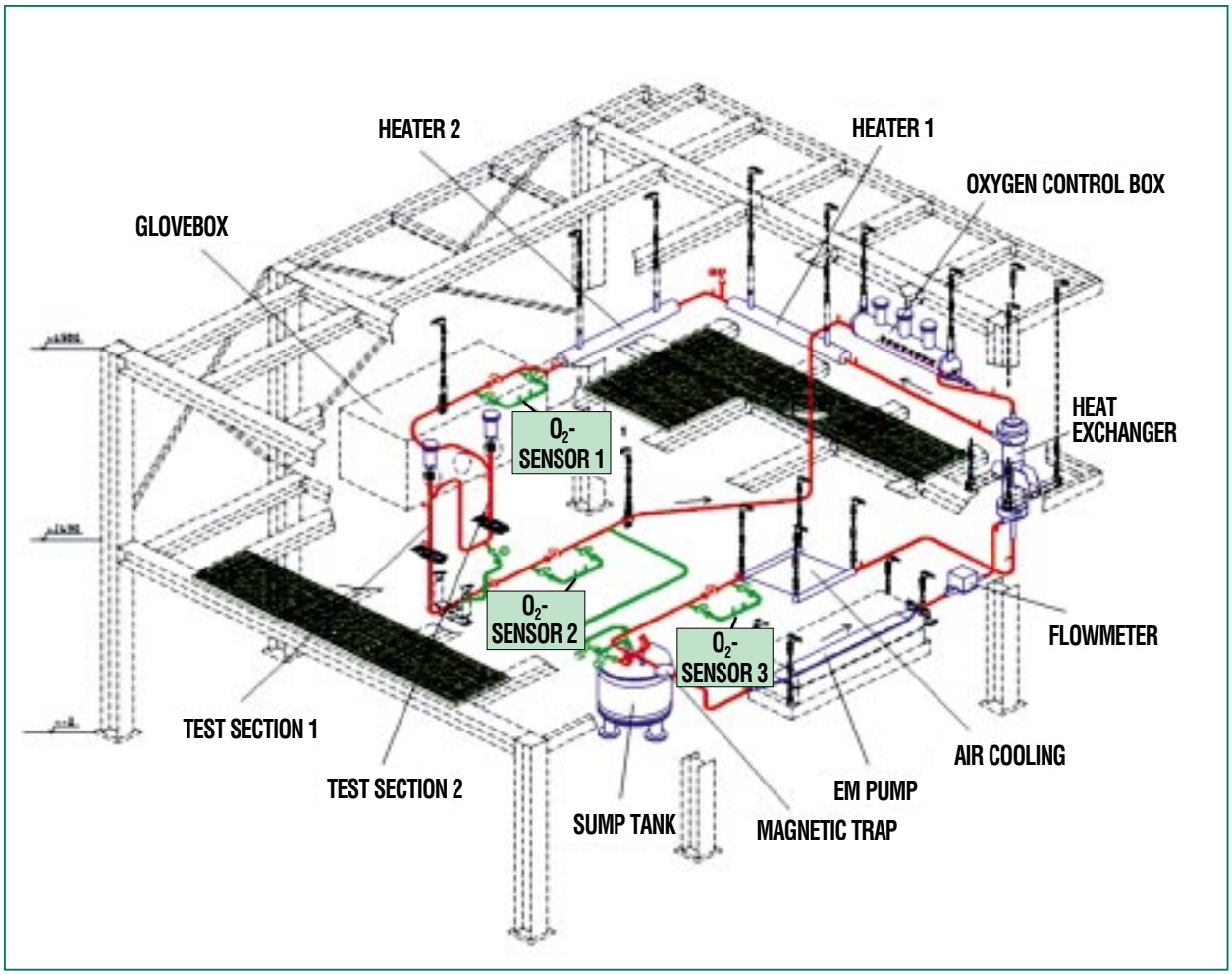

Fig. 6: Schematic representation of the components of the CORRIDA loop.

Summary

Partitioning and transmutation (P&T) opens up a new perspective of transforming longlived radionuclides into shortlived and stable elements, respectively, and in this way reducing to a technically manageable period of time the long-term hazard potential associated with them. At the present state of knowledge, accelerator-driven systems are expected to show good rates of incineration and transmutation.

The most important strategic cornerstones of systems development are fuel development, development of the technology of liquid metals as coolants, and development of suitable structural materials. In addition, there are a number of open questions with respect to steady-state neutron physics design and evaluation in terms of technical safety of the new systems designs, the solution of which is furthered by the research activities of the Karlsruhe Research Center. All these activities are part of work carried out and supported within the framework of the EU Research Program.

Literature

[1] C.D. Bowman et al., *Nuclear Instruments and Methods, 1992, p. 336*

[2] G.J. van Tuyle, H. Takahashi, M. Todoscow, *BNL 52279, 1991*

[3] F. Carminati, R. Klapisch. J.P. Revol, J.A. Rubio, C. Rubbia, *CERN AT/93-47(ET), 1993*

[4] *The European Technical Working Group on ADS, A European Roadmap for Developing Accelerator Driven Systems (ADS) for Nuclear Waste Incineration, ENEA, April 2001*

[5] J.U. Knebel, G. Heusener, *Sonderheft Radioaktivität und Kernenergie, Forschungszentrum Karlsruhe, 2001*

[6] C.H.M. Broeders, R. Dagan, V. Sanchez, A. Travleev, *Proc. Reaktortagung Düsseldorf, 2004*

[7] R.J.M. Konings (ed), *EUR 19928 EN, Institute for Transuranium Elements, 2001*

[8] S. Pillon, P. Smitz, J. Wallenius, W. Maschek, *GLOBAL 2003, New Orleans, Nov. 16 – 20, 2003*

[9] G.Y. Lai, *ASM Int., Materials Park, OH 44073, 1990*

[10] R.C. Asher, D. Davies, S.A. Beetham, *Corrosion Sci., 17, 1977, p. 545*

[11] B.F. Gromov et al., *Liquid Metal Systems, Plenum, New York, 1995, p. 339*

[12] G. Müller, G. Schumacher, F. Zimmermann, *J. Nucl. Mater. 278, 2000, p. 85*

[13] G. Müller, *FZKA 6422, 2000*

[14] G. Müller, A. Heinzel, G. Schumacher, A. Weisenburger, *J. Nucl. Mater., 321, 2003, p. 256*

Geochemical Behavior of Radionuclides in the Multi-barrier System of a Nuclear Waste Repository

H. Geckeis, V. Metz, B. Kienzler, INE

Introduction

There is still no alternative to final storage in deep geologic formations for the safe disposal of high-level radioactive waste [1]. Isolating radioactive waste from the biosphere in a geologically stable environment over periods of several hundreds of thousands of years offers maximum safety, which cannot be guaranteed at present by other concepts, such as transmutation of longlived radionuclides into shortlived fission products. The development of multi-barrier systems is being pursued internationally (Fig. 1): A system consisting of several independent barriers is to prevent effectively the release of contaminants from the repository. The multi-barrier system is composed of

- the engineered barrier consisting, e.g., of vitrified waste (HLW glass) and spent nuclear fuel, respectively, and, if applicable, a thick-walled container;
- the geotechnical barrier consisting of materials minimizing the remaining voids in order to increase mechanical stability, prevent the penetration of solutions, and influence chemically any solutions which may have entered. In addition, these substances are to absorb radionuclides and achieve good heat transfer from the high-level radioactive waste. The selection of suitable materials depends on the host rock. For final storage in rock salt, mainly crushed salt is being considered while, for other host rock varieties, plastic clays, such as bentonites, are being discussed;
- the geologic barrier comprising the host rock and the caprock.

In order to achieve maximum safety over long periods of time for the repository, all barriers must be optimized. Research into the safety of nuclear repositories serves (1) to quantify as a function of geochemical conditions and, where possible (2), optimize by suitable measures the mobility and retention, respectively, of radionuclides in the different barriers. As no decision has as yet been taken in Germany about a specific host rock and a repository site, respectively, the Institute for Nuclear Waste Disposal (INE) is engaged in studying the processes relevant to final storage in rock salt, clay rock, and crystalline rock.

The examples referred to below will show how a suitable choice of geochemical buffer materials can significantly reduce the solubility of radionuclides in a saline repository, and how radionuclide migration in the fractured system of a crystalline host rock (granite) is influenced by the interaction of radionuclides with mineral surfaces and colloidal components of the groundwater.

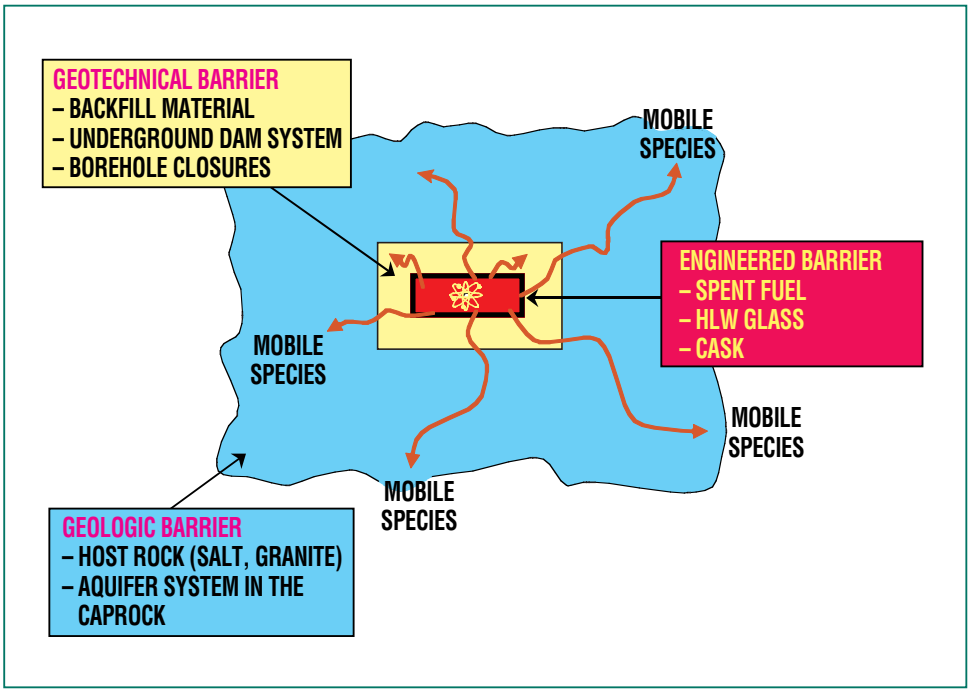

Fig. 1: Schematic representation of the barriers in a repository for radioactive waste.

Selection of a Geochemical Buffer Material as Demonstrated for the Asse Salt Mine

Between 1967 and 1978, approximately 125,000 casks con-

taining low-level radioactive waste and approx. 1300 casks containing medium-level radioactive waste, part of it from the Karlsruhe Research Center and the Karlsruhe Reprocessing Plant (WAK), respectively, were emplaced in this former salt mine. At present, the activity inventory amounts to approx. 10^{15} Bq, comprising approximately 120 t of uranium, 80 t of thorium, and 12 kg of plutonium. Since 1992, the open cavities outside the emplacement chambers have been filled up with crushed salt. Decommissioning the mine requires an integral demonstration of long-term safety for the radioactive materials emplaced, which includes statements about radionuclide mobilization and retention in the emplacement chambers (Fig. 2).

The scenario used to demonstrate long-term safety is based on the assumption that the present access of solutions (11 – 12 m^3 a day) cannot be reduced by technical means, and the remaining cavities and porous spaces in the backfilling therefore will be flooded. The solution currently entering is saturated with NaCl. As a consequence of the existence of highly soluble $KMgCl_3 \cdot 6\ H_2O$ (carnallite) in the deep levels of the salt mine, redissolution processes occur which could impair the mechanical stability of the Asse mine. To avoid these dissolution processes, the remaining voids will be filled up with a saturated $MgCl_2$ solution as a so-called "protective fluid" [2]. As this solution will contact the waste forms emplaced, there is great interest in improving radionuclide retention by specific additives.

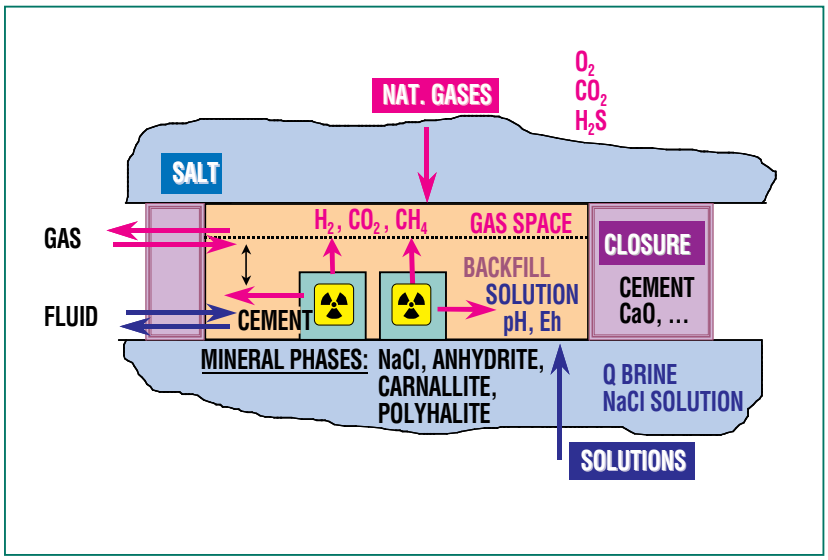

Fig. 2: Demonstration of the long-term safety of the Asse salt mine requires the interactions to be taken into account which exist between the cemented radioactive waste forms, any solutions and gases potentially entering, the mineral phases in the environment, backfill material, and closure material. The chemical and microbial reactions give rise to secondary mineral phase and gas formation and also to the composition of the solution being changed, which has a decisive influence on radionuclide behavior.

The choice of a suitable material is based on geochemical equilibrium calculations. The chambers were treated as "quasi-closed systems" for which the anticipated geochemical environment, i.e. the composition of solutions and of the newly produced solid phases, the pH, the gas phases, and the resultant radionuclide concentrations, were calculated by means of the EQ3/6 geochemical equilibrium code [3] [4]. The code allows modeling of highly concentrated brines by means of Pitzer's ion interaction model [5]. One precondition for reliable results to be obtained from these model calculations is a reliable database.

Important input data for the model calculations are the standardized inventories of the materials in the emplacement chambers relative to the volumes of solutions accessing. In total, more than 30,000 t of Portland cement, about 1000 t of nitrate salts, and approx. 2800 t of carbon bound in organic compounds (as components of radioactive waste) are emplaced. The organic material can be decomposed into CO_2 gas by means of microbes consuming nitrate as an energy source; this carbon dioxide gas is in equilibrium with the solutions as a function of the systems pressure in

the mine. This equilibrium decreases the pH of the solution unless a suitable buffer material is present. Although the presence of cement and magnesium (Mg^{2+}) in the solutions causes buffering and precipitation, respectively, of solid carbonate phases, the quantities of Ca^{2+} and Mg^{2+} are not sufficient in some chambers to prevent the pH from dropping into the acid range (pH < 4). As a consequence, the solubility of the uranium, plutonium, and thorium would increase by several orders of magnitude. To avoid this acidification, INE proposed to introduce into the chambers a buffer material based on brucite/Sorel cement ($Mg(OH)_2$ + $MgCl_2$ solution). This material will form a solid remaining in the chambers even in case of flow processes. In the long term, this material guarantees a pH in the range of 8. In this pH range, the solubilities of actinides are low. In addition, the magnesium contained in this buffer material binds the carbonate, thus preventing the formation of soluble carbonate complexes of the actinides and the production of carbonic acid, respectively.

In order to verify these model calculations, an extensive experimental program was carried out. The experiments comprised

- the evolution of the geochemical environment and of the pH in the presence of the Mg buffer material;
- demonstration of the precipitation of carbonate phases;

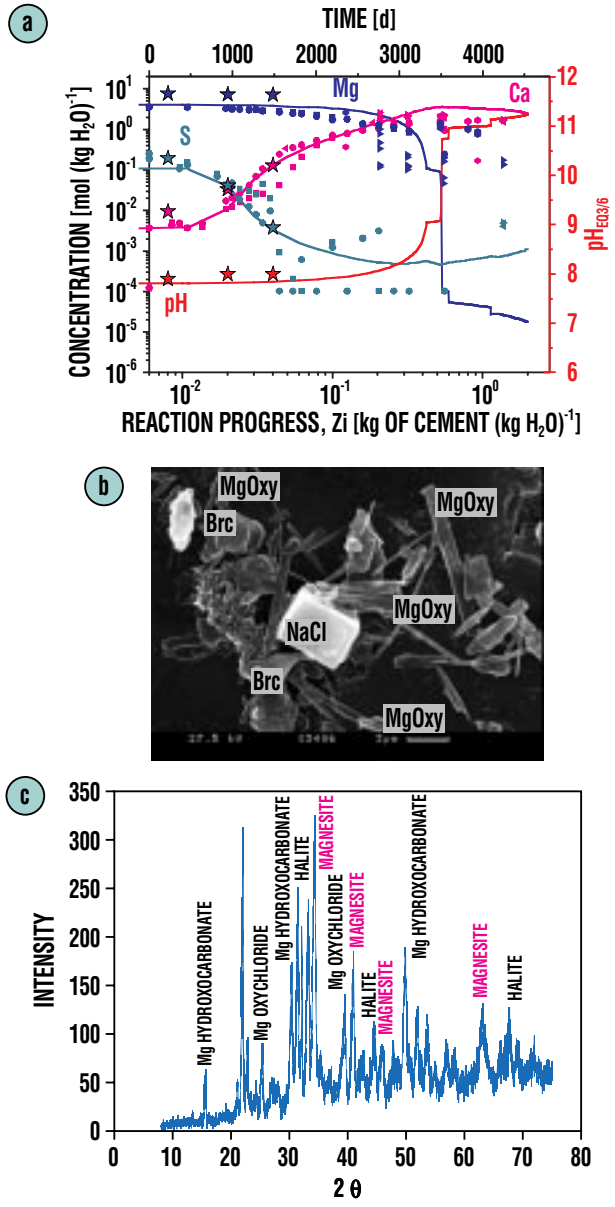

Fig. 3: The computed development of the solution composition (concentrations of dissolved species and pH) for the reaction of cemented waste simulates in a solution saturated with $MgCl_2$ (lines in Fig. (a)) is in good agreement with the development determined experimentally (symbols in Fig. (a)). The scanning electron micrograph (Fig. (b)) shows the main components of the buffer material, brucite (Brc), Mg oxychloride (MgOxy), and halite (NaCl). The precipitation of solid carbonate phases, such as magnesite and Mg hydroxocarbonate, as a result of the reaction of the buffer material with CO_2 gas and a solution saturated with $MgCl_2$ is demonstrated also in the X-ray diffractogram (Fig. (c)).

- the influence of the Mg buffer material on the solubility and sorption of radionuclides.

The agreement achieved between calculations and experiments was very high [2, 6], and a corresponding Mg buffer material is to be introduced into the storage chambers of the Asse salt mine within the framework of final decommissioning.

Radionuclide Migration in Fractured Granite

Several international projects with various partner organizations are devoted to studies of radionuclide migration in saturated fractures in granite. For this purpose, experiments were conducted in laboratories and in underground laboratories under in-situ conditions in Sweden (Äspö HRL, SKB) and Switzerland (Grimsel GTS, NAGRA).

Geochemical reactions can cause both mobilization and retention of radionuclides. Sorption reactions, such as ion exchange or surface complexing at the mineral-groundwater interface, retard radionuclide transport relative to the groundwater flow up to the point of radionuclide immobilization as a result of incorporation into newly formed mineral phases. Actinide ions in an oxidized form, such as $Np(V)O_2^+$, which are highly mobile in natural waters, can be reduced to Np(IV) in contact with minerals containing Fe(II). This clearly reduces the solubility and mobility of Np. Figure 4 shows results of a photoelectron spectroscopic (XPS) examination of $Np(V)O_2^+$ sorption onto natural granite (Äspö, Sweden) [7]. The pictures and the associated spectra show that Np is sorbed almost exclusively at those points where also Fe(II) can be found, and that it is sorbed or reduced to a solid Np(IV) phase, respectively.

On the other hand, sorption onto groundwater colloids can cause radionuclide mobilization. Groundwater colloids consist of organic degradation products (humic acids, fulvic acids) or mineral particles in a size range of 1 – 1000 nm. Specific geochemical conditions, such as low ionic strength and high pH, favor the production of colloidal solutions. Incorporation in, or sorption onto, colloids with large specific surfaces mobilize especially those radionuclides, such as the actinides Pu and Am, which, because of their pronounced sorption characteristics and low solubility, respectively, normally are considered not very mobile. Figure 5 shows breakthrough curves for various radionuclide ions as obtained in an in-situ experiment in the Grimsel, Switzerland rock laboratory [8]. Radionuclides together with clay

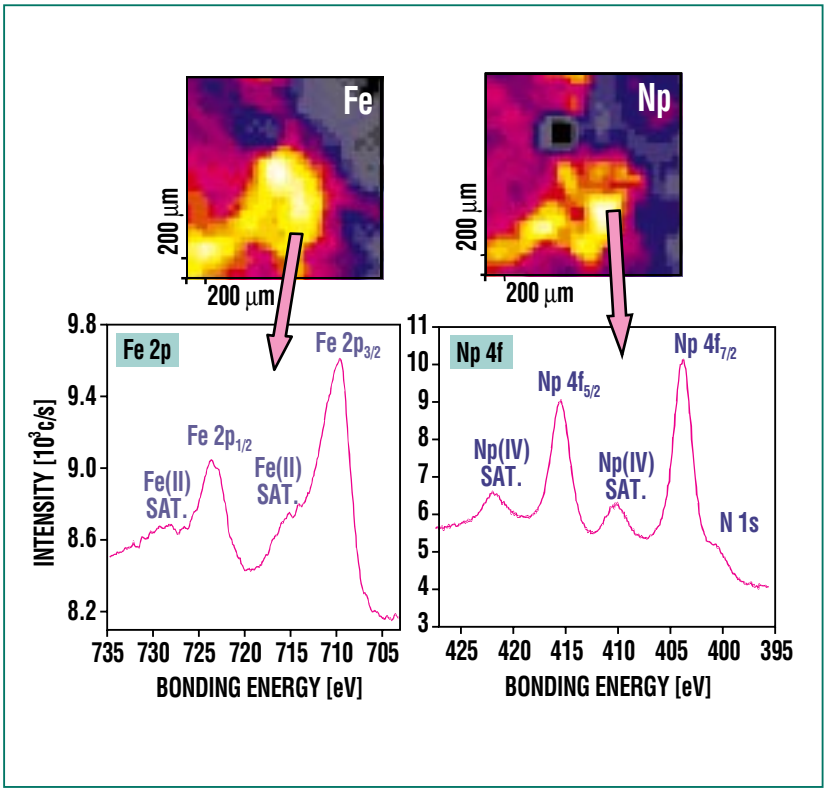

Fig. 4: Studies of the sorption of Np(V) onto a granite specimen (Äspö, Sweden). The distribution of elements measured by photoelectron spectroscopy (XPS) shows Np to be sorbed mainly onto mineral phases containing Fe(II). The XPS spectra allow the determination of oxidation states of Fe (divalent) and of the Np sorbed (tetravalent).

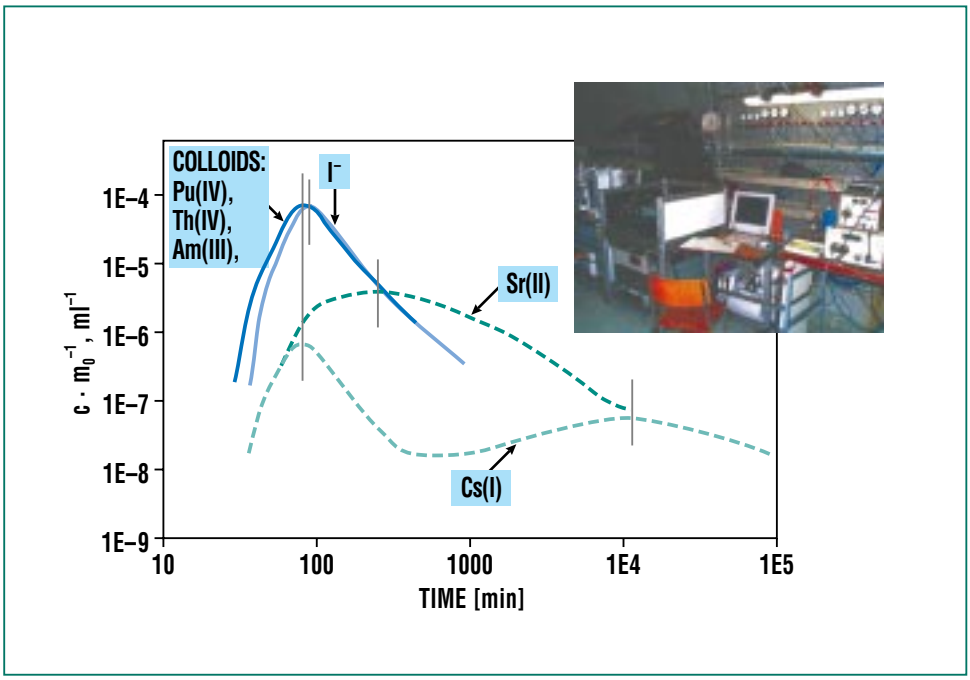

Fig. 5: Migration behavior of colloids, Am (III), Pu/Th(IV), I^-, Sr(II), and Cs(I) in a granite fracture (Grimsel, Switzerland). The colloid and radionuclide concentrations, c, were normalized to the total quantity injected, m_o, which makes them directly comparable. The photograph in the insert in the upper right hand corner shows the experimental setup for tracer detection in the rock laboratory. The unit in the middle is the mobile LIBD arrangement for colloid measurement [9, 10].

colloids were injected into a natural shear zone, and their migration behavior was studied by analyzing the groundwater at the outlet of the granite fracture. While Sr(II) and a large part of Cs(I) were retarded by sorption onto the rock surfaces and, consequently, eluted from the fracture with some delay, the trivalent and tretravalent actinides, Am(III), Pu(IV), Th(IV), and a small fraction of Cs(I) showed a different behavior. They were bound to clay colloids and were transported through the migration zone almost completely and without any delay. Radionuclides bound to colloids migrated even a bit faster than non-sorbing tracers, such as I^-, as a result of the exclusion of colloids from penetrating into rock pores. In order to be able to measure the colloids, which were present partly in the concentration range of µg/l, a mobile arrangement for colloid detection by means of laser induced breakdown (LIBD) developed at INE was used. LIBD allows very small colloids to be measured (diameter ~ 10 nm) down to concentrations below 1 ng/l [9, 10].

Consequently, one important criterion for judging the caprock as a barrier against radionuclide migration is the overall influence of the prevailing geochemical environment on radionuclide migration. In contrast to the near field of the repository, optimization in this case can be achieved only by careful choice of the repository site. Thus, higher salinity and pH levels of ~7 in the groundwater reduce the stability of many groundwater colloids due to their surface charge characteristics [11]. This decreases the relevance of colloidal radionuclide transport. Low permeability to water of the caprock, together with the low flow velocity of the groundwater, cause increased radionuclide sorption, which is further enhanced by diffusion of the dissolved radionuclide species in rock pores.

Fundamental understanding of the geochemical processes going on in the near and far fields of a repository allows mathematical models to be developed which enable forecasts to be made of the long-term behavior of dissolved radionuclides. In addition, problems can be identified in this way which may be solved, for instance, by exerting specific influences on the geochemical environment in the near field of the repository.

Literature

[1] *Auswahlverfahren für Endlagerstandorte, Empfehlungen des AKEnd-Arbeitskreis Auswahlverfahren Endlagerstandorte, December 2002 (www.akend.de)*

[2] V. Metz, W. Schüßler, P. Vejmelka, A. Bauer, J. Lützenkirchen, B. Kienzler, *Conference Proceedings of the 9th International Conference on Chemistry and Migration Behaviour of Actinides and Fission Products in the Geosphere, Migration '03, Gyeongju, Korea, September 19 – 26, 2003*

[3] T.J. Wolery, *EQ3NR, A Computer Program for Geochemical Aqueous Speciation Solubility Calculations: Theoretical Manual, User's Guide and Related Documentation (Version 7.0), UCRL-MA-110662 PT III, 1992*

[4] B. Kienzler, V. Metz, *Conference Proceedings of the International High-Level Radioactive Waste Management Conference, IHLRWMC 2001, Las Vegas, 2001*

[5] K.S. Pitzer, *in: Activity Coefficients in Electrolyte Solutions, R.M. Pytkowicz, ed., CRC Press, Inc., Boca Raton Fl., 1979, vol. 7, pp. 157 – 208*

[6] V. Metz, W. Schüßler, P. Vejmelka, J. Lützenkirchen, B. Kienzler, *Conference Proceedings of the 9th International Conference on Radioactive Waste Management and Environmental Remediation, Oxford, UK, September 21 – 25, 2003*

[7] B. Kienzler, P. Vejmelka, J. Römer, D. Schild, F. Enzmann, E. Soballa, M. Fuss, F.W. Geyer, T. Kisely, A. Görtzen, *2003 Actinide Migration Experiment in the Äspö HRL in Sweden: Results from Core # 5 (Part III), FZKA-6925, December 2003*

[8] A. Möri, W.R. Alexander, H. Geckeis, W. Hauser, Th. Schäfer, J. Eikenberg, Th. Fierz, C. Degueldre, T. Missana, *Colloids & Surfaces, 217, 2003, pp. 33 – 47*

[9] W. Hauser, H. Geckeis, J.I. Kim. Th. Fierz, *Colloids & Surfaces, 203, 2002, pp. 37 – 45*

[10] C. Walther, W. Hauser, H. Geckeis, Th. Fanghänel *Nachrichten, 35, 2003, pp. 179 – 84*

[11] W. Hauser, R. Götz, H. Geckeis, B. Kienzler, *In-situ Colloid Detection in Granite Groundwater along the Äspö Hard Rock Laboratory Access Tunnel. In: M. Laaksoharju (ed.), Äspö Hard Rock Laboratory: Status Report of the Colloid Investigation Conducted at the Äspö HRL During the Years 2000 – 2003, Swedish Nuclear Fuel and Waste Management Co. (SKB), International Progress Report, IPR-03-38, 2003*

Aquatic Chemistry and Thermodynamics of Actinides

R. Klenze, Th. Rabung, V. Neck, Th. Fanghänel, INE

Introduction

The work performed at INE in a geochemically-based approach to the long-term safety analysis of final storage (see contribution about multi-barriers) focuses on nuclear fuels and on the transuranium elements, respectively, produced by neutron capture in the reactor. Chemically, these elements are part of the actinide series, i.e., the thorium, protactinium, uranium, neptunium, plutonium, americium, curium elements following after actinium, and seven other elements. Why this interest in actinides for an analysis of long-term safety? While the radiotoxicity potential of high-level radioactive waste arising from nuclear fission is dominated by the fission products (β- and γ-emitters) for roughly 300 years, Pu and the minor actinides (Np, Am, and Cm), and their disintegration products determine the potential over a period of hundreds of thousands of years. This is due to the longlived nuclides of the transuranium elements (e.g. Pu-239: 24,000 years) and the twenty times higher dose factor of α-emitters compared to β- and γ-emitters. As transuranium elements do not occur in nature in any sizable quantities, no direct knowledge exists of their geochemical behavior over geologic time periods, as is the case for stable elements. Another reason for focusing research at INE on actinides is seen in the fact that there are only very few institutions worldwide where transuranium elements can be handled.

In actinides, the 5f shell is filled up with electrons in an analogous way to the 4f shell of the lanthanides. While most lanthanides exist in the trivalent state, the lighter actinides have oxidation levels between III and VII, exhibiting a correspondingly complex chemical behavior. Figure 1 shows the known oxidation states of the light actinides and those which are stable in an aqueous medium. One characteristic of actinide chemistry are the dioxo cations with a linear O = An = O (An: actinide) structure which are present in the V-VI oxidation states, and the highly charged trivalent and tetravalent cations coordinating preferably with "hard" bases, such as F^-, OH^-, and CO_3^{2-}, through electrostatic interaction.

To quantify actinide releases from the repository in case of water ingress, and the migration of these actinides along an aqueous propagation path into the biosphere, the mobilizing and the immobilizing reactions must be considered. The former include dissolution, complexing, and colloid formation, while the latter comprise the precipitation of pure and secondary mixed phases as well as sorption onto mineral surfaces. The mobilizing reactions of tetravalent actinides will be discussed below for the example of ternary hydroxo-carbonate complexes. When discussing immobilizing reactions, a more detailed account will be given of sorption reactions as explained by the example of

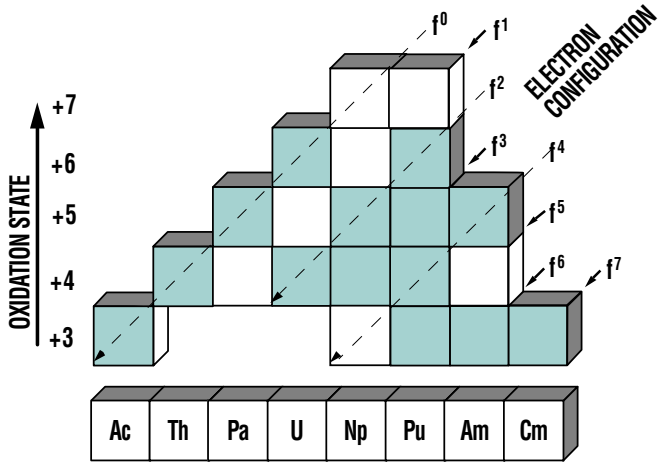

Fig. 1: Familiar oxidation states (+3 to +7) of the light actinide ions and their respective electron configurations (i.e. numbers of 5f electrons). The oxidation states stable in an aqueous solution are shown in color. The chemical behavior of actinides in the geosphere depends primarily on the oxidation states present under the given geochemical conditions. The complexity of aquatic actinide chemistry is apparent from the large number of oxidation states, some of which exist side by side.

laser spectroscopic examination of the boundary phase reactions of Cm(III) on sapphire single-crystal faces.

Reactions Determining Actinide Solubility in an Aquatic System

Geochemical modeling of actinides in systems related to repository conditions requires understanding aquatic chemistry and establishing a comprehensive thermodynamic database. Equilibrium constants for trivalent, pentavalent, and hexavalent actinides were elaborated for a broad range of boundary conditions of natural aquatic systems some time ago, especially also for concentrated brines of the type which can occur in a repository in salt formations.

A major gap in the thermodynamic database existed for the tetravalent actinides, for which only sparse and conflicting data were available even on such elementary reactions as hydrolysis. As a consequence, the chemical behavior of plutonium, which may exist in the III, IV, V, and VI oxidation states side by side in an aquatic system, cannot so far be described reliably in the environment. This lack of knowledge is due to the instability of highly charged ions in a not very acid or complexing medium. This results in the formation of polynuclear and colloidal solution species, respectively, and of sparingly soluble amorphous solid phases. It also makes studies difficult because of the pronounced sorption of ions onto the vessel walls. Moreover, sensitive spectroscopic speciation techniques, which can be used very successfully, for instance, with Cm(III) (see contribution about spectroscopic speciation of actinides), are available for tetravalent actinides only to a limited extent.

In recent years, extensive studies have been carried out at INE of the solubility and hydrolysis of the tetravalent actinides (Th, U, Np, and Pu) and the formation and stability of eigencolloids. This resulted in a consistent description of the reactions occurring [1 - 3]; the thermodynamic data were incorporated into international databases [4]. In neutral and alkaline solutions, solubility is determined always by amorphous oxyhydroxides, $An(OH)_4(am)$; compared to crystalline dioxides, $AnO_2(cr)$, their solubility is six orders of magnitude higher. It was also seen that the generation of An(IV) eigencolloids, i.e of dispersed $An(OH)_4(am)$ particles in the nanometer range, increases solubility by several orders of magnitude. These colloids are in equilibrium with ionic species and were seen to be surprisingly stable in the neutral to alkaline pH ranges even at higher ionic strengths.

Other actinide reactions increasing solubility result from complexing with substances contained in the water, such as chloride, sulfate, carbonate, phosphate, and natural organic compounds (humic substances), etc. Carbonate plays a special role because of its strong complex formation with actinides and its omnipresence in all kinds of water. Trivalent and pentavalent actinides only generate binary complexes, $An(CO_3)_n$, under relevant conditions [4]. For tetravalent actinides, however, because of the much more pronounced tendency to hydrolyze, also the formation of numerous ternary complexes with hydroxide and carbonate can be assumed:

$$An^{4+} + y\,OH^- + z\,CO_3^{2-} <=> An(OH)_y(CO_3)_z^{4-y-2z} \quad (1)$$

As it is possible, under different boundary conditions, that two or more complexes always exist side by side, the complex stoichiometries and complexing constants, $logb_{1yz}$, as proposed in the literature, are mostly uncertain [4]. Any reliable description of complexing in the An(IV)-OH-CO_3 ternary system requires experiments in which the OH^- and CO_3^{2-} ligands are varied over the widest possible range. Studies performed with redox-stable Th(IV) are discussed below.

On the one hand, solubility experiments were carried out with $Th(OH)_4(am)$ in 0.5 M $NaHCO_3$-NaCl solutions in a pH range of 4.5 – 7.5 in equilibrium with a CO_2 gas phase (open system). On the other hand, solubility in a closed system was studied in the pH range of 8.5 – 13.5 at constant total carbonate concentrations. Figure 2 shows the increase in solubility in carbonate solutions as against solutions containing no carbonate in open

and closed systems for the boundary conditions indicated.

The studies performed provide no indication of the formation of a carbonate-bearing solid phase; consequently, it may be assumed that $Th(OH)_4(am)$ is the phase determining solubility. The solubility product and the hydrolysis constants of Th(IV) are well known from previous studies [1 - 3]. The shaded area in Fig. 1b illustrates the scattering of experimental data caused by contributions by incompletely separated Th(IV) colloids.

Simultaneous fitting of the complexing constants, log β_{1yz}, according to Equation 1, to the experimental series shown in Fig. 2 and to comparable data from the literature [5] indicated that the solubility data can be described unequivocally by relatively few complexes (solid lines in Fig. 2). The $Th(OH)(CO_3)_4^{5-}$ complex (log $\beta^0_{114} = 35.8 \pm 0.3$) dominates solubility at pH 8 – 11 (Fig. 2b). Below $pCO_2 = 1$ and 0.1 bar, in addition also the $Th(OH)(CO_3)_2^{2-}$ (log $\beta^0_{122} = 37.0 \pm 0.4$) complex becomes dominant. In addition, only $Th(OH)_2(CO_3)^0$, $Th(OH)_3(CO_3)^-$, and $Th(OH)_4(CO_3)^{2-}$ furnish significant, though less important, contributions to solubility. Other ternary complexes as well as pure carbonate complexes, $Th(CO_3)_z^{4-2z}$, do not play a role under these conditions. The complexing system in the Th(IV)-OH-CO_3 ternary system can be seen in Fig. 3. The two most important ternary complexes, $Th(OH)(CO_3)_4^{5-}$ and $Th(OH)_2(CO_3)_2^{2-}$, lie on a diagonal between the binary species, $Th(OH)_4^0$ (dominating at low carbonate concentrations above pH 5) and $Th(OH)_5^{6-}$ (dominating at high carbonate concentrations [6]).

Analogous experiments are planned to derive corresponding complexes of Np(IV) and Pu(IV). The importance of ternary hydroxo-carbonate complexes compared to strictly binary complex species is relevant also to other complex ligands, such as humic substances, and takes a much greater effort in determining thermodynamic data than for

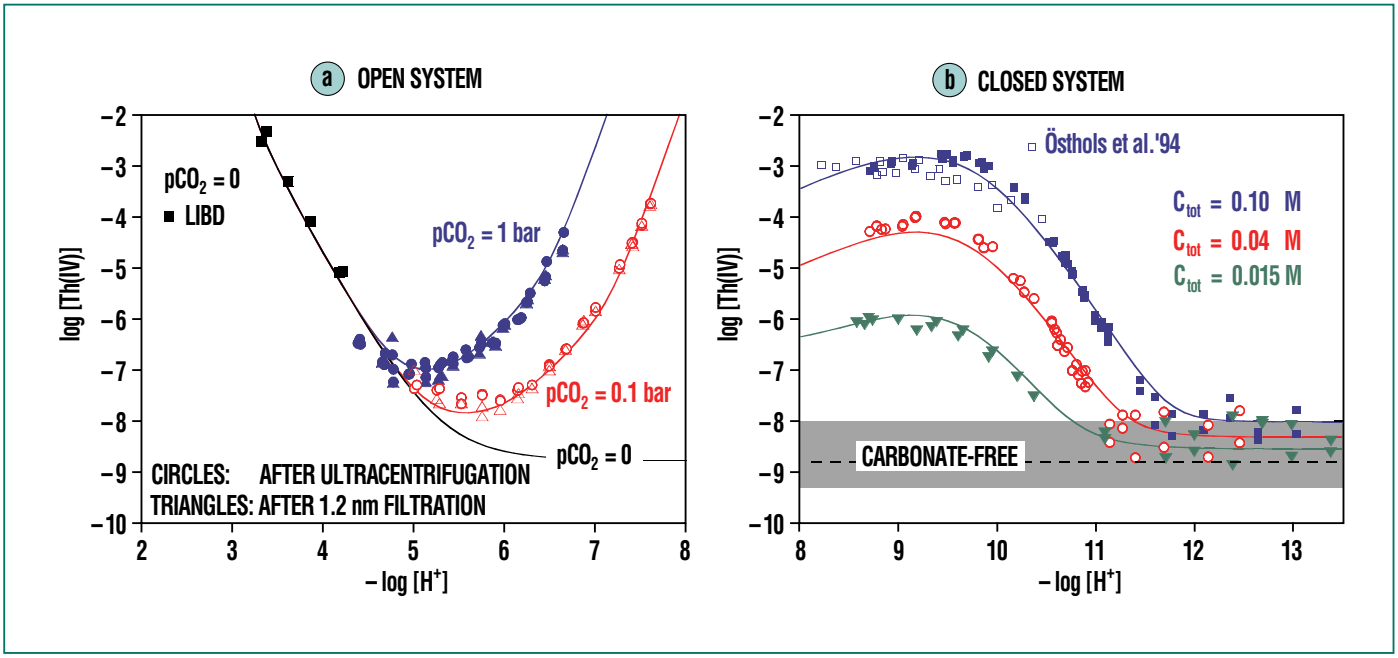

Fig. 2: Solubility of $Th(OH)_4(am)$ in a carbonate solution (I = 0.5 M, 22°C); (a) in the pH range of 3-8 at a CO_2 partial pressure, $pCO_2 = 1.0$ (blue), 0.1 bar (red) and, for comparison, carbonate-free (black); (b) in the pH range of 8-13.5 for total carbonate concentrations, ($C_{tot} = [HCO_3^-] + [CO_3^{2-}]$), of 0.1 (blue), 0.04 (red), and 0.015 M (green). Black squares in Fig. 2a: Solubility measurements by laser-induced breakdown detection (LIBD) under the exclusion of carbonate [1]; open squares in Fig. 2b: Östhols et al. [5]. The solid lines were obtained by simultaneous fitting of the experimental data, including the complexes mentioned in the text.

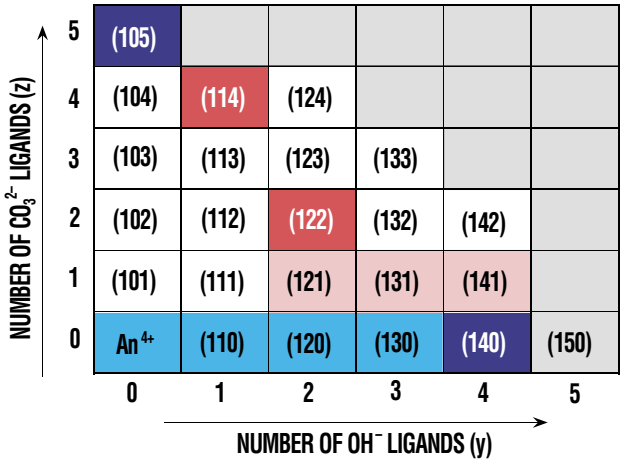

Fig. 3: Possible mononuclear complexes, (1yz) = $An(OH)_y(CO_3)_z^{4-y-2z}$. Dark boxes: dominant complexes in neutral and alkaline solutions (binary complexes in blue; ternary complexes in red); bright boxes: less important complexes, shaded: complexes unlikely for steric reasons and charge reasons, respectively.

other actinide oxidation levels. The important finding of this study, namely that only very few mixed complexes out of the many possible ones are relevant, opens up a perspective for calculating the relative stabilities of complexes, and estimating them, respectively, in theoretical approaches.

Interactions of Actinides with Mineral Phases

While the reactions discussed above determine the solubility and, hence, mobility of actinides in a given chemical environment, the interaction of actinides with mineral phases in the near and far fields of a repository in general results in retention or retarded transport. Most of these interactions so far have been described phenomenologically by a distribution coefficient, K_D, between the aqueous and the solid phases and taken into account in transport calculations. However, this sorption coefficient applies only to the given system and can be translated into other chemical boundary conditions only in a very limited way. Moreover, the K_D value encompasses different sorption mechanisms, such as ion exchange, specific adsorption to functional groups on the mineral surface, and surface precipitation and incorporation in secondary phases, all of which may have very different sorption and desorption kinetics. Quantitative descriptions of sorption in the absence of any knowledge of the processes going on therefore appear to be not very reliable. Over the past few years, thermodynamics-based sorption models have increasingly been used, such as the surface complexing model (SCM), which covers a broad range of pH levels and concentrations. Model fitting of hypothetical surface complexes is achieved by distribution coefficients determined as a function of pH and concentrations of metal and sorbent.

To test the reliability of SCM in all its variants when applied to actinide ions of higher valencies, the sorption of Cm(III) onto model mineral phases (amorphous SiO_2, γ-Al_2O_3, clay minerals, etc.) was investigated by time-resolved laser fluorescence spectroscopy (TRLFS) [7, 8]. It was seen that this allows direct differentiation among sorption mechanisms, such as ion exchange in clay interlayers, specific adsorption onto aluminol groups of γ-Al_2O_3, and clay minerals, as well as the incorporation of non-hydrated Cm ions into alumosilicates (see contribution about speciation). Moreover, the pH-dependence not only permits the usual pH-edge to be determined but also a differentiation to be made among various ternary surface complexes.

However, no information about the influence of heterogeneity of the binding sites and the interface potential, respectively, can be derived from sorption measurements of colloidal solid phases. Consequently, the studies were extended to single crystals with clearly defined crystal faces. Sapphire single crystals (α-Al_2O_3) were chosen as a suitable, easily available substrate because of their favorable spec-

troscopic properties and their model character for the spectroscopically inaccessible iron oxides. Sapphire wafers with different orientations ((018), (104), (012), (110), (001)) were cleaned thoroughly and characterized by various techniques (XPS, AFM, LEED). The orientation of UO_2^{2+} on the surface was determined by polarized X-ray absorption spectroscopy under a grazing angle of incidence (GI-XAFS) [9] while, for characterization of the functional aluminol groups, sum frequency IR spectroscopy was used (see contribution about speciation). Some preliminary results about interface reactions of Cm(III) will be discussed below.

Sorption of a Cm solution of 6.5×10^{-7} mol/l at pH 5.1 on the crystal faces of 1 cm^2 autoradiographically indicated a uniform cover, after two days of contact time, of 0.02 – 0.4 atoms/nm^2 for the different orientations. As is shown in Fig. 4, excellent emission spectra can still be obtained for a surface coverage of 0.2 – 2.0 % of the maximum binding capacity. Significant differences are found for Cm(III) on the (001) surface with respect to the peak position and fluorescence lifetime compared to the other four crystal surfaces, which have practically identical spectra and lifetimes. Analogous observations are obtained also by means of XPS. The quantity of Cm(III) sorbed strongly depends on the single-crystal faces. The highest sorption is found for the (001) surface, while the lowest sorption is found for the (018) orientation. Because of the very similar spectra for Cm(III) on the (001) surface and on colloidal γ-Al_2O_3 particles [4], the surface species can be assumed to be very similar. Most probably, they consist of γ-$Al(OH)_3$ formed on the surface as a result of contact with water [10]. This effect is much less pronounced for the other sapphire single-crystal surfaces. These preliminary results exhibit a large potential for obtaining fundamental insights into interface reactions by sensitive complementary spectroscopic methods.

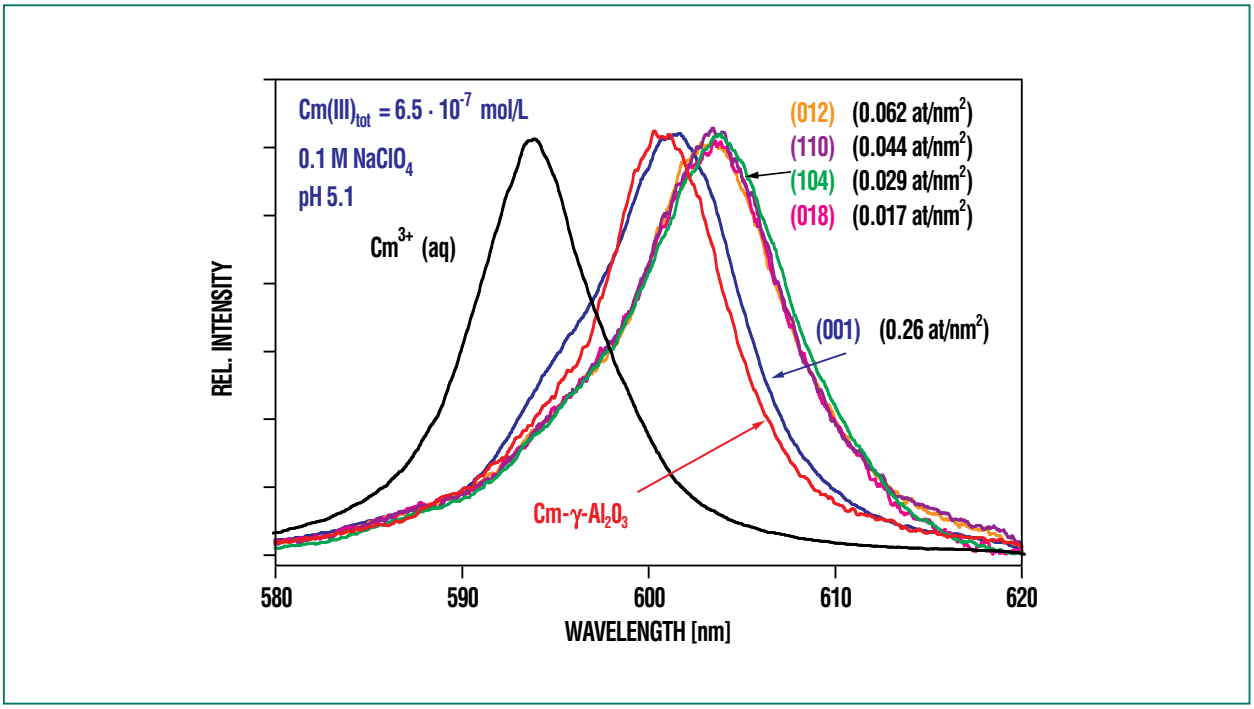

Fig. 4: Fluorescence emission spectra for Cm(III) sorbed at pH 5.1 to various sapphire single-crystal surfaces, (001), (110), (018), (012), and (104). The spectra have been normalized to identical peak heights. For comparison, the spectra are shown for free Cm^{3+}(aq) and for the first Cm(III) sorption species to γ-Al_2O_3 colloids [8].

Outlook

INE plays a leading role internationally in the speciation and thermodynamics of aquatic actinides. Its findings are incorporated in thermodynamics databases and constitute the basis of geochemical and reactive transport modeling for safety analyses. The importance of this line of research is underlined by the European Network of Excellence for Actinide Sciences (ACTINET), which is currently being built up and will serve to revive the actinide sciences by opening research facilities to universities and train highly qualified young scientists. INE together with ITU[1)], SCK-CEN[2)], and CEA[3)] as the coordinator is one of the main players in this network.

[1)] ITU: Institute for Transuranium Elements

[2)] SCK-CEN: Studiecentrum voor Kernenergie / Centre d'Étude Nucléaire

[3)] CEA: Commissariat à l'Énergie Atomique

Literature

[1] V. Neck, J.I. Kim, *Radiochim. Acta, 89, 2001, 1*

[2] V. Neck, M. Altmaier, R. Müller, A. Bauer, Th. Fanghänel, J.I. Kim, *Radiochim. Acta 91, 2003, 253*

[3] V. Neck, R. Müller, M. Bouby, M. Altmaier, J. Rothe, M. A. Denecke, J.I. Kim, *Radiochim. Acta 90, 2002, 485*

[4] R. Guillaumont, Th. Fanghänel, J. Fuger, I. Grenthe, V. Neck, D.A. Palmer, M.H. Rand, (OECD, NEA-TDB), *Chemical Thermodynamics, vol. 5, Update on the Chemical Thermodynamics of Uranium, Neptunium, Plutonium, Americium and Technetium. Elsevier, North-Holland, Amsterdam, 2003*

[5] E. Östhols, J. Bruno, I. Grenthe, *Geochim. Cosmochim. Acta, 58, 1994, 613*

[6] A.R. Felmy, D. Rai, S. M. Sterner, M. J. Mason, N.J. Hess, S. D. Conradson, *J. Solution Chem. 26, 1997, 399*

[7] H. Geckeis, R. Klenze, J. I. Kim, *Radiochim. Acta, 87, 1999, 13*

[8] T. Stumpf, T. Rabung, R. Klenze, H. Geckeis, J. I. Kim, *J. Colloid Interface Sci., 238, 2001, 219*

[9] M. A. Denecke, J. Rothe, K. Dardenne, P. Lindqvist-Reis, *Phys Chem Chem Phys, 5, 2003, 939*

[10] P. J. Eng, T. P. Trainor, G. E. Brown, G. A Waychunas, M. Newville, S. R. Sutton, M. L. Rivers, *Science, 288, 2000, 1029*

Spectroscopic Methods of Actinide Speciation

M. A. Denecke, P. J. Panak, M. Flörsheimer, INE

Introduction

One factor of decisive importance in assessing the long-term safety of high-level nuclear repository waste is the extent to which radionuclides released by the waste (for instance, as a result of an ingress of water) will migrate from the repository region into the biosphere, causing unacceptable exposure levels. Highly sensitive and selective spectroscopic methods are employed at the Institute for Nuclear Waste Disposal (INE) of the Karlsruhe Research Center to quantify radionuclide migration and elucidate the reactions and mechanisms involved. The focus of these investigations is on the migration behavior of actinides because, over very long periods of time, these are the radionuclides contributing most to the radiotoxicity of the waste. The spectroscopic methods used at INE constitute the latest state of the art and are continuously advanced and adapted to complex problems arising in actinide speciation.

Selected spectroscopic techniques will be presented in the sections below, and their application to problems of actinide speciation will be explained using current examples. The following will demonstrate how better understanding of reaction mechanisms through application of a combination of various methods is achieved.

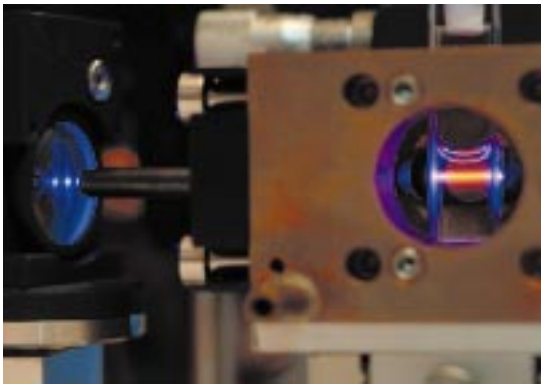

Fig. 1: Fluorescence emission of Eu(III).

Time-resolved Laser Fluorescence Spectroscopy (TRLFS)

Basic Principles: Time-resolved laser fluorescence spectroscopy is a speciation technique, which allows actinides to be characterized and quantified without disturbing the chemical equilibrium. One representative of trivalent actinide ions is trivalent curium (Cm(III)), which has excellent fluorescence spectroscopic properties and thus can be used for speciation studies down to the nanomol range. The method can be used both to characterize solution species and for speciation in suspensions and solids.

Besides quantification, TRLFS also provides information about the structure of the actinide complexes under study. The fluorescence emission spectra allow information to be obtained about the number and coordination of actinide species, while fluorescence lifetime measurements allow determination of the number of water molecules bound to the actinide in the inner coordination sphere. In the case of Cm(III), the exchange of bound water molecules for complexing ligands causes a red shift of the emission band and the fluorescence lifetime is increased. There is a linear relation between the reciprocal fluorescence lifetime and the number of water molecules in the coordination sphere of Cm(III).

Application of TRLFS Example: The production of hydroxyalumosilicate (HAS) colloids from dissolved mono- and polysilicic acids and aluminium ions and the incorporation of trivalent actinides, such as Cm(III) and americium (Am(III)), into the structure of colloids can lead to increased mobility of radionuclides in natural groundwaters. In-situ characterization of the Cm species during Cm incorporation into HAS colloids was performed by means of TRLFS as a function of pH_c in the range between 1.5 and 9.0. Analysis of the spectra shows that, in addition to the Cm^{3+} aquo ion, three Cm-HAS species, Cm-HAS*(1)*, Cm-HAS*(2)*, and Cm-HAS*(3),* are generated in the solution (Fig. 2a). The species distribution as a function of pH_c is shown in Fig. 3. At low pH_c levels, the Cm^{3+} aquo ion dominates. Cm-HAS*(1)* is produced above $pH_c = 4$, attaining a maximum relative amount at pH_c of 5.8. From $pH_c = 5$ onward, the second species is generated, Cm-HAS*(2)*. For pH_c-levels > 6.3, Cm-HAS*(3)* represents the dominant species. From measured fluorescence lifetimes, we find (Fig. 2b) that the number of coordinating water molecules drops from 9 for the Cm^{3+} aquo ion to 6.9 ± 1 for Cm-HAS*(1),* and to 6.5 ± 1 for Cm-HAS*(2).* This confirms that the production of Cm-HAS complexes is accompanied by an exchange of

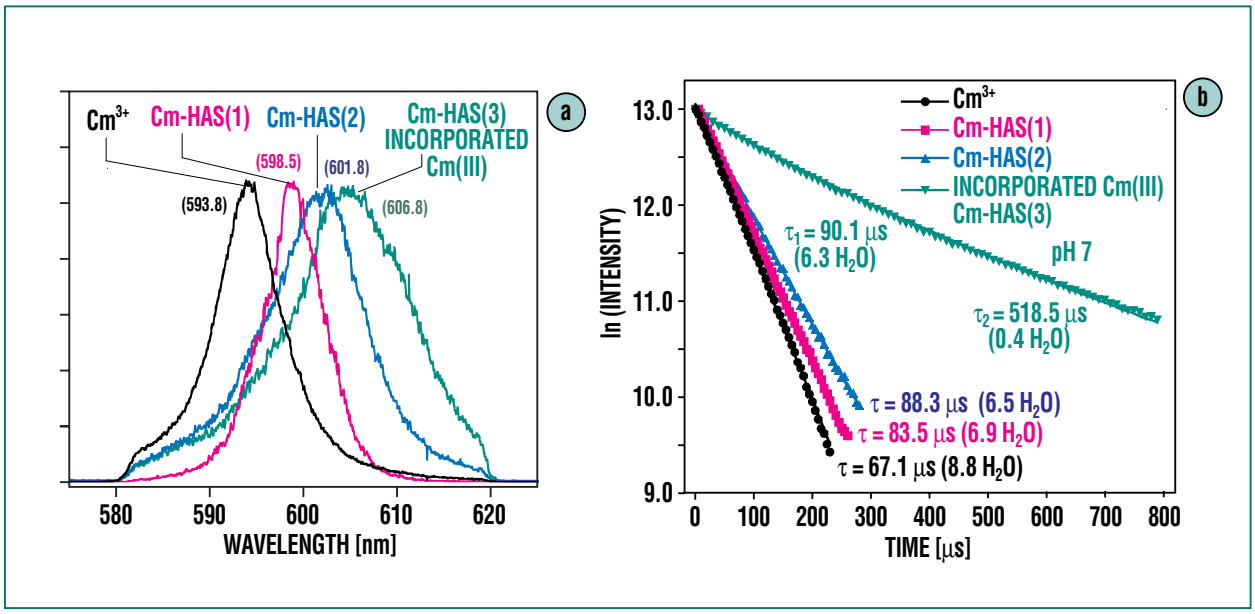

Fig. 2a (left) and 2b (right): Emission spectra and fluorescence lifetimes of the Cm(III)-HAS complexes.

water molecules. The Cm-HAS*(3)* species has a very long fluorescence lifetime corresponding to 0. 4 water molecules in the inner coordination sphere. This almost complete displacement of the water molecules proves that the Cm^{3+} cation is incorporated into the molecular structure of HAS. As long-term studies document the stability of the actinide-bearing HAS colloids even over long periods of time, there may be a significant increase in mobility of trivalent actinides in the pH_c range relevant to repository conditions.

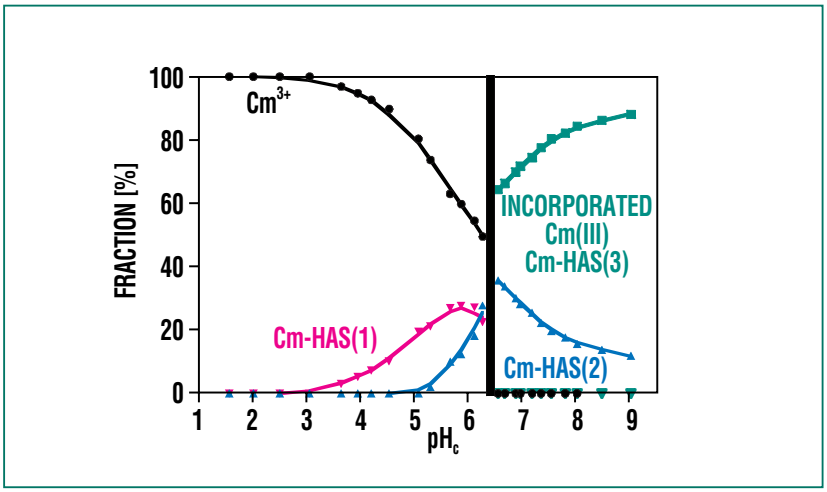

Fig. 3: Species distribution of the Cm(III)-HAS complexes as a function of pH_c.

X-ray Absorption Fine Structure Spectroscopy (XAFS)

Basic Principles: X-ray absorption spectroscopy is an element-specific method for determining structural short-range order, oxidation states, and the electron structures of atoms. In an XAFS experiment, the change in the absorption coefficient is registered as a function of varying energy of the X-radiation. The specimen is excited by high-intensity monochromatic synchrotron radiation from an electron or positron storage ring, such as ANKA at the Karlsruhe Research Center. XAFS spectra are subdivided into two energy regimes (Fig. 4): XANES (X-ray absorption near-edge structure) and EXAFS (extended X-ray absorption fine structure). The frequency and amplitude of

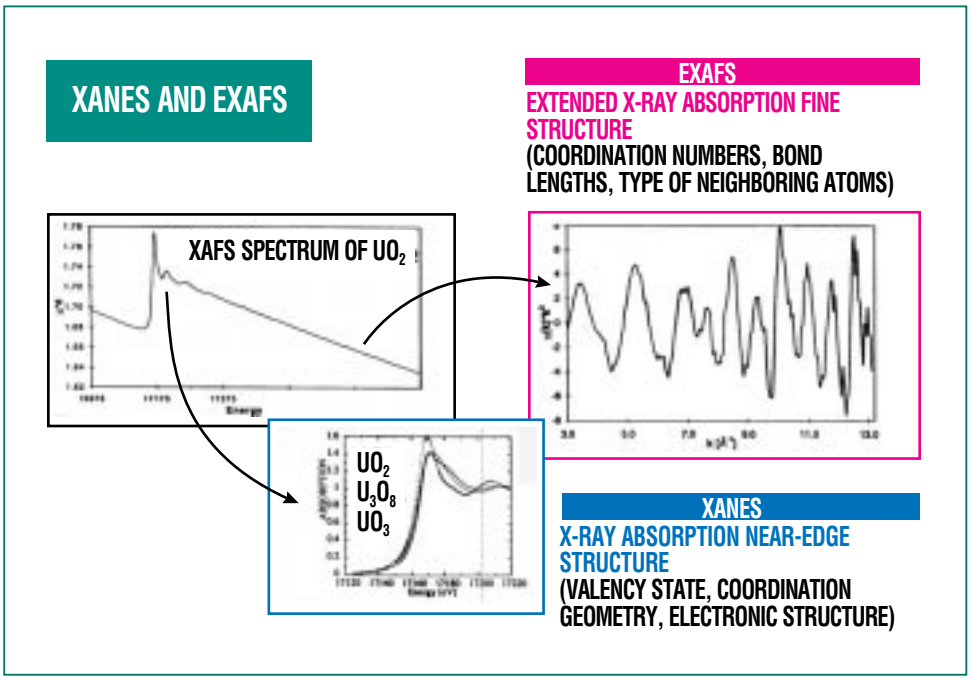

Fig. 4: Classification of X-ray absorption fine structure spectra into the XANES and EXAFS regimes and their information contents using the U L3 spectra of uranium oxides as an example.

the EXAFS oscillations contain information about interatomic distances (R) and the number (N) and type of neighboring atoms. The XANES region lies near photon energies close to the ionization potential of the element to be studied and contains valency state and coordination geometry information.

XANES Application Example: The influence of colloids on the transport behavior of actinide ions is a central research topic in the aquatic chemistry of the actinides in natural groundwaters. Humic substance (HS) colloids, for instance, may form complexes with actinide ions which are mobile in groundwater. Actinide-HS complexes can also be immobilized by coagulation and precipitation. In this study, we combined high-resolution XANES spectroscopy and STXM (scanning transmission X-ray microscopy) in order to elucidate the chemical properties of an HS aggregate, while simultaneously visualizing its morphology, before and after the addition of trivalent europium (Eu(III)) as a homologue of trivalent actinides [1]. The STXM image of HS at pH_c = 4.3 shows different structures, with particles and leafy morphologies embedded in a fibrous carbon matrix (Fig. 5a). After the addition of Eu(III), these structures

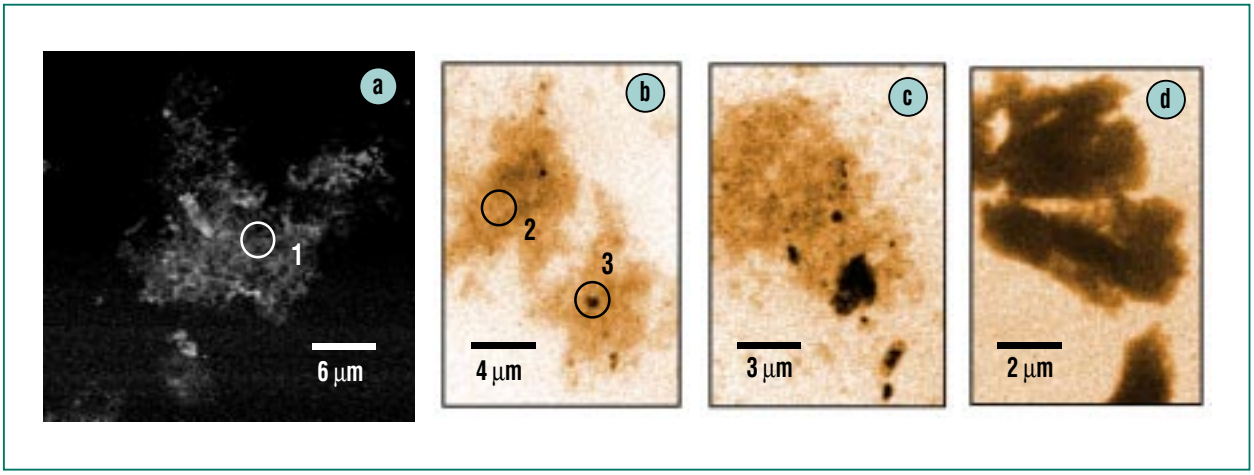

Fig. 5: (a) Negative STXM image of an HS agglomerate at pH_c = 4.3; HS agglomerates after various reaction times following the addition of Eu(III); (b) 1 h, (c) four weeks, (d) 7 months. Circles indicate areas from which the XANES spectra in Fig. 6 are extracted. All pictures are taken at a photon energy of 290 eV.

change drastically. In a sort of pseudo-phase separation, dark spots are observed to develop within brighter, i.e. optically less dense, material. The density of the Eu(III)-HS agglomerates is also observed to increase with time (Fig. 5c and d) [2].

Prior to the addition of Eu(III), the HS shows two intense peaks in its carbon (C 1s) XANES spectrum (Fig. 6), which are attributed to aromatic carbons and carboxylate and carbonyl groups, respectively. The changes in morphology of the aggregates after the addition of Eu(III) are also apparent in changes in their XANES spectra. In general, the intensity of the carboxylate peak decreases strongly after complexation, which is indicative of participation of the carboxylate groups in complexing Eu(III). This confirms the interpretation of XAFS results in the hard X-ray regime [3]. The observed phase separation into dark, dense and brighter, less dense regions of the HS-Eu(III) agglomerates results in differences in the XANES spectra in the range of peaks normally attributed to phenolic and aliphatic carbon atoms. This can be explained by a separation of HS components with different phenolic and aliphatic contents and/or with different complexing capabilities of various HS constituents. These processes influence the solubility of the HS-Eu(III) agglomerates, and the ability of HS to bind more actinide ions.

EXAFS Application Example: The solubility of tetravalent plutonium (Pu(IV)) in an aqueous medium is very low because of the formation of sparingly soluble hydroxides and oxides (approx. 10^{-10} mol/l). These hydroxides and oxides exhibit a pronounced tendency to form colloidal particles in the nm range, which can lead to increased Pu concentration in the mobile aqueous phase by several orders of magnitude. Determining the generation, quantity, and stability of such aquatic Pu(IV) colloids is thus the decisive factor in predicting the migration behavior of Pu(IV). We were able to determine the structures of the Pu(IV) colloids formed in the hydrolysis reaction of the Pu^{4+} cation at various pH_c levels between 0 and 1.75 from their Pu EXAFS spectra [4].

Pu L3 EXAFS (Fig. 7) exhibits the following trends going from sample A to F with increasing pH_c: the Pu-O coordination shell (O: oxygen) becomes asymmetric, while the amplitude of Pu-Pu interaction rises continuously. The asymmetry of the Pu-O shell is indicative of the binding of different ligands ($-O^-$, -OH, OH_2) to Pu(IV). The Pu-Pu interaction present in all spectra implies the existence of a rather rigid -Pu-O-Pu-backbone in the colloid structure. Simulation of the data clearly shows that the -Pu-O-Pu-backbone of the colloids is derived from a PuO_2 structure (CaF_2 lattice: face-centered cubic) and consists of a cubic Pu sublattice rich in defects.

Combination of the structural information obtained from EXAFS with results obtained by LIBD

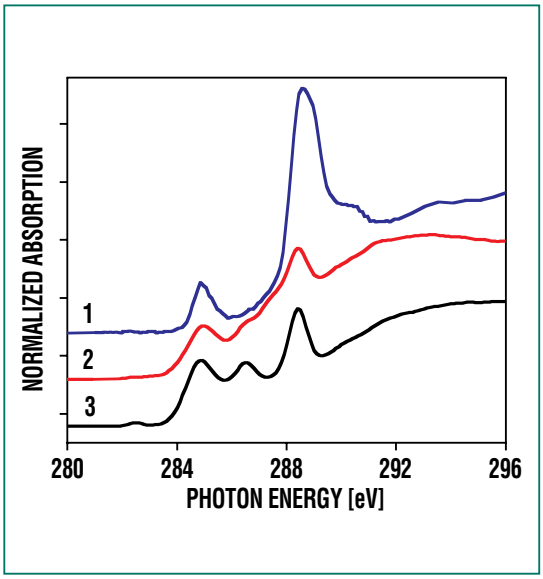

Fig. 6: C 1s XANES of HS before (1) and after (2, 3) the addition of Eu(III).

(laser-induced breakdown detection) allows us to postulate a mechanism of Pu-colloid formation. It is known from LIBD studies [5] that the hydrolytic generation of colloids is associated with a release of two protons. We postulate a mechanism in which the Pu colloids are formed by agglomeration of small Pu-oxyhydroxide oligomers ($Pu_nO_{2n-x}(OH)_{2x}(H_2O)_z$) (Fig. 8). The oligomers are formed from successive condensation of monomeric units ($Pu(OH)_2(H_2O)_6^{2+}$) linked at cubic polyhedron edges, hereby releasing two protons per Pu^{4+} ion in the process. The asymmetry of the Pu-O shell is a direct result of this mechanism. Condensation reactions of cubic units and agglomeration of the oligomers produced automatically result in a three-dimensional structure with a cubic Pu-sublattice.

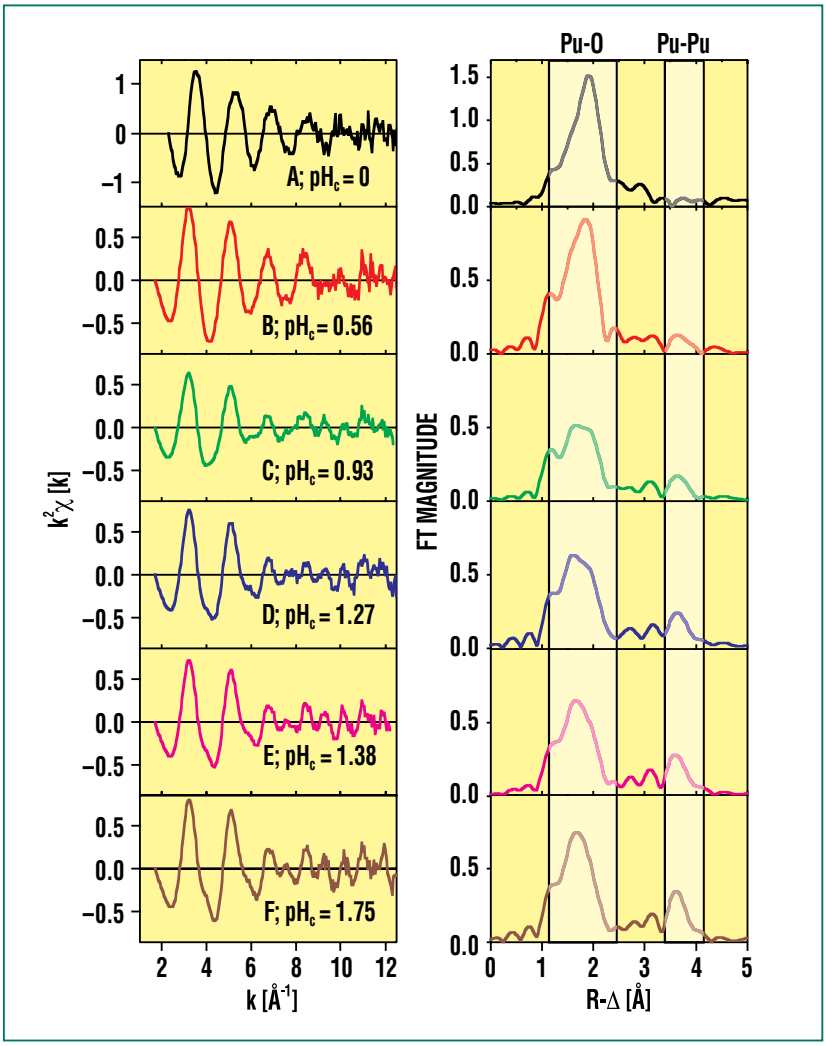

Fig. 7: Pu L3 EXAFS of aqueous Pu(IV) solutions (1 mM) at varying pH$_c$.

Sum Frequency Spectroscopy (SFS)

Basic Principles: In the non-linear optic technique of sum frequency (SF) spectrocopy [6], a sample is exposed to intense light from two lasers of the frequencies ω_1 and ω_2. Because of the high intensities, photons of both types of radiation can simultaneously couple at the sample and generate photons of the frequency, $\omega_{SF} = \omega_1 + \omega_2$. An SF signal can always be generated at a surface or interface, thus supplying interface selective information.

At INE, SF spectroscopy is applied systematically for the first time to the speciation of the functional groups of mineral/electrolyte interfaces, which can play a major role in migration and retention of radionuclides in natural groundwater. This technique allows the identification and quantification of such surface functional groups responsible for its reactivity and the adsorp-

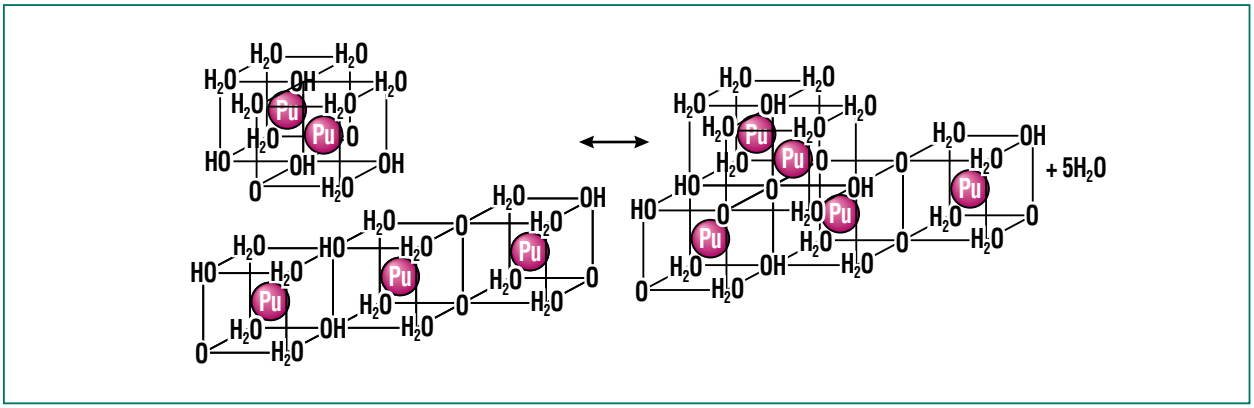

Fig. 8: Schematic representation of the agglomeration of a $Pu_2O_2(OH)_4(H_2O)_8$ dimer with a $Pu_3O_4(OH)_4(H_2O)_{12}$ trimer.

tion/desorption properties of the interface.

SF Spectroscopy Application Example: The SF spectrum of a specific surface of sapphire (aluminium oxide mineral) under an aqueous electrolyte solution at pH_c 12.0 is shown in Fig. 9. The infrared (IR) laser is tuned over the spectral range in which the OH-stretching vibrations are expected. Figure 9 shows the square root of SF intensity as a function of the IR wave number. Deconvolution of the spectrum yields seven bands. The two bands shown as dashed lines are from water molecules in the direct vicinity of the interface which have a preferred polar orientation. The other five bands originate from a surprisingly large number of up to five aluminol species (aluminium in a combination with OH groups) and of water molecules bound in a specific way. The dominant peak of these five bands at 3693 cm^{-1} is interpreted as an OH-group whose oxygen acts as a bridge between two Al atoms [7]. When interpreting this spectrum, it must be borne in mind that the intensities of the individual bands, unlike the intensities in a fluorescence experiment, are not simply additive.

From SF signals it is possible to determine the absolute orientation of molecular dipoles. We conclude from these results that the OH dipole of the aluminium species shown in the small frame in Fig. 9 points in the direction of the electrolyte solution. The water molecules with their polar arrangement in the immediate vicinity of the interface (dashed bands) show a reverse orientation (upper right-hand corner in Fig. 9), which is what we expect at high pH_c. Measurement of the dipole orientation and quantification of the surface concentration of different species as a function of pH_c is underway. The interaction of the chemical species on the mineral surface with actinide ions will also be studied by SF spectroscopy. These studies, in combination with other speciation methods, are expected to furnish a detailed quantitative model of the interaction of actinide ions with mineral surfaces.

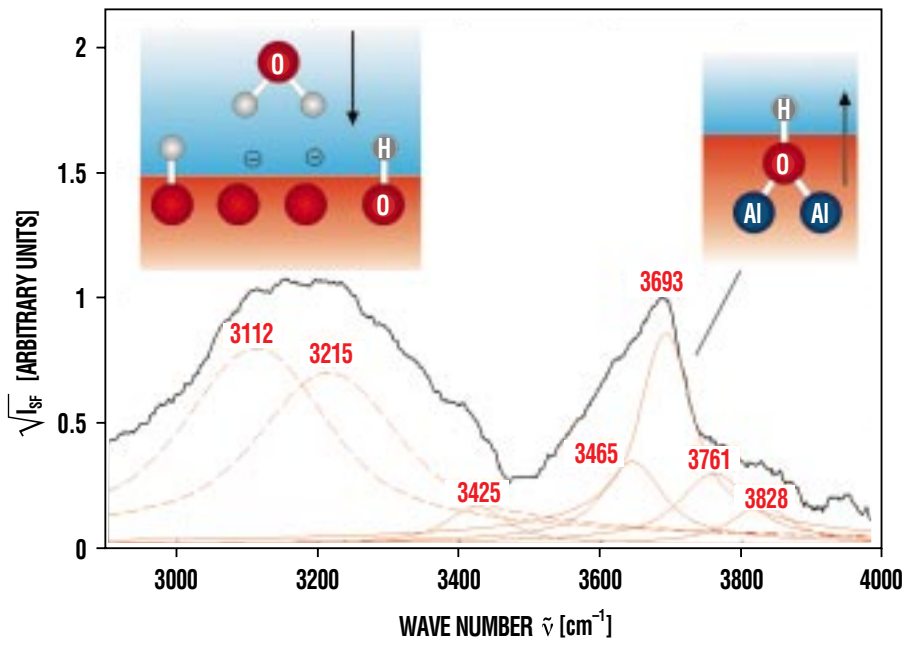

Fig. 9: Sum frequency spectrum of a sapphire surface under water at pH_c = 12 together with the result of deconvolution and its interpretation. The arrows symbolize dipoles of the ordered water film and the dipoles of the aluminol-OH groups acting as a bridge between two Al atoms.

Summary

The speciation of actinides by spectroscopic methods and by the combination of various spectroscopic methods is indispensable to the assessment of the long-term safety of radioactive waste repositories. Only when the migration behavior of the actinides is understood can long-term safety be ensured. Understanding the migration behavior of actinides, in turn, can be achieved only by elucidating the reaction mechanisms leading to the mobilization/immobilization of actinides in the geosphere and hydrosphere. Elucidation of reaction mechanisms is possible through the application of spectroscopic speciation techniques.

Literature

[1] M. Plaschke, J. Rothe, M.A. Denecke, Th. Fanghänel, *J. Electron Spec. Relat. Phenom., 135, 55-64 (2004)*

[2] J. Rothe, M. Plaschke, M.A. Denecke, *J. Phys. IV France, 104, 421-4, 2003*

[3] M.A. Denecke, D. Bublitz, J.I. Kim, H. Moll. I. Farkes, *J. Synchrotron Rad., 6, 394-6, 1999*

[4] J. Rothe, C. Walther, M.A. Denecke, Th. Fanghänel, *Inorg. Chem (in the press)*

[5] C. Walther, W. Hauser, H. Geckeis, Th. Fanghänel, *Nachrichten, 4, 179-84, 2003*

[6] Y.R. Shen *Nature, 357, 519, 1989*

G.L. Richmond, *Chem. Rev., 102, 2693, 2002*

[7] K.C. Hass, W.F. Schneider, A. Curioni, W. Andreoni, *J. Phys. Chem B, 104, 5527, 2000*

V. Barrón, J. Torrent, *J. Colloid Interface Sci., 177, 407, 1996*

Individual Calibration of Whole-body and Partial-body Counters by Means of Voxel Phantoms

H. Doerfel, B. Heide, M. Streckenbach, M. Urban, HS; H. Çakmak, IAI

Introduction

At the present state of the art, the accuracy of activity determination by means of whole-body and partial-body counters is no longer determined by errors in counting statistics, but by the bias caused by calibration. This is true in particular of low-energy photon emitters, such as Pb-210, U-235, Th-234 (daughter product of U-238), and Am-241. In addition, these nuclides in general show a very inhomogeneous distribution in the body (bone surface, lung, lymph nodes, liver, kidneys). These problems cannot be solved completely even by the most advanced physical phantoms, as these phantoms always represent one standard distribution only.

The Karlsruhe Research Center has a whole-body counter for measurements of photon emitters in the energy range between 100 and 3000 keV, and two partial-body counters for measuring photon emitters in the energy range between 15 and 200 keV. The whole-body counter is made up of four NaI(Tl) scintillation detectors with a crystal diameter of 20 cm and a crystal thickness of 10 cm. The partial-body counters, on the other hand, use large-area phoswich detectors or smaller HPGe detectors. The phoswich detectors each consist of a thin NaI(Tl) scintillation crystal for detection of low-energy photon radiation, and a comparatively thick CsI(Tl) scintillation crystal acting as an anti-Compton shield to reduce the background of the NaI(Tl) crystal. In partial-body counting, the phoswich detectors are in direct contact with the body and are moved as close as possible to the organ under study. Figure 1 shows the example of a detector arrangement in lung counting. As a result of anti-Compton discrimination, the phoswich detectors have a relatively high sensitivity specifically to low-energy photon emitters. However, their energy resolution is relatively bad, which may give rise to major problems in the presence of spurious emitters, such as Cs-137. For this reason, another partial-body counter with special HPGe sandwich detectors was developed at the Research Center. These detectors constitute a solid-state analog of phoswich detectors in which a planar HPGe crystal assumes the role of the NaI(Tl) crystal, and a coaxial HPGe detector assumes the function of the CsI(Tl) crystal. Four such detectors are used in the Karlsruhe HPGe partial-body counter (Fig. 2).

Four different physical phantoms are available for calibration of the partial-body counters. Figure 3 shows the example of a disassembled trunk phantom used at the Research Center. The models of organs in this phantom each contain a matrix of holes into which radioactive standard sources can be introduced to simulate almost any nuclide deposition. Both partial body counters are regularly calibrated with this trunk phantom and with a comparable torso phantom. Nevertheless, inconsistent results are frequently encountered in practice when (a) the proportions of the body of the subject do not match those of the phantom, and

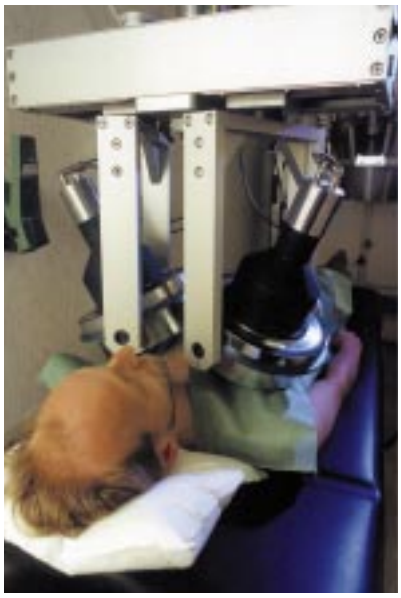

Fig. 1: Partial-body counter with two NaI(Tl)/CsI(Tl) phoswich detectors for measurements of photon emissions in the energy range between 15 and 100 keV in the lung.

Fig. 2: Partial-body counter with four HPGe sandwich detectors for measurements of photon emissions in the energy range of 15 to 200 keV in the lung.

Fig. 3: Physical phantom for calibration of whole-body and partial-body counters for nuclide depositions in major organs and tissue structures of the body.

Fig. 4: MEET-Man, front view, partly dissected.

(b) the nuclide distributions and the organs of the subject do not correspond to those in the phantom.

One solution to this problem is offered by the voxel phantoms recently introduced into internal dosimetry. These voxel phantoms allow mathematical simulations of photon transport from a source organ to a target organ in the body, and have proved to work excellently in the calculation of dose coefficients for internal dosimetry. The voxel phantoms also allow photon transport from a source organ within the body to a detector outside the body to be simulated, thus basically permitting the efficiency of this detector to be calculated for the radiation emitted by the nuclide deposition. This mathematical calibration of whole-body and partial-body counters has the decisive advantage of allowing voxel phantoms, unlike physical phantoms, to be matched easily to the individual body proportions and activity distributions of the subject.

Mathematical Simulation of a Subject

Basic Dataset

The "MEET-Man" dataset of the Institute of Biomedical Engineering of the University of Karlsruhe is used to simulate the subject [1]. Originally, this dataset was designed to simulate physics processes in the body, especially electromagnetic, elastomechanical and thermal processes.

The basis of this MEET-Man is the Visible-Man dataset produced in 1994 within the framework of the Visible Human project run by the National Library of Medicine (NLM), Bethesda, Maryland, USA [2, 3]. The Visible-Man dataset is composed of tomograms of a male body generated by computerized tomography (CT), nuclear magnetic resonance tomography (NMR), and thin-film color photography. The man was 180 cm tall and weighed 92 kg. The tomograms were processed by the Institute for Biomedical Engineering. Geometric errors and errors in color were corrected, missing or useless tomographic slices were interpolated in a special process (image warping). Then the images were segmented. In this case, each three-dimensional element was assigned precisely one out of 28 characteristic tissue and organ numbers, respectively. Figure 4 shows a picture of the structures of the MEET-Man.

Individual Matching of the Dataset

Matching the MEET-Man to the individual proportions of a subject's body can be achieved by linear extension and compression, respectively, of the voxels or by non-linear morphing. Linear extension is a congruent transformation in which the structures of the phantom are extended or compressed in the three directions in space, x, y, and z, with the fixed extension factors, f_x, f_y, and f_z. In this way, the dimensions of all structures of the phantom change in the same way. In morphing, however, the structures

are extended and compressed, respectively, in different ways, thus causing the shape of the phantom or of individual structures of the phantom to change. Matching is achieved on the basis of a surface model of the subject. To generate a surface model of this kind, the RAMSIS (Computer-assisted Anthropological Mathematical System for Subject Simulation) process developed at the Munich Technical University [4, 5] can be used. However, a comparatively simple surface scan can also be carried out by means of a laser scan. Figure 5 shows the example of a surface model of a subject produced with a laser scanner of the Munich Technical University [6].

Linear Matching

When the proportions of the body of a subject differ only slightly from those of the basic dataset, linear matching is possible. In this case, first the voxel representations of the MEET-Man organs are transformed into the surface envelope of the subject. This transformation is achieved by means of the KisMo code developed at the Research Center [7]. The voxel organs are positioned in such a way that their centers of mass are in the anatomically correct positions. Afterwards, the voxel organs are extended and compressed, respectively, in the three directions in space, x, y, and z, until their shapes correspond to the criteria contained in a three-dimensional anatomical atlas. Figure 6 shows the organs (brain, lung, stomach, liver, spleen, kidneys) of the MEET-Man dataset implemented into the surface model of a subject in this way.

Non-linear Matching

In non-linear matching, surface representations of the organs of the phantom are produced in a first step by means of the KisMo code. They are construed interactively with check points and derivation vectors by means of form surfaces, with tomograms of MEET-Man serving as models. First of all, the organ to be modeled is identified in the tomograms, a design level is selected, and the contours of the object in the tomograms are generated by interactive placing and erasing of check points. The contours of the object must not be construed for all tomograms, as final linear interpolation will automatically generate missing contours and produce the 3D object surface. Four check points each with the associated derivation vectors constitute a so-called patch with the associated interpolation points calculated by means of a spline function. Figure 7 shows the example of a surface representation of the left lung of the MEET-Man dataset, with the patches being shown in red and the check points being shown in yellow.

In a second step, the surfaces are now modified by clicking and moving the check points in such a way that the organs assume the desired shape and the desired volume. Also ultrasonic images may be used for orientation. Movement is in any plane in

Fig. 5: Surface model of a subject produced with a laser scanner.

Fig. 6: Implementation of a few organs of the MEET-Man voxel phantom in the surface model of a subject; the person is identical with the subject in Fig. 7, but the surface is represented as a wire frame for better clarity.

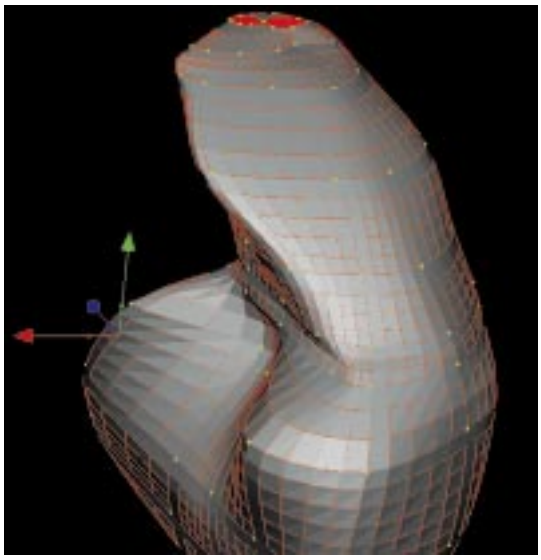

Fig. 7: Surface representation of the left lung of the MEET-Man voxel phantom; the red grids represent the patches, the yellow points, the checkpoints.

three-dimensional space and is indicated by the code simultaneously both in a perspective view and in the xy, xz, and yz planes.

In the third and last step, voxel representations are generated again from the surface representations. For this purpose, a circumscribing block is construed around the respective surface area and filled with voxels of the desired size. Next, each voxel will be checked with respect to whether it will be used or not, i.e. whether it lies within or outside the surface area.

It is assumed that the surfaces are closed, simply connected, and free from double points in the mathematical sense. This is generally assured for the surfaces generated by KisMo.

Simulation of Photon Transport

The MEET-Man phantom matched to the test person serves as a basis for simulating photon transport from a specific organ or tissue of the phantom to a specific detector of the whole-body or partial-body counter. Simulation is carried out by means of the Visual Monte Carlo Code (VMC) [8]. First, a random number generator is used to select a voxel of the respective organ or tissue from which a photon is emitted at the given energy. Then a random value is determined for the angle of emission, and the next interaction of the photon in the respective direction in space is determined by means of the corresponding cross sections. If this interaction is a photo effect, the photon is fully absorbed at this point. If it is a Compton effect or pair production effect, the random number generator is employed to determine the starting parameters of the scattered photon and those of the annihilation quanta, respectively, produced after pair production. This simulation is continued until the photons generated in the interactions are absorbed by the photo effect or leave a given volume. After simulation of a sufficiently large number of processes, the number of those photons is determined which reach the detector without being scattered and are absorbed there by the photo effect. Relating this number to the total number of photons emitted yields the efficiency of the re-

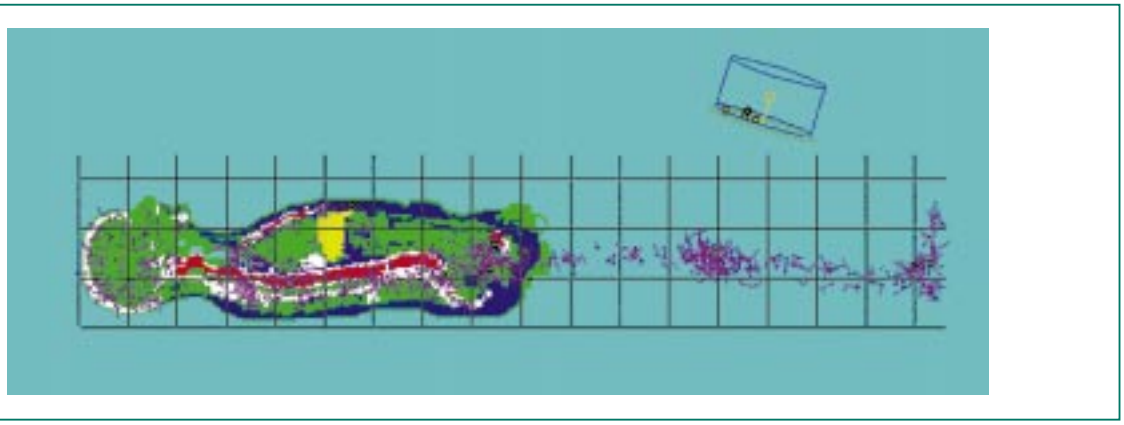

Fig. 8: Simulation of photon transport by the VMC code [8] for a deposition of Am-241 in the skeleton of a voxel phantom; the short violet lines indicate the directions of photon emission. The green circles (mainly in the middle and in the feet) stand for interactions of the photons with air molecules, while the yellow circles in the detector symbolize absorption events due to the photo effect.

spective detector for nuclide deposition in the respective organ or tissue. For illustration, Figure 8 shows the simulation of photon transport by the VMC code for a deposition of Am-241 in the skeleton of a voxel phantom. The short violet lines indicate the directions of photon emission. The green circles (mainly in the center and around the feet) stand for interactions of the photons with air molecules, while the yellow circles in the detector symbolize absorption events due to the photo effect.

Experience so far has shown this method to produce a sufficiently accurate simulation of photon transport from any nuclide deposition in the body to any detector of a whole-body or partial-body counter. However, the method is unable to simulate subsequent processes in the detector and in the downstream electronics. These processes can be determined experimentally in a simple way. On the basis of those experiments, empirical correction factors can be derived to take into account electronic effects and can be implemented in the simulation program. This is the subject of further studies.

Literature

[1] F.B. Sachse, C. Werner, M. Müller, K. Meyer-Waarden, *Meet-Man Models for Simulation of Electromagnetic, Elastomechanic and Thermic Behavior of Man, Erstellung und technische Parameter, Institut für Biomedizinische Technik, University of Karlsruhe, 1997*

[2] M. J. Ackerman, *Viewpoint: The Visible Human Project, Journal Biocommunication, 18, No. 2, p. 14, 1991*

[3] V. Spitzer, M.J. Ackerman, A.L. Scherzinger, D. Whitlock, *The Visible Human Male: A Technical Report, Journal of the American Medical Informatics Association, 3, No. 2, pp. 118-30, 1996*

[4] H. Bubb, *RAMSIS – A Measuring and CAD-Tool Serving as a Standard for Ergonomic Assessments of Workplaces, Cars, and Other Products, In: Proc. of the 13th Triennial Congress of the International Ergonomics Association, Tampere, Finland, June 29 – July 4, 1997, edited by P. Seppala, T. Luopajarvi, C.H. Nygard and M. Mattila, Finnish Institute of Occupational Health, Helsinki, vol. 2*

[5] T. Seitz, H. Bubb, *An Approach for a Low-Cost Alternative for Full-Body Posture and Movement Measurement and Analysis, In: Proceedings of the International Conference on Computer-Aided Ergonomics and Safety, Maui, Hawaii, July 29 – August 1, 2001*

[6] T. Seitz, Lehrstuhl für Ergonomie, Technische Universität München, *private communication*

[7] H.K. Çakmak, H. Maass, G. Strauss, C. Trantakis, E. Nowatius, U. Kühnapfel, *Modellierung chirurgischer Simulationsszenarien für das Virtuelle Endoskopie Trainingssystem (VEST), CURAC 2002, 1. Jahrestagung der Deutschen Gesellschaft für Computer- und Roboterassistierte Chirurgie e.V., Leipzig, Germany, electronically published by Medicstream.de, ISSN 1619-2745*

[8] J.G. Hunt, B.M. Dantas, E. Lucena, *Calibration of an In Vivo Measurement System Using a Voxel Phantom, Radiation Protection Dosimetry, vol. 79, 1998, pp. 425-27*